Supporting Information

for

Synthesis, coordination, and catalytic application of phosphinoferrocene ligands bearing flexible thienyl and thiazolyl pendants

Věra Varmužová, Ivana Císařová and Petr Štěpnička*

Department of Inorganic Chemistry, Faculty of Science, Charles University, Hlavova 2030, 128 00 Prague, Czech Republic; Email: stepnic@natur.cuni.cz

Contents

Additional experiments

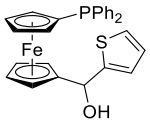

Synthesis of alcohol 7. An oven-dried 50mL flask equipped with a stirring bar was charged with 1-(diphenylphosphino)-1´-bromoferrocene (**6**; 225 mg, 0.5 mmol), flushed with nitrogen, and sealed. Anhydrous THF (5 mL) was added, and the solution was cooled to −78 °C in a dry ice/ethanol bath. *n*-Butyllithium (0.2 mL, 2.5 M solution in THF, 0.5 mmol) was added, and the mixture was stirred for 45 min, during which time an orange precipitate formed. Neat 2-formylthiophene (0.05 mL, 0.55 mmol) was added dropwise, and the resulting mixture was stirred with cooling for 15 min and then at room temperature for 2 h. The reaction was terminated by adding distilled water (10 mL) and ethyl acetate (10 mL). The orange organic layer was separated, washed with brine (15 mL), dried over $MgSO_4$, filtered, and evaporated under vacuum. The orange residue was taken up with dichloromethane (5 mL) and evaporated with chromatographic alumina. The crude, preadsorbed product was transferred onto an alumina column packed with hexane-ethyl acetate (8:1). Elution with the same solvent mixture led to the development of three bands. The first yellow band and the second red band were discarded. Then, the mobile phase was changed to cyclohexane-ethyl acetate (1:1) to elute the product as an orange band. After evaporation, compound **7** was obtained as an orange powder. Yield: 126 mg (52%).

^{1}H NMR (400 MHz, $CDCl_3$): δ 2.83-2.87 (m, 1 H, CHO*H*), 4.06-4.09 (m, 1 H, C_5H_4), 4.09-4.12 (m, 1 H, C_5H_4), 4.14-4.17 (m, 1 H, C_5H_4), 4.17-4.21 (m, 2 H, C_5H_4), 4.25-4.30 (m, 1 H, C_5H_4), 4.41-4.45 (m, 2 H, C_5H_4), 5.60 (d, *J* = 3.4 Hz, 1 H, C*H*OH), 6.82-6.86 (m, 1 H, C_4H_3S), 6.89 (dd, *J* = 5.1, 3.5 Hz, 1 H, C_4H_3S), 7.20 (dd, *J* = 5.1, 1.3 Hz, 1 H, C_4H_3S), 7.27-7.46 (m, 10 H, PPh_2). ^{31}P{^{1}H} NMR (161.9 MHz, $CDCl_3$) δ −17.1 (s, PPh_2). ^{13}C{^{1}H} NMR (100.6 MHz, $CDCl_3$): δ 67.04 (s, CH C_5H_4), 68.10 (s, CHOH), 68.31 (s, CH C_5H_4), 69.22 (s, CH C_5H_4), 69.27 (s, CH C_5H_4), 71.35 (d, J_{PC} = 3 Hz, CH C_5H_4), 71.45 (d, J_{PC} = 4 Hz, CH C_5H_4), 73.01 (d, J_{PC} = 13 Hz, CH C_5H_4), 73.81 (d, J_{PC} = 16 Hz, CH C_5H_4), 76.49 (d, J_{PC} = 5 Hz, C^{ipso}-P C_5H_4), 93.61 (s, C^{ipso}-C C_5H_4), 124.27 (s, CH C_4H_3S), 124.70 (s, CH C_4H_3S), 126.30 (s, CH C_4H_3S), 128.23 (d, J_{PC} = 3 Hz, CH PPh_2), 128.30 (d, J_{PC} = 3 Hz, CH PPh_2), 128.65 (s, CH PPh_2), 128.83 (s, CH PPh_2), 133.32 (d, J_{PC} = 19 Hz, CH PPh_2), 133.69 (d, J_{PC} = 19 Hz, CH PPh_2), 138.27 (d, J_{PC} = 8 Hz, C^{ipso} PPh_2), 138.65 (d, J_{PC} = 8 Hz, C^{ipso} PPh_2), 147.48 (s, C^{ipso} C_4H_3S). HRMS (ESI+), *m/z* calc. for $C_{27}H_{24}FeOPS$ ($[M + H]^+$): 483.0635, found: 483.0620.

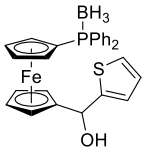

Synthesis of 7·BH_3. An oven-dried 50mL flask equipped with a stirring bar was charged with 1-(diphenylphosphino)-1´-bromoferrocene–borane (1:1) (**6**·BH_3; 2.315 g, 5.0 mmol), flushed with nitrogen, and sealed. Anhydrous THF (25 mL) was added, and the solution was cooled to −78 °C in a dry ice/ethanol bath. *n*-Butyllithium (2.0 mL, 2.5 M solution in THF, 5.0 mmol) was introduced, and the resulting mixture was stirred for 45 min (an orange precipitate formed during this time). Neat 2-formylthiophene (0.51 mL, 5.5 mmol) was added dropwise, and the reaction mixture was stirred with cooling for 15 min and then at room temperature for 2 h. The reaction was terminated by adding distilled water (40 mL) and ethyl acetate (40 mL). The orange organic layer was separated, washed with brine (40 mL), dried over $MgSO_4$, filtered, and evaporated under vacuum. The orange residue was dissolved in dichloromethane (40 mL) and evaporated with chromatographic alumina. The preadsorbed crude product was transferred onto an alumina column packed with hexane-ethyl acetate (8:1). Elution with the same solvent mixture produced three bands. The first yellow band and the second red band were discarded. Next, the eluent was changed to cyclohexane-ethyl acetate (1:1) to remove an orange band of the product. Following evaporation, compound **7**·BH_3 was obtained as an orange powder. Yield: 1.556 g (63%).

^{1}H NMR (400 MHz, $CDCl_3$): δ 0.75-1.83 (br m, 3 H, BH_3), 2.35 (d, *J* = 3.9 Hz, 1 H, CHO*H*), 4.06-4.11 (m, 2 H, C_5H_4), 4.20-4.24 (m, 1 H, C_5H_4), 4.29-4.32 (m, 1 H, C_5H_4), 4.45-4.49 (m, 2 H, C_5H_4), 4.52-4.58 (m, 2 H, C_5H_4), 6.81-6.84 (m, 1 H, C_4H_3S), 6.89 (dd, *J* = 5.1, 3.5 Hz, 1 H, C_4H_3S), 7.19 (dd, *J* = 5.1, 1.3, 1 H, C_4H_3S), 7.36-7.52 (m, 6 H, PPh_2), 7.52-7.65 (m, 4 H, PPh_2). ^{31}P{^{1}H} NMR (161.9 MHz, $CDCl_3$) δ 15.7 (br s, PPh_2·BH_3). ^{13}C{^{1}H} NMR (100.6 MHz, $CDCl_3$): δ 67.45 (s, CH C_5H_4), 67.89 (s, CHOH), 69.14 (s, CH C_5H_4), 69.58 (d, J_{PC} = 68 Hz, C^{ipso}-P C_5H_4), 69.76 (s, CH C_5H_4), 70.02 (s, CH C_5H_4), 72.57 (d, J_{PC} = 8 Hz, CH C_5H_4), 72.71 (d, J_{PC} = 8 Hz, CH C_5H_4), 73.31 (d, J_{PC} = 10 Hz, CH C_5H_4), 73.63 (d, J_{PC} = 10 Hz, CH C_5H_4), 93.90 (s, C^{ipso}-C C_5H_4), 124.33 (s, CH C_4H_3S), 124.80 (s, CH C_4H_3S), 126.34 (s, CH C_4H_3S), 128.47 (d, J_{PC} = 3 Hz, CH PPh_2), 128.57 (d, J_{PC} = 3 Hz, CH PPh_2), 130.73 (d, J_{PC} = 10 Hz, C^{ipso} PPh_2), 131.01 (d, J_{PC} = 3 Hz, CH PPh_2), 131.07 (d, J_{PC} = 3 Hz, CH PPh_2), 131.32 (d, J_{PC} = 10 Hz, C^{ipso} PPh_2), 132.63 (2× d, J_{PC} = 10 Hz, CH PPh_2), 147.33 (s, C^{ipso} C_4H_3S). HRMS (ESI+), *m/z* calc. for $C_{27}H_{26}BFeNaOPS$ ($[M + Na]^+$): 519.0782, found: 519.0775.

Reduction of 7·BH_3 with Et_3SiH/CF_3CO_2H. Compound **7**·BH_3 (135 mg, 0.27 mmol) was dissolved in anhydrous dichloromethane (5 mL) under nitrogen and the solution was cooled to 0 °C in an ice bath. Neat triethylsilane (48 μL, 0.30 mmol) and then trifluoroacetic acid (22 μL, 0.30 mmol) were added dropwise, and the resulting brown-orange solution was stirred at room temperature overnight (18 h). Next, the reaction mixture was diluted with dichloromethane (5 mL), washed with saturated aqueous $NaHCO_3$ (2× 10 mL) and brine (10 mL). The organic layer was separated, dried over $MgSO_4$ and evaporated, leaving an orange oil. The oil was taken up with dichloromethane (5 mL) and evaporated with chromatographic silica gel. The crude preadsorbed product was purified by chromatography over a silica gel column using cyclohexane-ethyl acetate (8:1) as the eluent. The first yellow-orange band afforded after evaporation a mixture of **1**·BH_3 and **1** in a 65:35 ratio. Yield: 58 mg, orange solid.

Characterization data for **1**·BH_3. ^{1}H NMR (400 MHz, $CDCl_3$): δ 3.53 (s, 2 H, CH_2), 4.02 (vt, *J*′ = 1.8 Hz, 2 H, C_5H_4), 4.13 (vt, *J*′ = 1.9 Hz, 2 H, C_5H_4), 4.37 (vq, *J*′ = 1.9 Hz, 2 H, C_5H_4), 4.46 (vt, *J*′ = 1.8 Hz, 2 H, C_5H_4). The spectrum could not be analysed in full due to overlaps of the signals due to 1 and **1**·BH_3. Data for the reaction mixture. ^{31}P{^{1}H} NMR (161.9 MHz, $CDCl_3$) δ 15.9 (br s, PPh_2·BH_3), –16.9 (s, PPh_2).

Attempted synthesis of [PdCl(μ-Cl)(1-κ*P*)]$_2$. A solution of ligand **1** (11.1 mg, 0.024 mmol) in $CDCl_3$ (1.0 mL) was added to solid [$PdCl_2(MeCN)_2$] (6.2 mg, 0.024 mmol), and the resulting red mixture was stirred for 30 min, whereupon it deposited a dark precipitate. Subsequent evaporation produced a black insoluble powder.

The reaction of [$PdCl_2(MeCN)_2$] with 1 and triphenylphosphine. To solid [$PdCl_2(MeCN)_2$] (5.2 mg, 0.020 mmol) were added in rapid succession a solution of ligand **1** (9.2 mg, 0.020 mmol) in $CDCl_3$ (1.0 mL) and solid triphenylphosphine (5.3 mg, 0.020 mmol). The resulting red mixture was stirred for 30 min and analysed by ^{1}H and ^{31}P NMR spectroscopy. The ^{31}P NMR spectra revealed the presence of *trans*-[$PdCl_2(PPh_3)$(**1**-κ*P*)] (δ_P 22.4 and 16.9, $^2J_{PP}$ = 481 Hz; the data were analysed as an AB spin system), and the symmetrical bis(phosphine) complexes **25** (δ_P 15.1) and [$PdCl_2(PPh_3)_2$] (δ_P 23.2), in approximately 2:1:1 molar ratio (Figure S1).

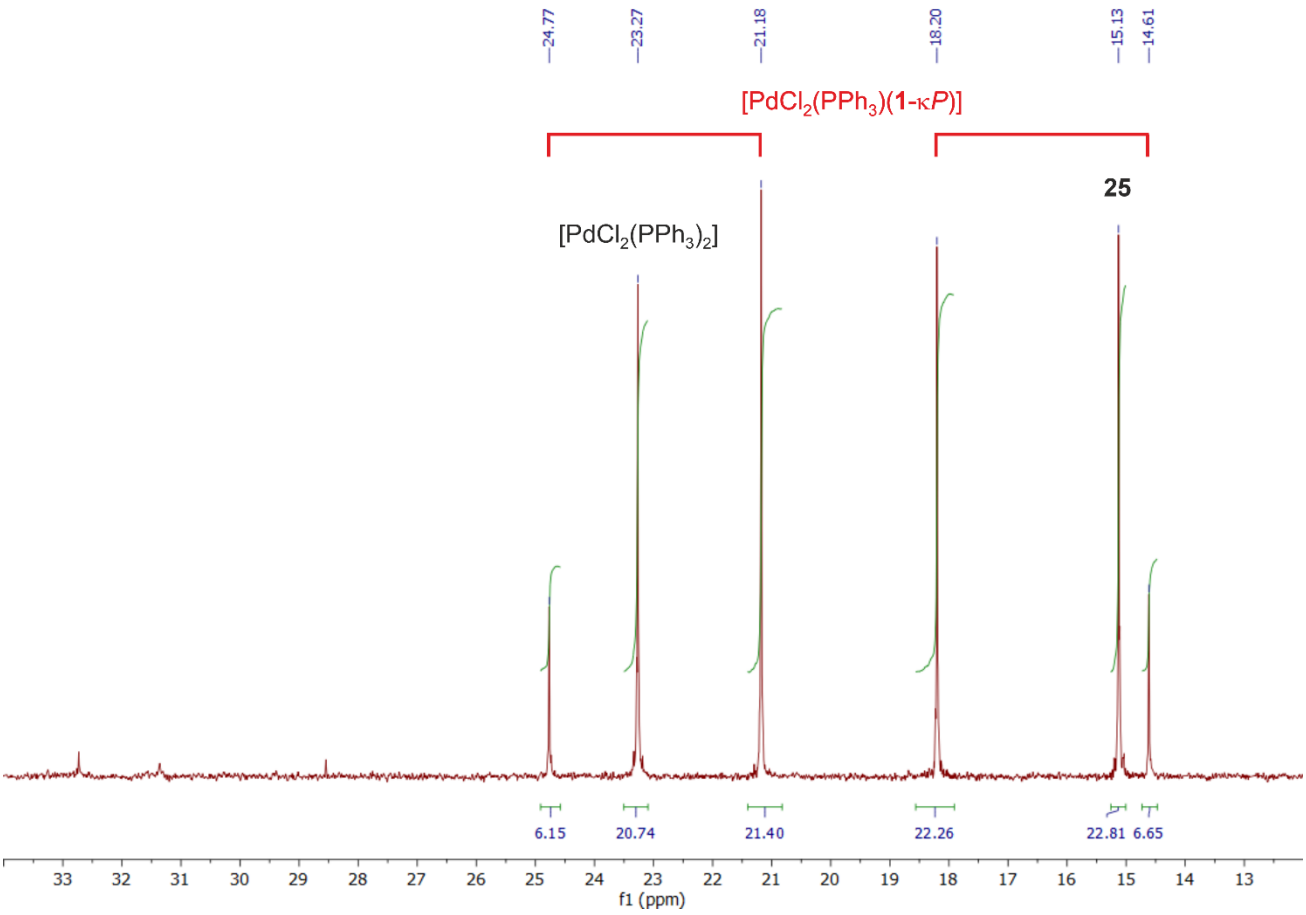

Figure S1. $^{31}P\{^{1}H\}$ NMR ($CDCl_3$, 161.98 MHz, 25 °C) spectrum of the reaction mixture obtained from $[PdCl_2(MeCN)_2]$, **1** and PPh_3 at the 1:1:1 molar ratio.

Cleavage of [PdCl(μ-Cl)(1-κ*P*)]$_2$ with triphenylphosphine. A solution of ligand **1** (11.1 mg, 0.024 mmol) in $CDCl_3$ (1.0 mL) was added to solid $[PdCl_2(MeCN)_2]$ (6.2 mg, 0.024 mmol) and the resulting red mixture was stirred for 30 min. A dark precipitate separated. Solid triphenylphosphine (6.3 mg, 0.024 mmol) was added and the stirring was continued for 3 h. The most of the precipitate dissolved during this time to give a red brown solution. The resulting mixture was filtered through a PTFE syringe filter (0.45 μm porosity) and analysed by NMR spectroscopy. The composition of the reaction mixture was essentially the same as in the previous experiment.

X-ray crystallography

The diffraction data were collected with a Bruker D8 VENTURE Kappa Duo diffractometer equipped with an Oxford Cryostream cooler. Mo Kα radiation (λ = 0.71073 Å) was applied throughout. The structures were solved by the intrinsic phasing method using SHELXT (version 2014 or 2018),[1] and refined by full-matrix least-squares against F^2 with SHELXL (version 2014 or 2017).[2] All non-hydrogen atoms were refined with anisotropic displacement parameters. Hydrogen atoms were placed into their theoretical positions using the default parameters implemented in SHELXL, and refined as riding atoms with $U_{iso}(H) = 1.2U_{eq}(C)$.

The thienyl groups in the structures of **1**-**3** were disordered over two virtually isosteric positions related by a 180°-rotation along the pivotal C23-C24 bond. The refined occupancies were 58:42 for **1**, 74:26 for **2**, and 69:31 for **3**. Besides, the structure of **2** contained a relatively large residual electron density maximum (1.22 e Å^{-3}), which corresponds to the lone pair at the phosphorus atom.

The heterocyclic moieties in the structures of bisphosphine complexes **25**-**27**, **27,** and **30** were also disordered. In this case, however, the heterocyclic substituents were often found in general positions. They were refined with either the terminal heterocyclic substituent (complex **26**: occupancies 58:42; in this case, the disorder was similar to that in the free ligand **2**; complex **29**: occupancies 56:44) or the entire CH_2Het pendant (Het = heterocyclic group) over two positions (complex **25**: occupancies 50:50; complex **27**: occupancies 50:50, one of the phenyl rings, C(11-16) was also partly disordered (65:35 for two ring atoms); and complex **30**: occupancies 51:49). Notably, the diffraction patterns recorded for **27** contained weak satellite maxima, suggesting that the disorder was not entirely random.

The structure of **28** displayed a disorder of the $C_5H_4CH_2(C_4H_3S)$ moiety, which was refined over two positions (55:45). Compound **31**·CH_2Cl_2 crystallized as a two-component twin. The refined contributions from the two domains were 60:40. In addition, the solvent molecule in this structure was disordered and had to be refined over two positions (82:18). Lastly, compound **32**·CH_2Cl_2 crystallised with four complex and four solvent molecules in the asymmetric unit. Two of the four structurally independent dichloromethane molecules were partly disordered and were thus refined with one or two chlorine atoms split over two positions.

Complete crystallographic data were deposited with The Cambridge Crystallographic Data Centre and can be obtained free of charge via https://www.ccdc.cam.ac.uk/structures/, or by contacting The Cambridge Crystallographic Data Centre, 12 Union Road, Cambridge, CB2 1EZ, United Kingdom; phone: +44 (0)1223 336408. The deposition codes and parameters of the structure solution and refinement are presented in Table S1. Geometric parameters and structure diagrams were obtained using a recent version of the PLATON program.[3] All values are rounded according to their standard uncertainties.

Table S1. Selected crystallographic data and structure refinement parameters.

Compound	**1**	**2**	**3**
Formula	$C_{27}H_{23}FePS$	$C_{27}H_{35}FePS$	$C_{27}H_{23}FePS$
M [g mol^{-1}]	466.33	478.43	466.33
Crystal system	monoclinic	monoclinic	monoclinic
Space group	$P2_1/n$ (no. 14)	$P2_1/n$ (no. 14)	$P2_1/n$ (no. 14)
T [K]	120	120	120
a [Å]	8.5287(4)	13.6239(4)	8.6415(3)
b [Å]	18.4913(8)	7.8232(2)	9.5305(3)
c [Å]	13.9375(6)	21.8916(7)	26.4474(8)
α [°]	90	90	90
β [°]	99.727(2)	96.704(1)	94.896(1)
γ [°]	90	90	90
V [Å]^3	2166.4(2)	2317.3(1)	2170.2(1)
Z	4	4	4
F(000)	968	1016	968
μ(Mo Kα) [mm^{-1}]	0.878	0.822	0.877
Diffrns collected	29947	44325	68478
Independent diffrns	5379	5748	4990
Observed diffrns[a]	4926	5542	4925
R_{int}[b] [%]	3.02	2.08	2.46
No. of parameters	290	290	284
R[b] obsd diffrns [%]	3.18	2.44	2.32
R, wR[b] all data [%]	3.60, 6.95	2.52, 6.53	2.35, 5.80
Δρ [e Å^{-3}]	0.39, –0.26	1.22, –0.25	0.33, –0.28
CCDC deposition no.	2484154	2484155	2484156

[a] Diffractions with $I > 2\sigma(I)$. [b] Definitions: $R_{int} = \Sigma|F_o^2 - F_o^2(\text{mean})|/\Sigma F_o^2$, where F_o^2(mean) is the average intensity of symmetry-equivalent diffractions. $R = \Sigma||F_o| - |F_c||/\Sigma|F_o|$, $wR = [\Sigma\{w(F_o^2 - F_c^2)^2\}/\Sigma w(F_o^2)^2]^{1/2}$.

Table S1 continued

Compound	**4**	**25**	**26**
Formula	$C_{26}H_{22}FeNPS$	$C_{54}H_{46}Cl_2Fe_2P_2PdS_2$	$C_{54}H_{70}Cl_2Fe_2P_2PdS_2$
M [g mol^{-1}]	467.32	1109.97	1134.16
Crystal system	orthorhombic	monoclinic	triclinic
Space group	*Pbca* (no. 61)	$P2_1/n$ (no. 14)	$P\bar{1}$ (no. 2)
T [K]	120	120	120
a [Å]	9.3576(4)	11.0368(2)	10.8384(4)
b [Å]	16.7762(9)	12.7503(3)	10.8772(4)
c [Å]	27.556(1)	16.3510(4)	11.7745(4)
α [°]	90	90	80.317(1)
β [°]	90	98.395(1)	66.367(1)
γ [°]	90	90	88.618(1)
V [Å]^3	4325.9(4)	2276.30(9)	1252.14(8)
Z	8	2	1
F(000)	1936	1128	588
μ(Mo Kα) [mm^{-1}]	0.881	1.338	1.217
Diffrns collected	41233	42567	36012
Independent diffrns	5825	5192	5715
Observed diffrns[a]	5362	5123	5566
R_{int}[b] [%]	3.35	1.96	2.08
No. of parameters	271	341	293
R[b] obsd diffrns [%]	3.21	2.36	2.08
R, wR[b] all data [%]	3.55, 7.96	2.39, 5.87	2.13, 5.26
Δρ [e Å^{-3}]	0.65, –0.43	0.67, –0.47	0.80, –0.38
CCDC deposition no.	2484157	2484158	2484159

Table S1 continued

Compound	**27**	**28**	**29**
Formula	$C_{54}H_{46}Cl_2Fe_2P_2PdS_2$	$C_{54}H_{70}Cl_4Fe_2P_2Pd_2S_2$	$C_{52}H_{44}Cl_2Fe_2N_2P_2PdS_2$
M [g mol^{-1}]	1109.97	1311.46	1111.95
Crystal system	monoclinic	monoclinic	monoclinic
Space group	$P2_1/n$ (no. 14)	$P2_1/n$ (no. 14)	$P2_1/n$ (no. 14)
T [K]	120	120	120
a [Å]	10.9741(4)	10.629(1)	11.0056(4)
b [Å]	12.8369(4)	14.289(2)	12.7466(6)
c [Å]	16.3789(8)	17.484(2)	16.1630(7)
α [°]	90	90	90
β [°]	98.795(1)	99.942(4)	98.179(1)
γ [°]	90	90	90
V [Å]^3	2280.2(2)	2615.6(5)	2244.4(2)
Z	2	2	2
F(000)	1128	1336	1128
μ(Mo Kα) [mm^{-1}]	1.336	1.603	1.358
Diffrns collected	112800	50606	37029
Independent diffrns	5891	6011	5571
Observed diffrns[a]	5876	5010	5051
R_{int}[b] [%]	1.83	6.06	3.74
No. of parameters	342	374	323
R[b] obsd diffrns [%]	1.83	5.64	3.37
R, wR[b] all data [%]	1.84, 4.59	7.13, 10.3	3.77, 8.84
Δρ [e Å^{-3}]	0.45, −0.44	1.13, −1.03	1.41, −0.58
CCDC deposition no.	2484161	2484160	2484162

Table S1 continued

Compound	**30**	**31**·CH_2Cl_2	**32**·CH_2Cl_2
Formula	$C_{52}H_{44}Cl_2Fe_2N_2P_2PdS_2$	$C_{53}H_{46}Cl_6Fe_2N_2P_2Pd_2S_2$	$C_{27}H_{24}Cl_4FeNPPdS$
M [g mol^{-1}]	1111.95	1374.18	729.55
Crystal system	monoclinic	monoclinic	triclinic
Space group	$P2_1/n$ (no. 14)	$P2_1/c$ (no. 14)	$P\bar{1}$ (no. 2)
T [K]	120	120	120
a [Å]	10.9837(5)	19.452(1)	12.8754(7)
b [Å]	12.6909(5)	16.5443(7)	13.8595(8)
c [Å]	16.3131(7)	16.2609(8)	33.249(2)
α [°]	90	90	82.959(2)
β [°]	99.153(2)	91.825(2)	85.539(2)
γ [°]	90	90	75.627(2)
V [Å]^3	2245.0(2)	5230.3(5)	5697.2(6)
Z	2	4	8
F(000)	1128	2744	2912
μ(Mo Kα) [mm^{-1}]	1.358	1.708	1.664
Diffrns collected	34326	184633	379068
Independent diffrns	5558	19345	28196
Observed diffrns[a]	5453	18055	26635
R_{int}[b] [%]	2.03	5.60	3.14
No. of parameters	332	633	1326
R[b] obsd diffrns [%]	2.29	5.96	2.75
R, wR[b] all data [%]	2.33, 5.55	6.56, 12.3	2.96, 6.04
Δρ [e Å^{-3}]	0.44, −0.62	1.25, −1.58	2.19, −2.40
CCDC deposition no.	2484164	2484163	2484165

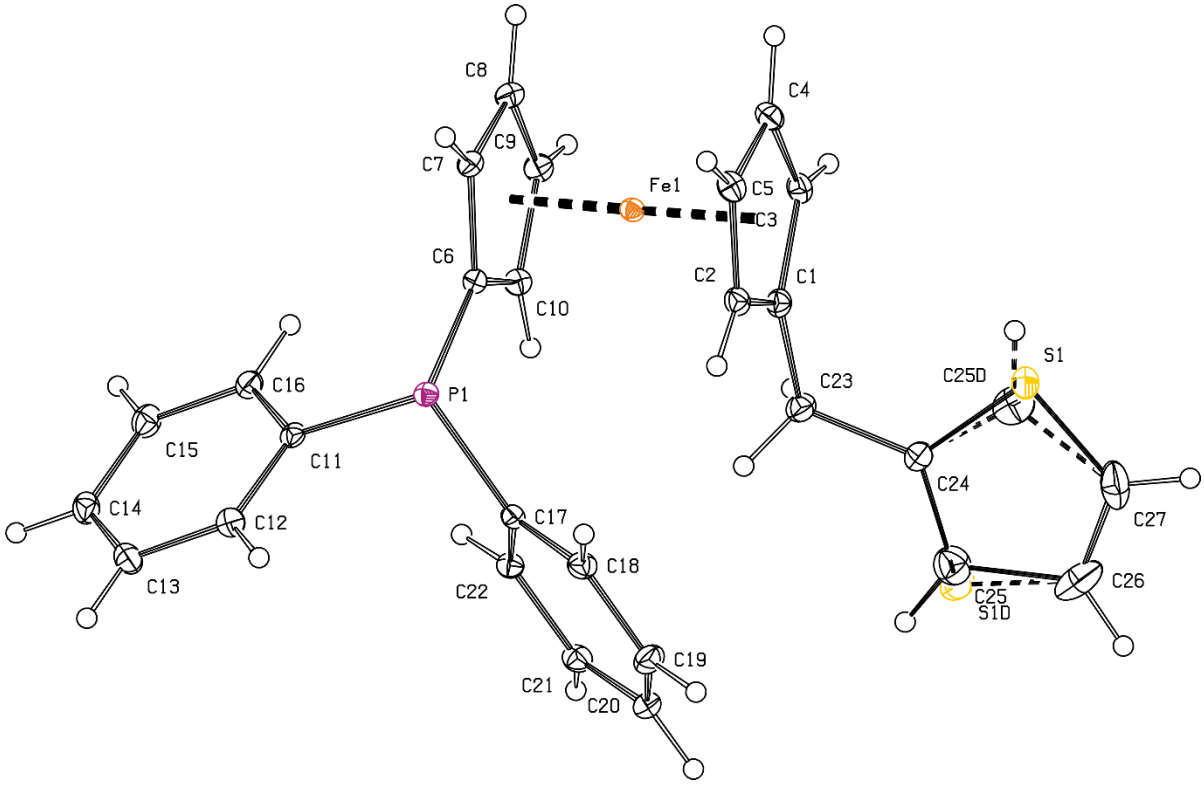

Figure S2. PLATON plot of the molecular structure of **1** (ellipsoids at the 30% probability level).

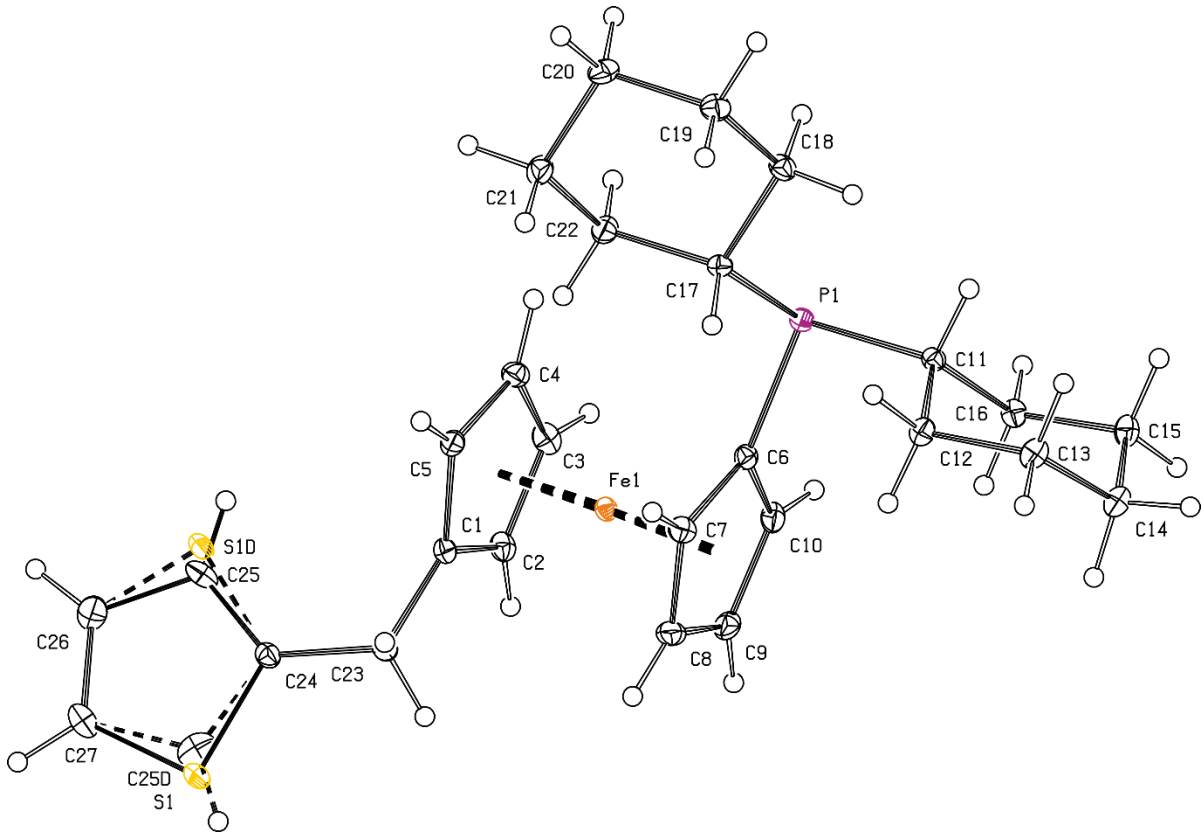

Figure S3. PLATON plot of the molecular structure of **2** (ellipsoids at the 30% probability level).

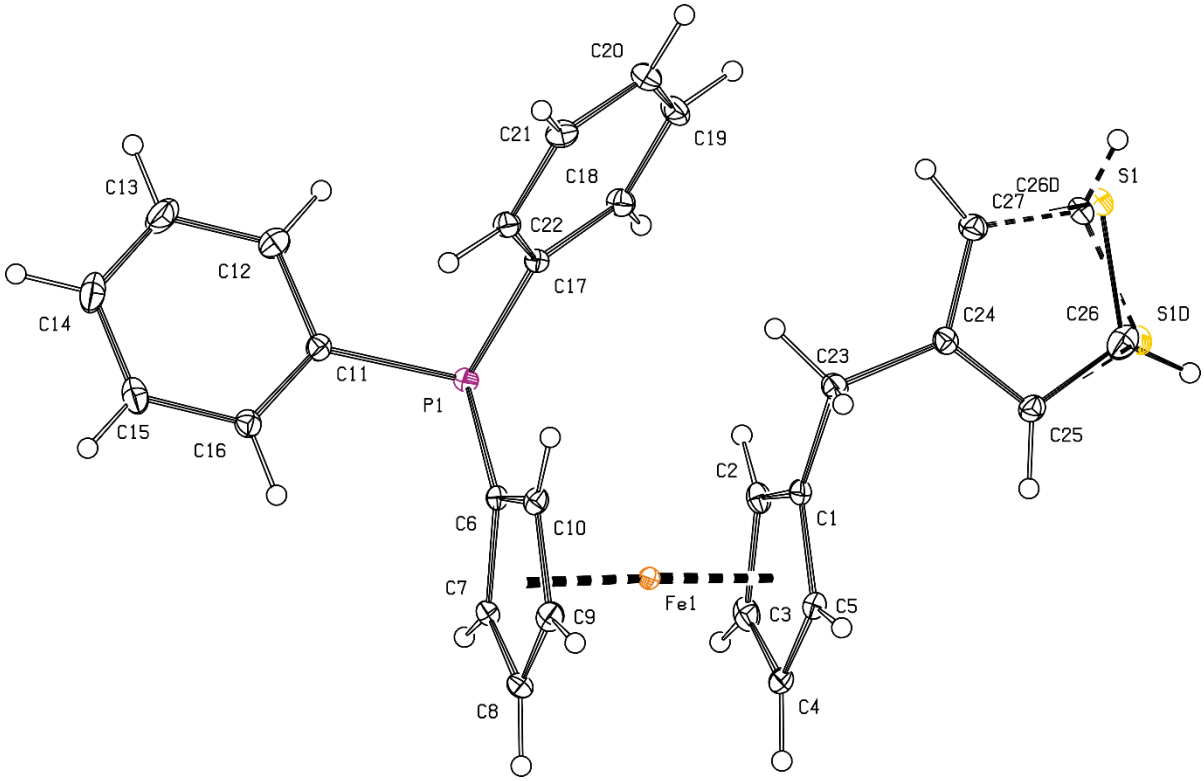

Figure S4. PLATON plot of the molecular structure of **3** (ellipsoids at the 30% probability level).

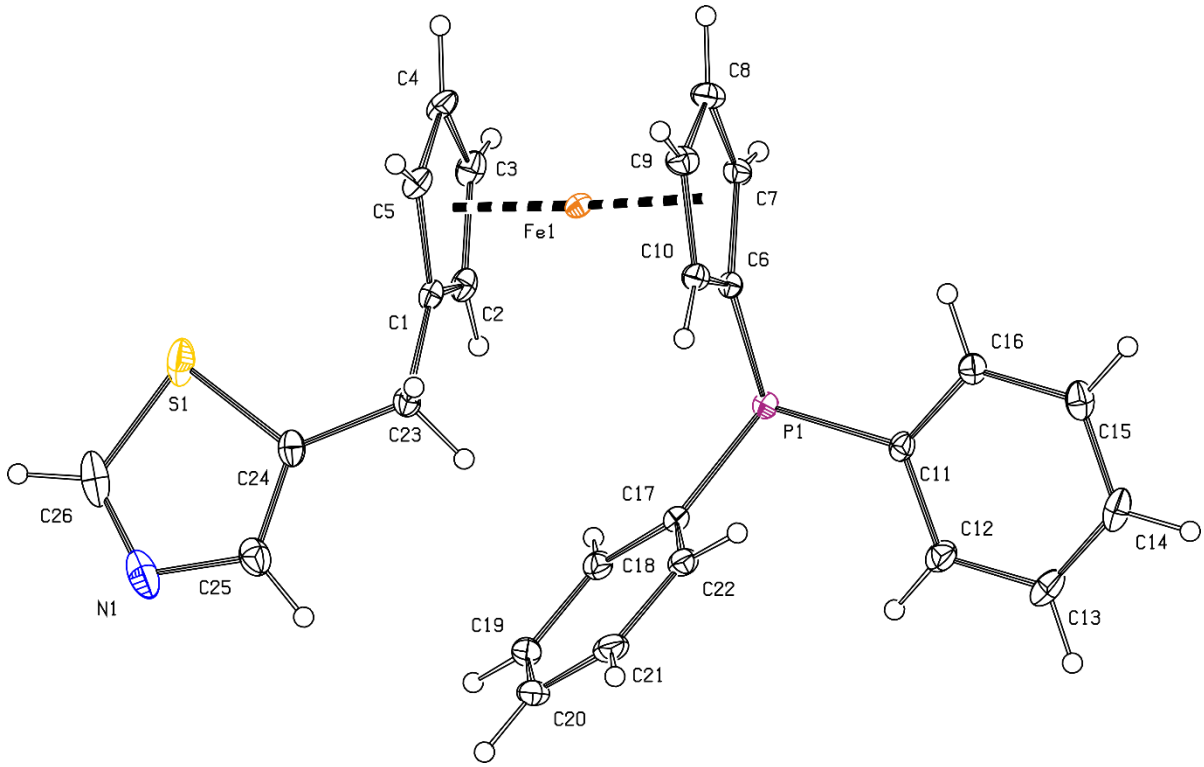

Figure S5. PLATON plot of the molecular structure of **4** (ellipsoids at the 30% probability level).

Table S2. Selected distances and angles for compounds **1**-**4** (in Å and deg).

Parameter[a]	**1**	**2**	**3**	**4**[b]
Fe-C range	2.031(2)-2.057(2)	2.033(1)-2.063(1)	2.031(1)-2.057(1)	2.038(2)-2.054(2)
tilt	0.34(9)	3.39(7)	2.48(7)	2.15(9)
τ	72.3(1)	–141.95(8)	68.56(9)	64.1(1)
P1-C6	1.803(2)	1.819(1)	1.808(1)	1.806(1)
P1-C11	1.835(2)	1.869(1)	1.838(1)	1.836(2)
P1-C17	1.832(2)	1.864(1)	1.834(1)	1.830(1)
C6-P1-C11	101.57(7)	99.35(5)	101.60(5)	101.22(7)
C6-P1-C17	104.36(7)	104.76(5)	103.06(5)	104.63(6)
C11-P1-C17	98.79(7)	101.43(5)	99.12(5)	100.48(6)
C1-C23	1.507(2)	1.498(2)	1.504(2)	1.499(2)
C23-C24	1.514(2)	1.507(2)	1.517(2)	1.503(2)
C1-C23-C24	112.9(1)	112.3(1)	110.8(1)	113.1(1)
C2-C1-C23-C24	–86.8(2)	–86.2(1)	–72.3(2)	–79.3(2)

[a] Tilt is the dihedral angle of the least-squares cyclopentadienyl planes C(1-5) and C(6-10); Cg1 and Cg2 denote the respective ring centroids. τ is the torsion angle C1-Cg1-Cg2-C6. [b] Further data: S1-C24 1.719(2), S1-C26 1.721(2), N1-C25 1.378(2), N1-C26 1.300(3), C24-C25 1.363(2), C24-S1-C26 89.2(1), S1-C26-N1 115.7(2), C26-N1-C25 109.7(2), N1-C25-C24 116.0(2), C25-C24-S1 109.4(1).

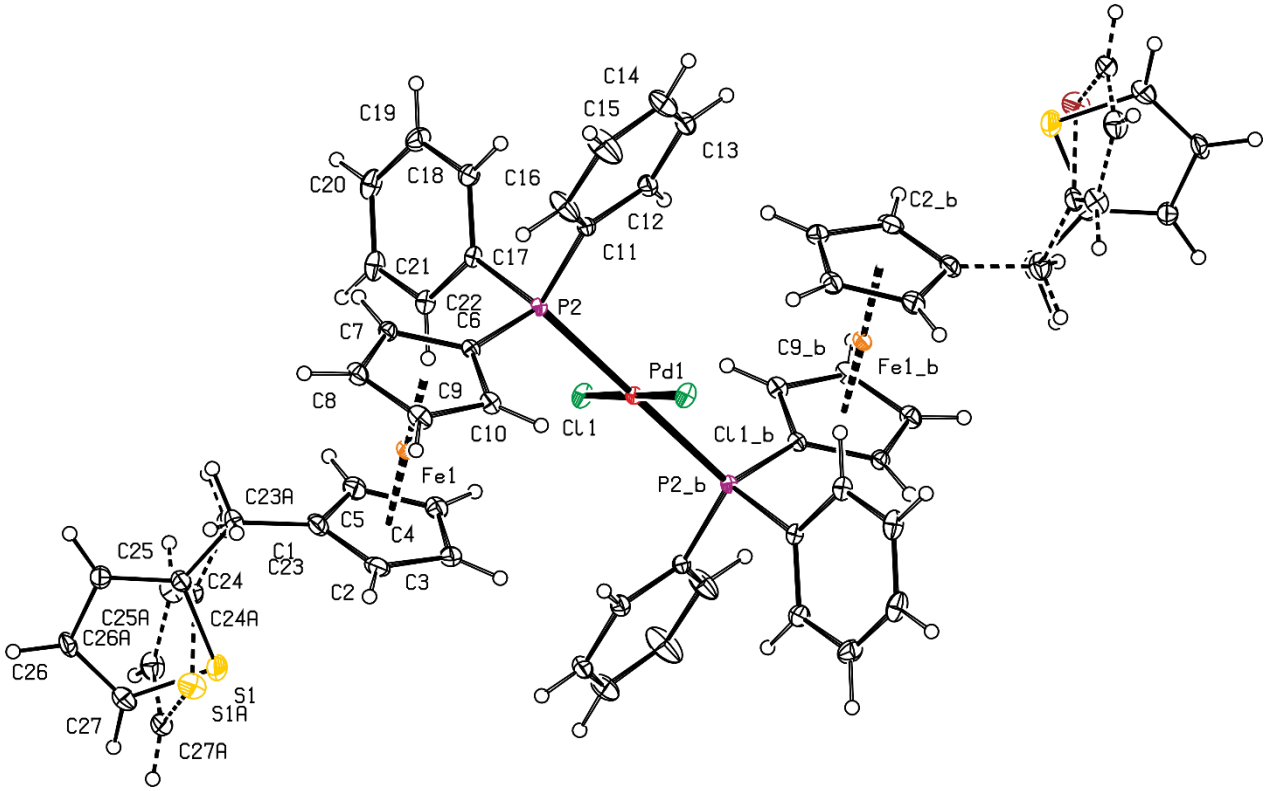

Figure S6. PLATON plot of the molecular structure of **25** (ellipsoids at the 30% probability level).

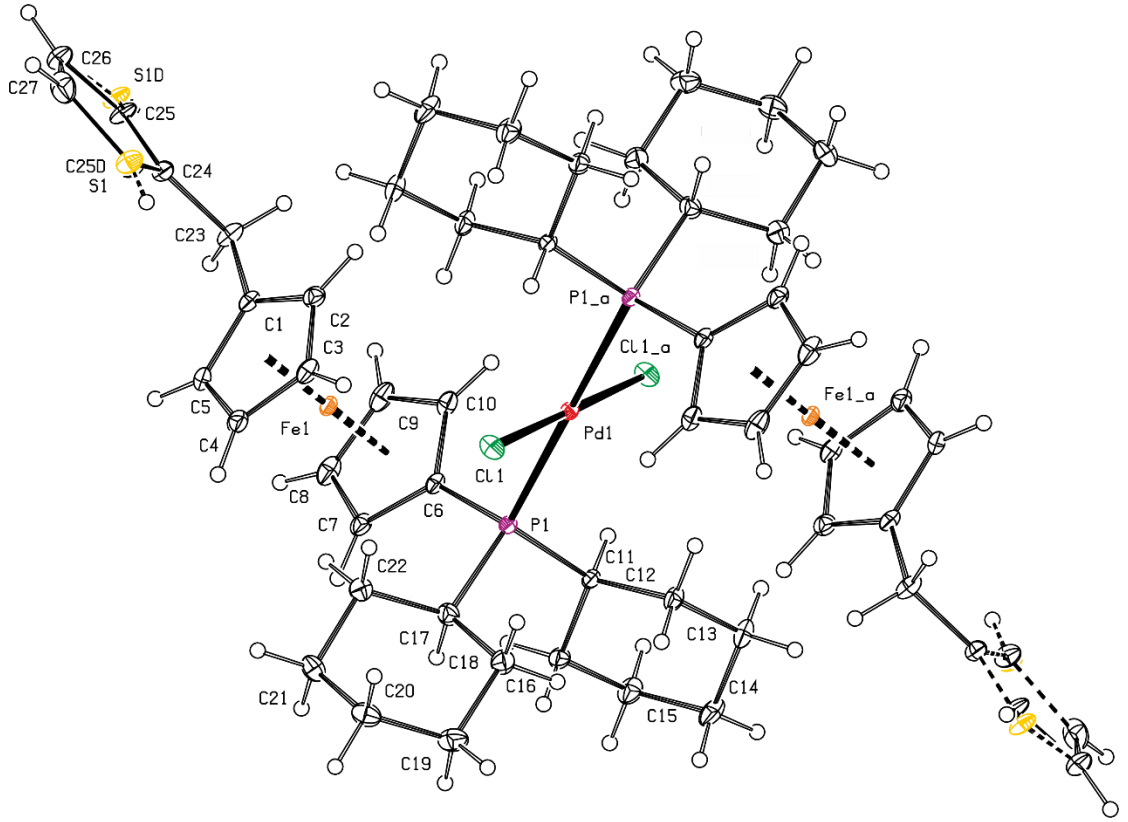

Figure S7. PLATON plot of the molecular structure of **26** (ellipsoids at the 30% probability level).

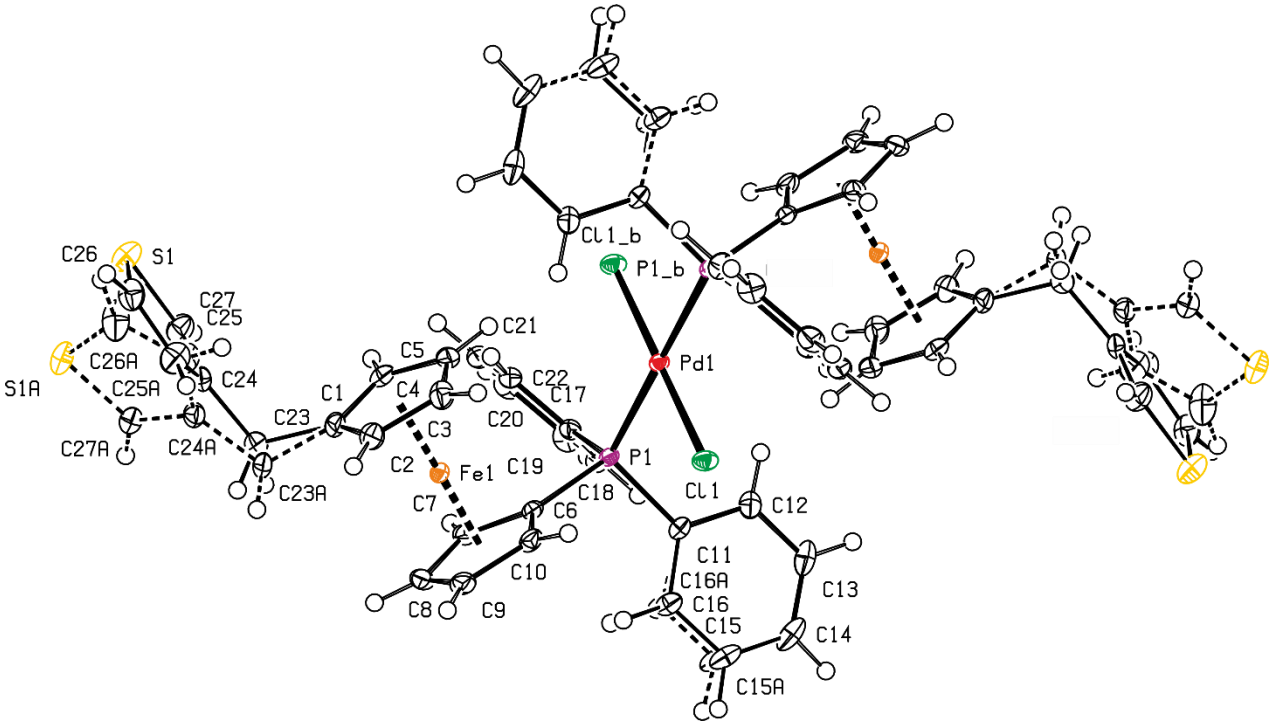

Figure S8. PLATON plot of the molecular structure of **27** (ellipsoids at the 30% probability level).

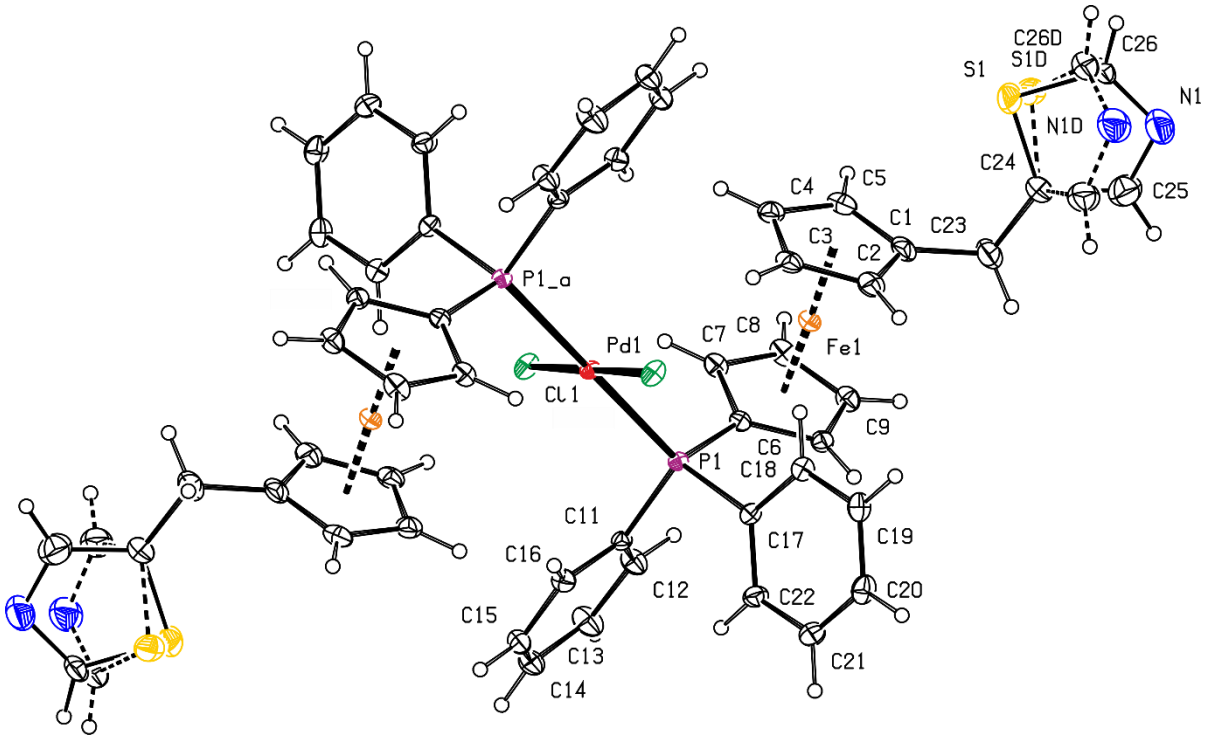

Figure S9. PLATON plot of the molecular structure of **29** (ellipsoids at the 30% probability level).

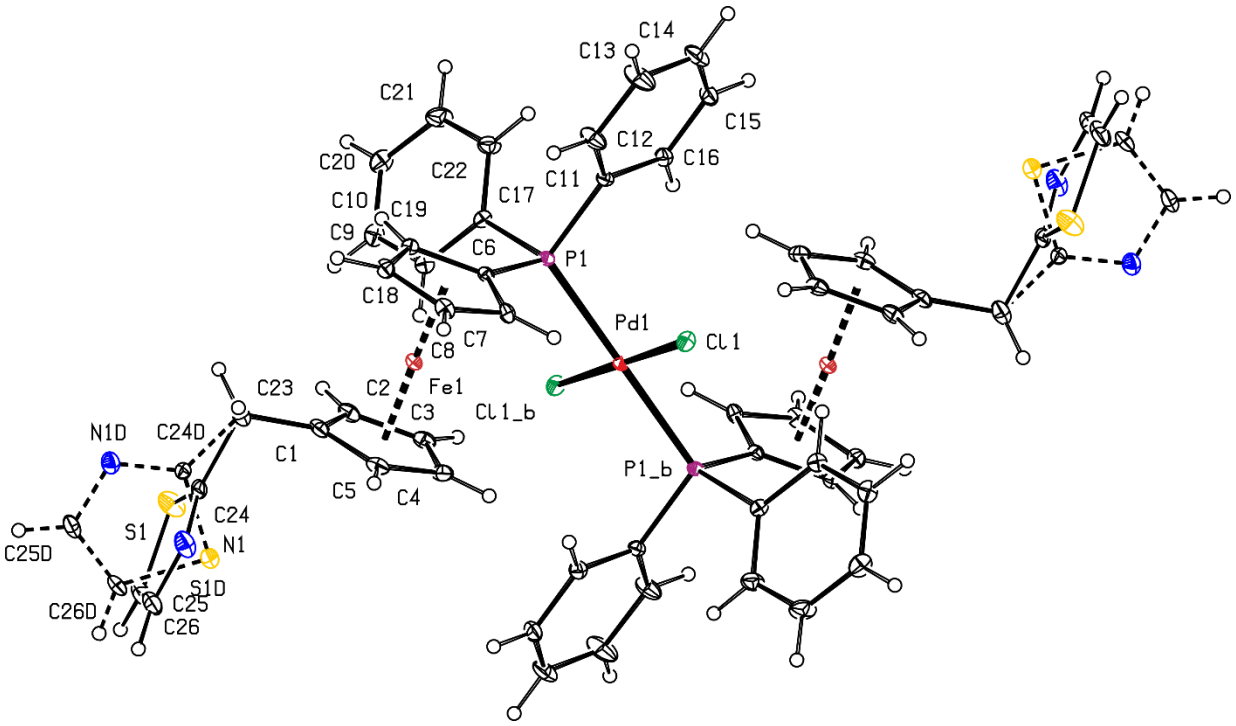

Figure S10. PLATON plot of the molecular structure of **30** (ellipsoids at the 30% probability level).

Table S3. Selected distances and angles for compounds **25-27**, **29**, and **30** (in Å and deg).

Parameter[a]	**25**	**26**	**27**	**29**	**30**
Pd1-Cl1	2.3061(5)	2.3058(3)	2.3076(3)	2.3058(6)	2.3051(3)
Pd1-P1	2.3472(4)	2.3570(3)	2.3469(3)	2.3458(6)	2.3454(4)
Cl1-Pd1-P1[b]	93.77(1)	91.86(1)	93.78(1)	94.23(2)	93.47(1)
Fe-C range	2.032(2)-2.053(2)	2.035(2)-2.057(2)	2.035(1)-2.055(1)	2.033(2)-2.051(2)	2.035(2)-2.051(2)
tilt	3.9(1)	4.21(9)	3.40(7)	3.9(2)	3.5(1)
τ	−139.3(1)	150.6(1)	138.3(1)	138.3(2)	−140.2(1)
P1-C6	1.796(2)	1.809(2)	1.795(1)	1.793(2)	1.799(2)
P1-C11	1.820(2)	1.856(1)	1.819(1)	1.815(2)	1.816(2)
P1-C17	1.827(2)	1.862(2)	1.824(1)	1.824(2)	1.823(2)
C6-P1-C11	104.50(7)	102.08(7)	104.20(5)	104.7(1)	104.76(7)
C6-P1-C17	102.61(8)	104.88(7)	102.38(5)	102.2(1)	103.04(7)
C11-P1-C17	104.21(8)	104.55(6)	104.04(5)	104.1(1)	103.70(7)

[a] Tilt is the dihedral angle of the least-squares cyclopentadienyl planes C(1-5) and C(6-10), Cg1 and denote the respective ring centroids. τ is the torsion angle C1-Cg1-Cg2-C6. Geometric parameters of the heterocyclic substituents are affected by disorder. [b] Because of the imposed inversion symmetry, two adjacent P-Pd-Cl angles always sum up to exactly 180°.

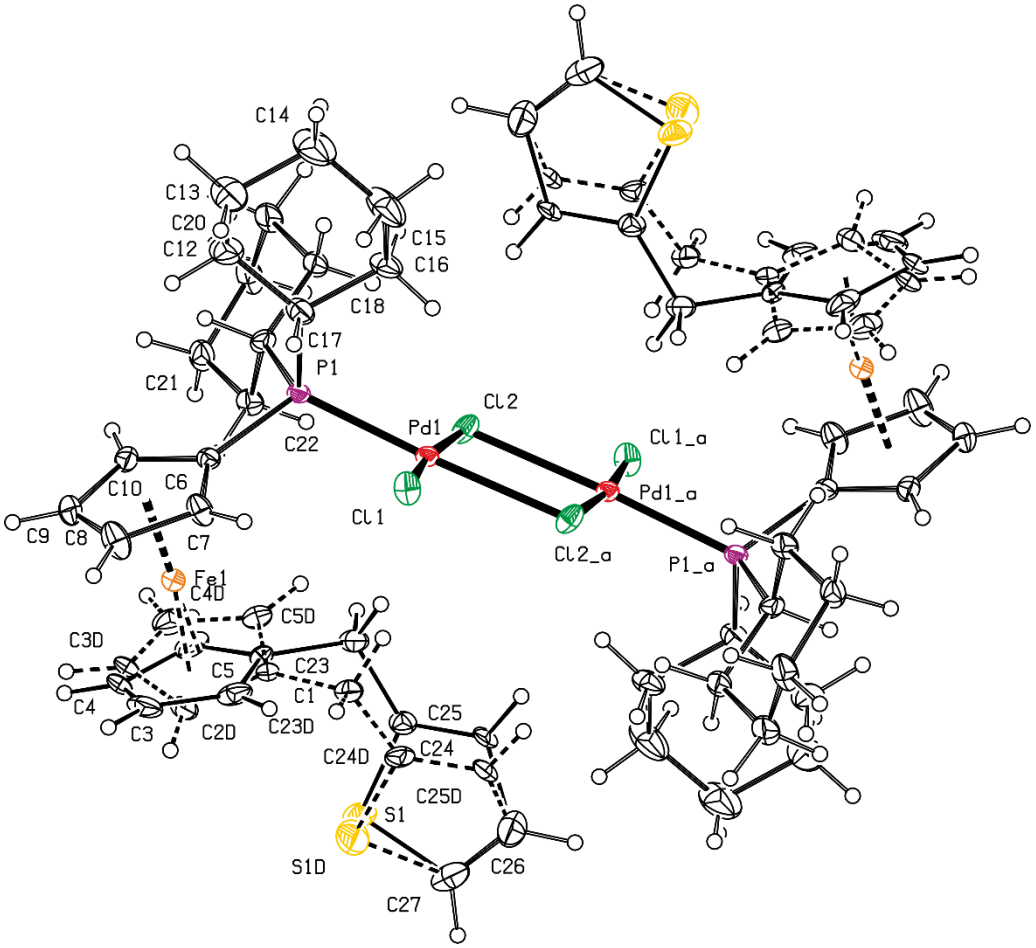

Figure S11. PLATON plot of the structure of complex **28** (ellipsoids at the 30% probability level).

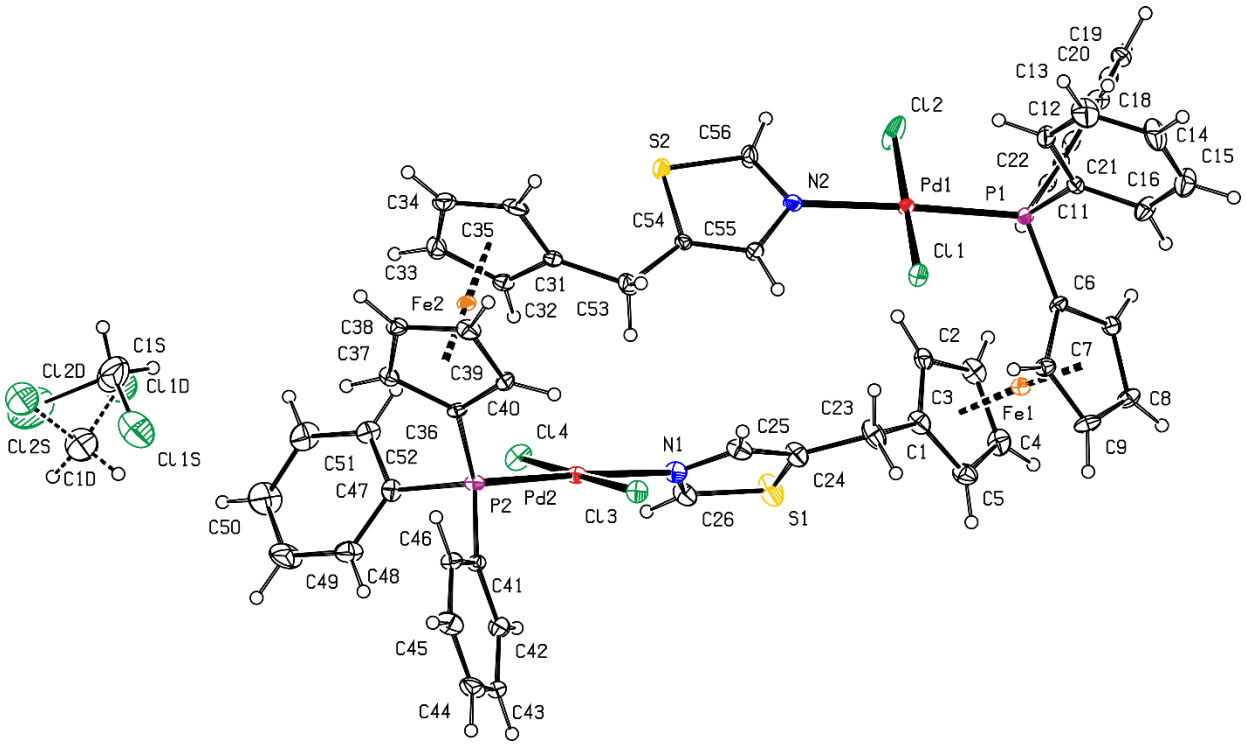

Figure S12. PLATON plot of the structure of **31**·CH_2Cl_2 (ellipsoids at the 30% probability level).

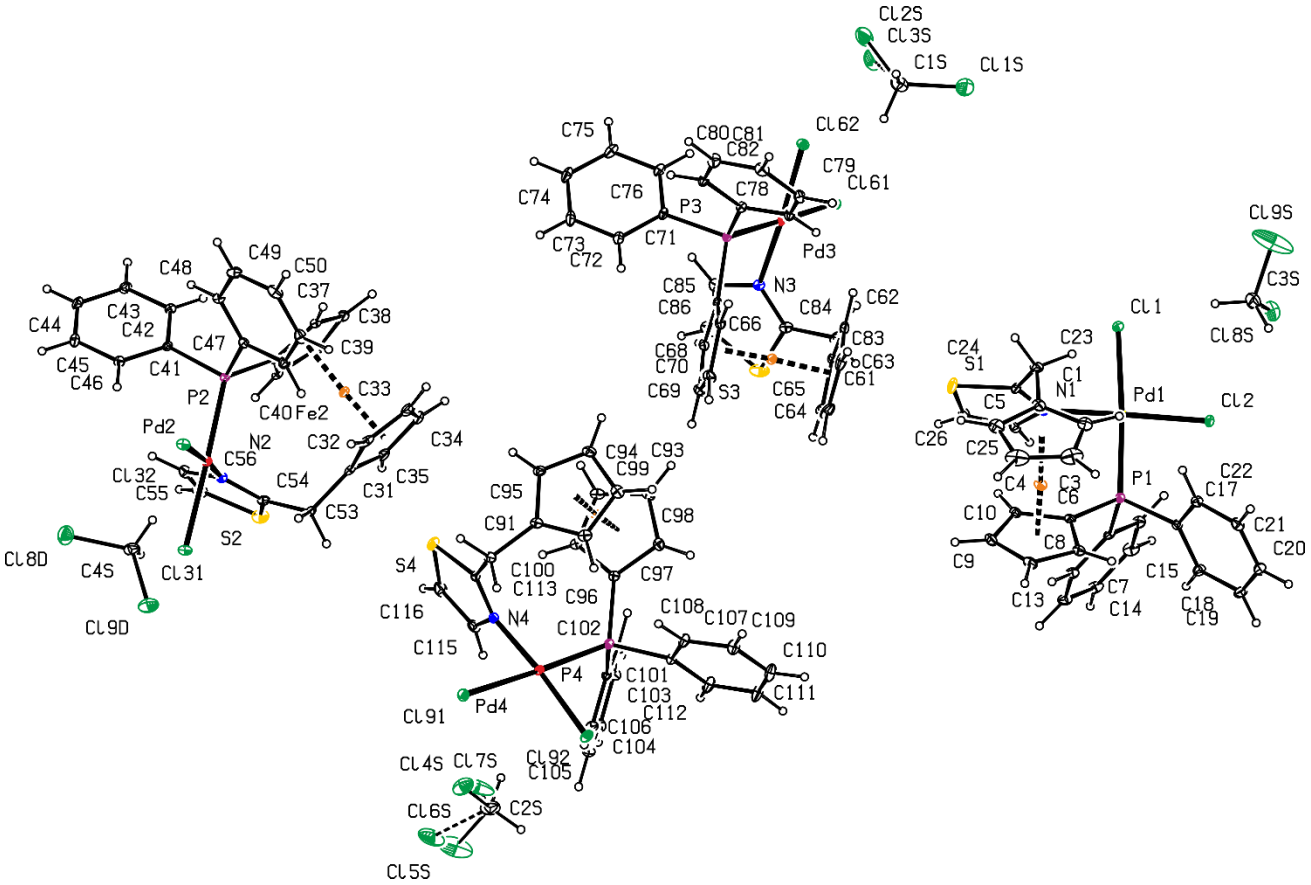

Figure S13. PLATON plot of the structure of **32**·CH_2Cl_2 (ellipsoids at the 30% probability level).

Table S4. Selected distances and angles for **32**·CH_2Cl_2 (in Å and deg).

Parameter[a]	molecule 1	molecule 2	molecule 3	molecule 4
Pd1-Cl1	2.3977(8)	2.3783(8)	2.3715(7)	2.3767(6)
Pd1-Cl2	2.2915(7)	2.2830(7)	2.2805(8)	2.2817(8)
Pd-P1	2.2421(8)	2.2498(8)	2.2532(7)	2.2490(6)
Pd-N1	2.024(2)	2.026(2)	2.032(2)	2.021(2)
Cl1-Pd1-Cl2	94.36(2)	92.28(2)	92.16(2)	93.15(2)
Cl1-Pd1-N1	85.17(5)	86.13(5)	85.84(5)	85.45(5)
Cl2-Pd1-P1	88.86(3)	89.06(3)	88.99(3)	89.73(3)
P1-Pd1-N1	91.31(5)	92.38(5)	92.83(5)	91.67(5)
Fe-C range	2.028(3)-2.055(2)	2.036(2)-2.058(3)	2.031(2)-2.048(2)	2.042(2)-2.062(2)
tilt	3.7(2)	2.0(2)	2.8(1)	2.8(1)
τ	48.4(2)(2)	46.9(2)	−54.7(2)	−49.8(2)
ψ	64.1(2)	62.6(1)	60.5(1)	63.9(1)
P1-C6	1.793(2)	1.797(2)	1.795(2)	1.800(2)
P1-C11	1.811(2)	1.816(2)	1.814(2)	1.820(2)
P1-C17	1.815(2)	1.813(2)	1.814(2)	1.814(2)
C6-P1-C11	104.6(1)	103.7(1)	104.5(1)	104.8(1)
C6-P1-C17	102.0(1)	103.2(1)	101.5(1)	102.3(1)
C11-P1-C17	106.6(1)	107.6(1)	106.0(1)	106.6(1)
C1-C23-C24	115.3(2)	115.2(2)	116.3(2)	114.4(2)
C2-C1-C23-C24	113.6(3)	117.5(2)	−107.5(3)	−113.1(3)

[a] The numbering of atoms in the four crystallographically independent molecules is strictly analogous. Tilt is the dihedral angle of the least-squares cyclopentadienyl planes C(1-5) and C(6-10), Cg1 and denote the respective ring centroids. τ is the torsion angle C1-Cg1-Cg2-C6 and ψ is the dihedral angle between the cyclopentadienyl plane C(1-5) and the thiazole ring.

Copies of the NMR spectra

(Note: solvent signals in the NMR spectra are marked by an asterisk.)

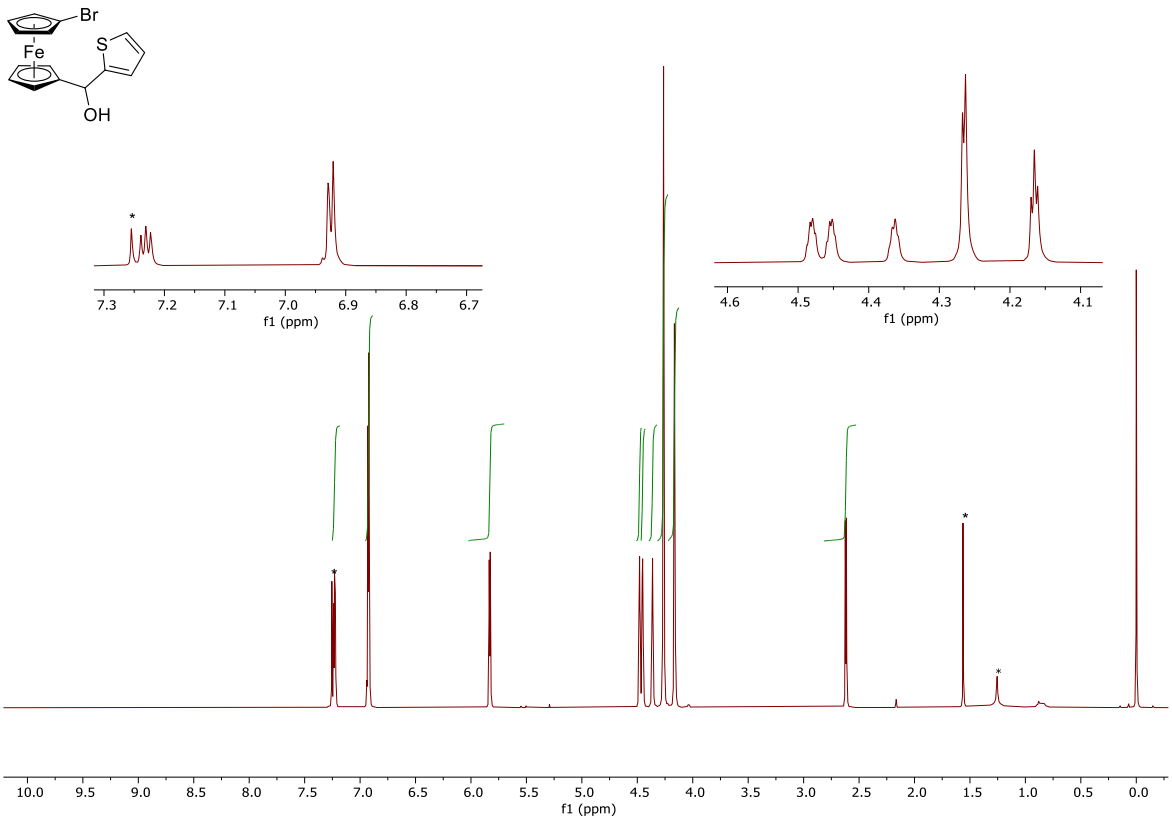

Figure S14. ^{1}H NMR spectrum (400 MHz, $CDCl_3$) of **9**.

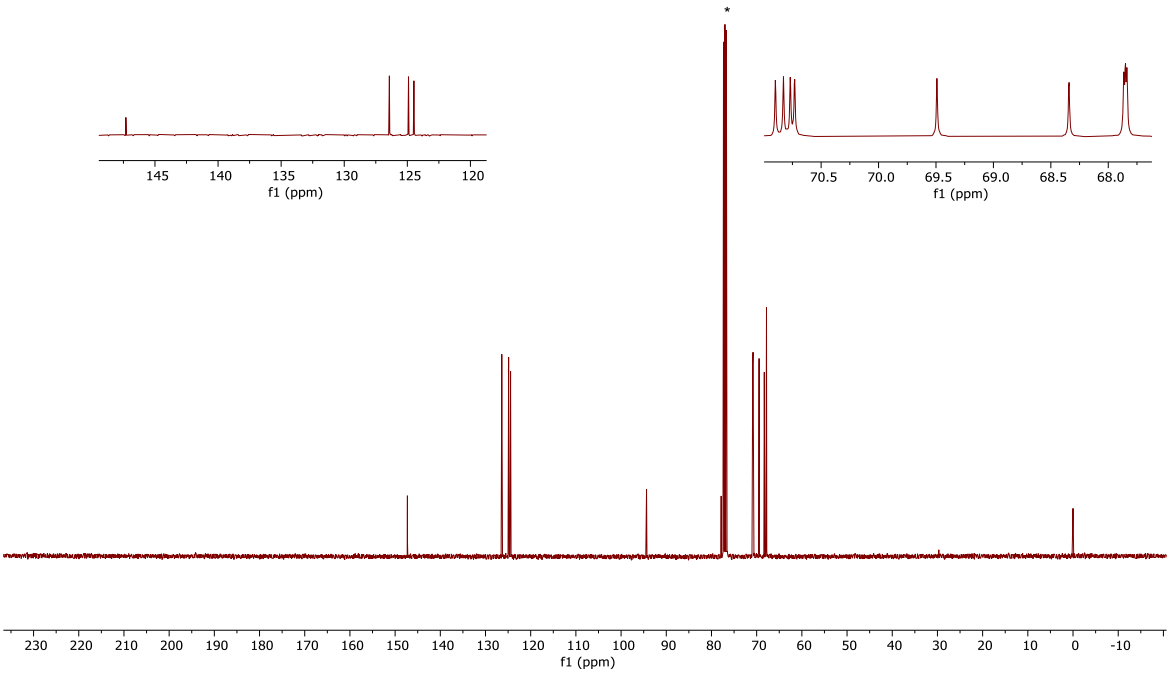

Figure S15. $^{13}C\{^{1}H\}$ NMR spectrum (101 MHz, $CDCl_3$) of **9.**

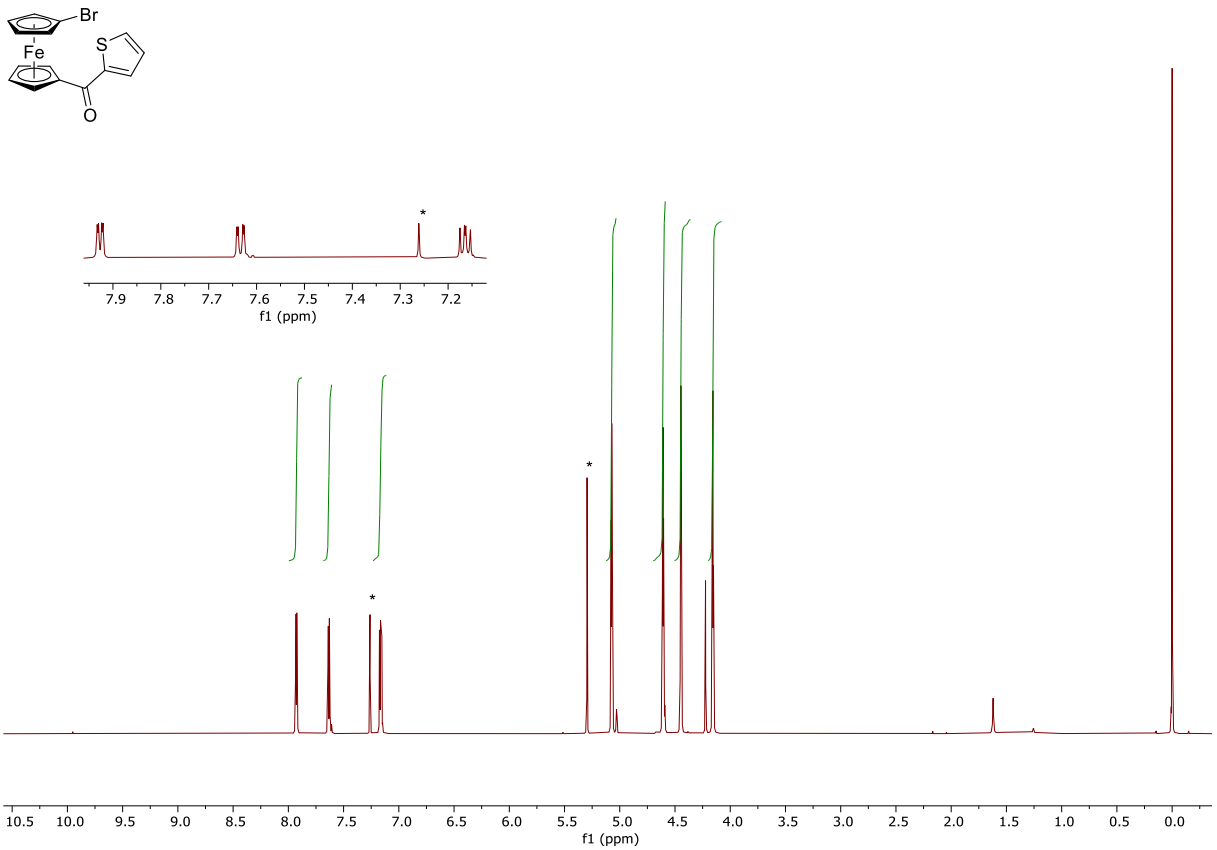

Figure S16. ^{1}H NMR spectrum (400 MHz, $CDCl_3$) of **10**.

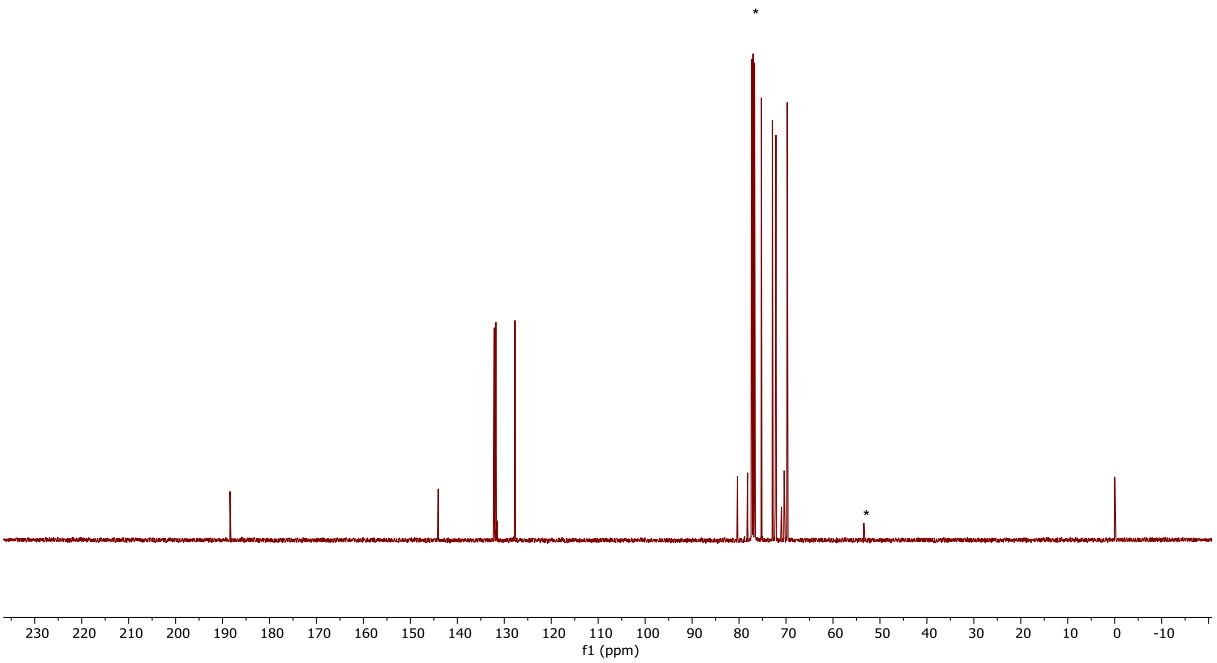

Figure S17. $^{13}C\{^{1}H\}$ NMR spectrum (101 MHz, $CDCl_3$) of **10**.

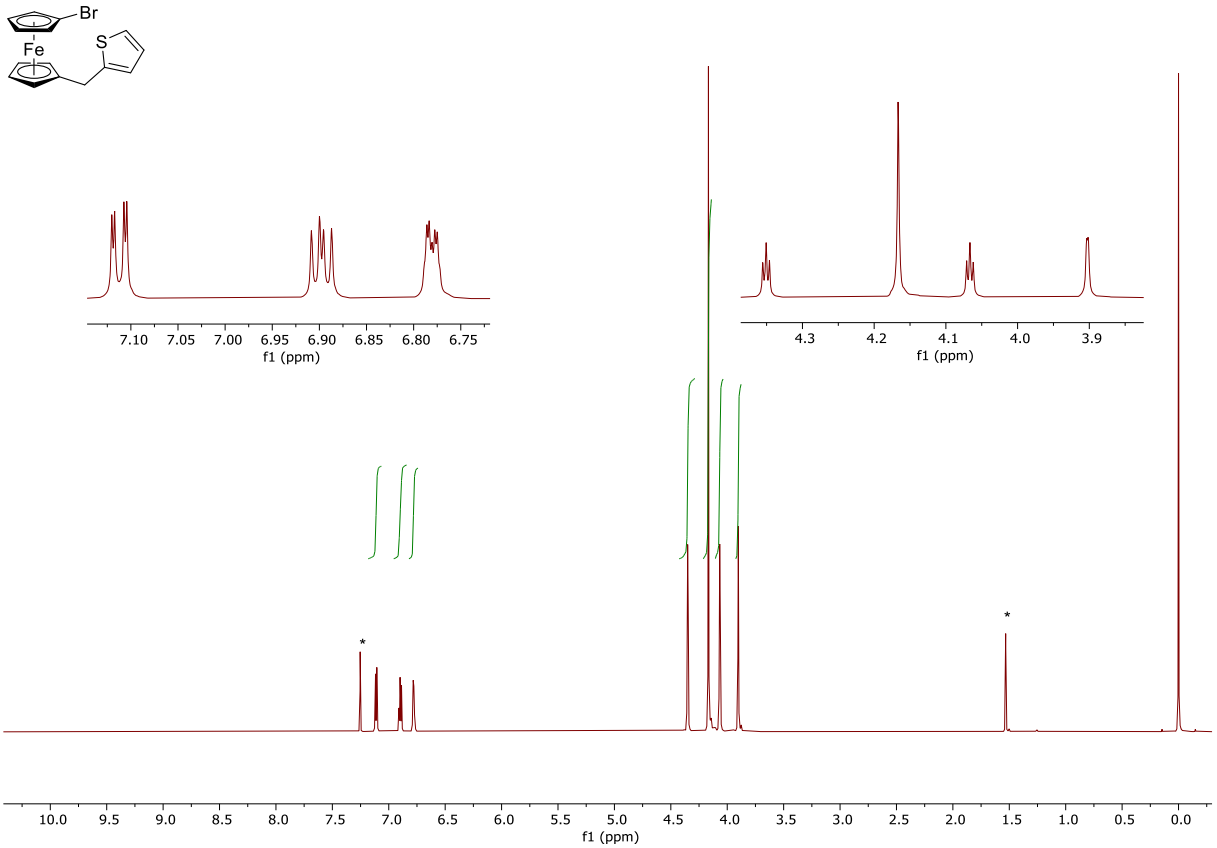

Figure S18. ^{1}H NMR spectrum (400 MHz, $CDCl_3$) of **11**.

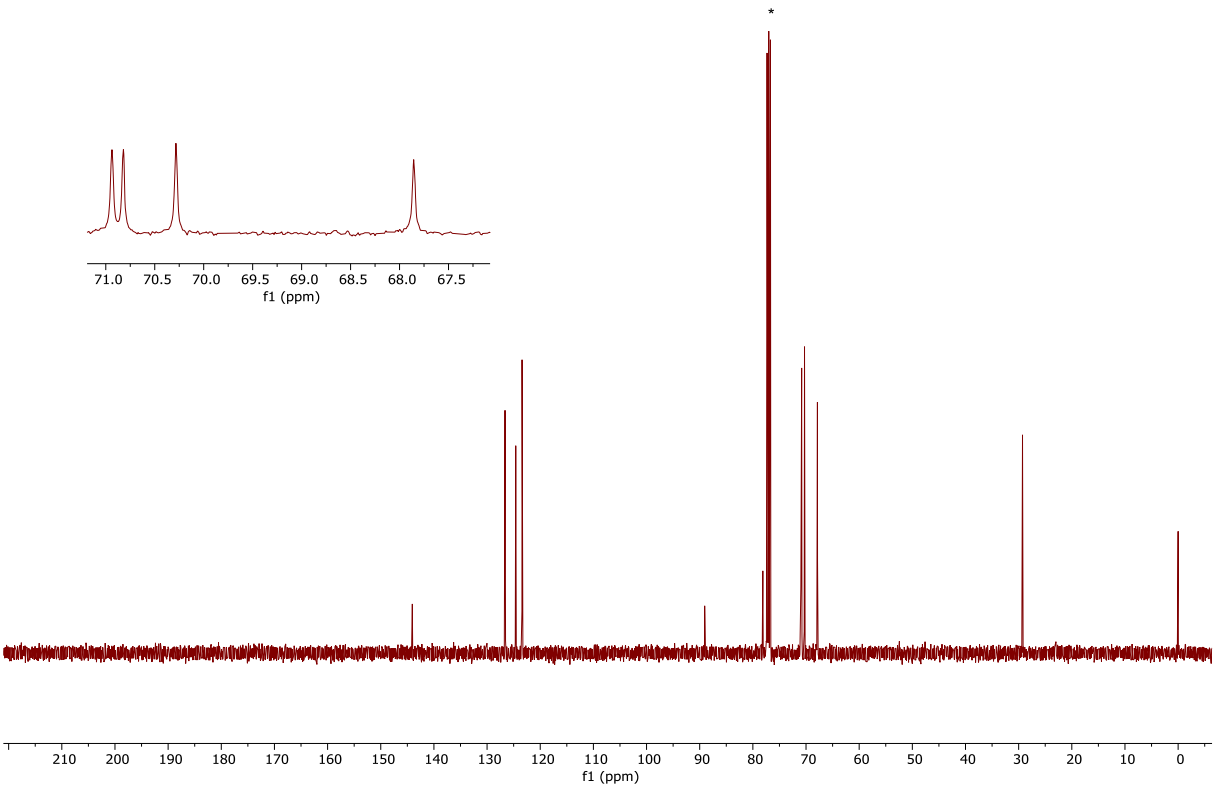

Figure S19. $^{13}C\{^{1}H\}$ NMR spectrum (101 MHz, $CDCl_3$) of **11**.

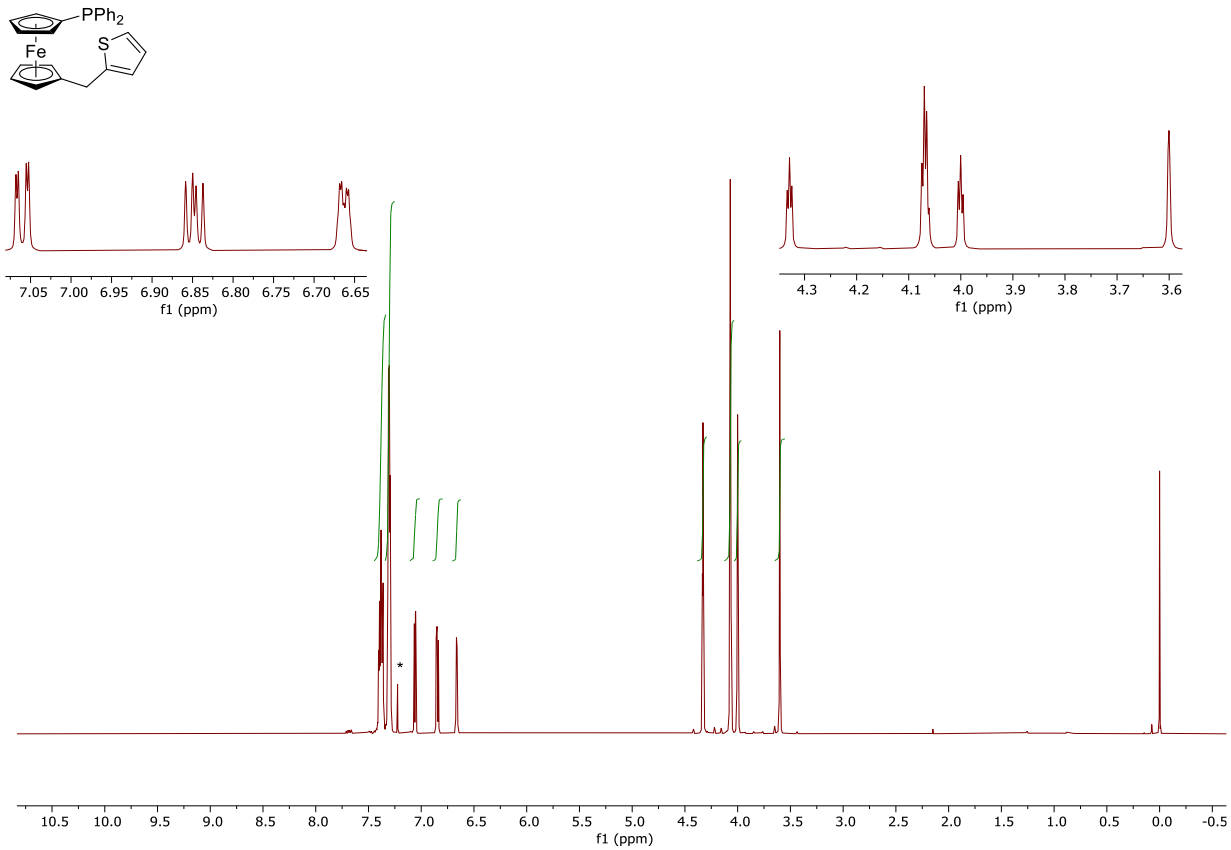

Figure S20. ^{1}H NMR spectrum (400 MHz, $CDCl_3$) of **1**.

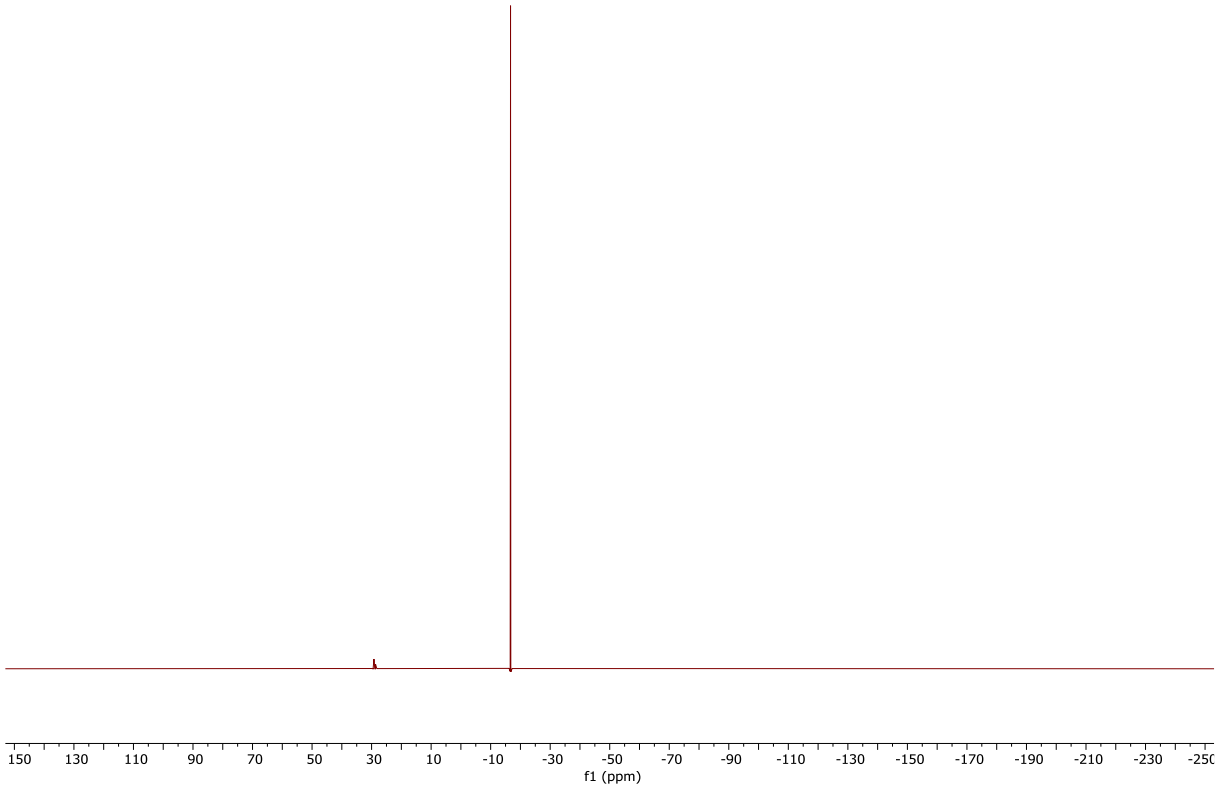

Figure S21. $^{31}P\{^{1}H\}$ NMR spectrum (162 MHz, $CDCl_3$) of **1**.

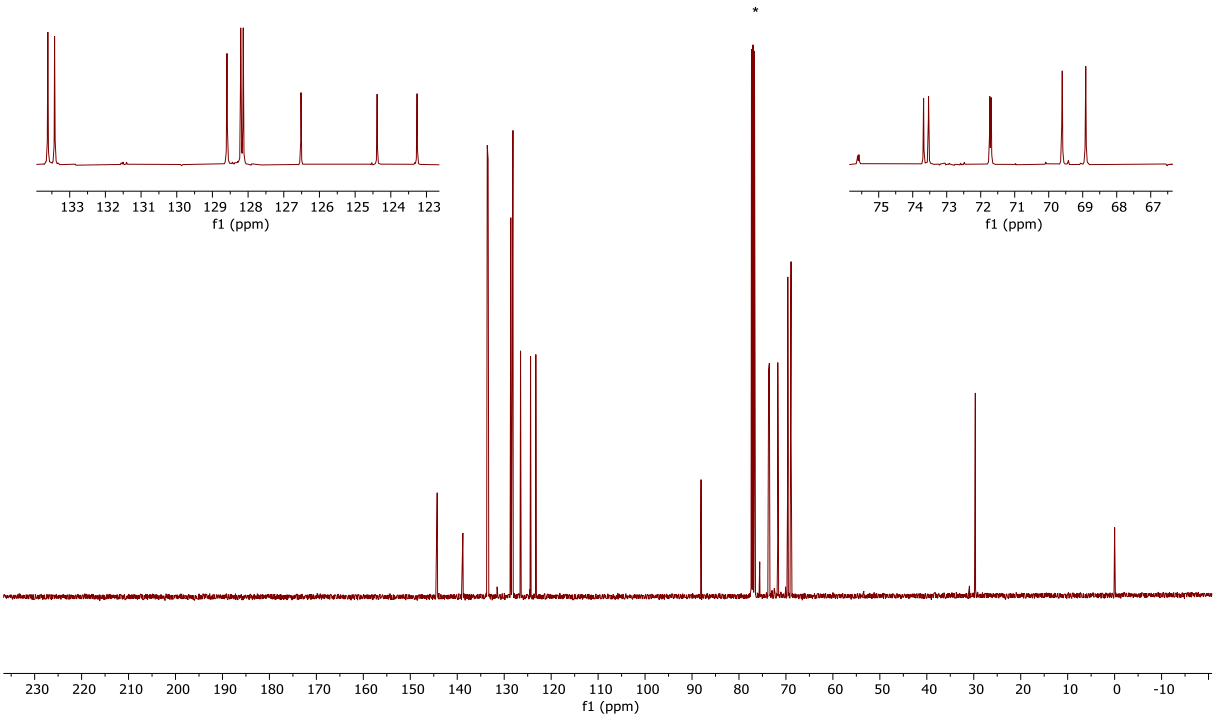

Figure S22. $^{13}C\{^{1}H\}$ NMR spectrum (101 MHz, $CDCl_3$) of **1**.

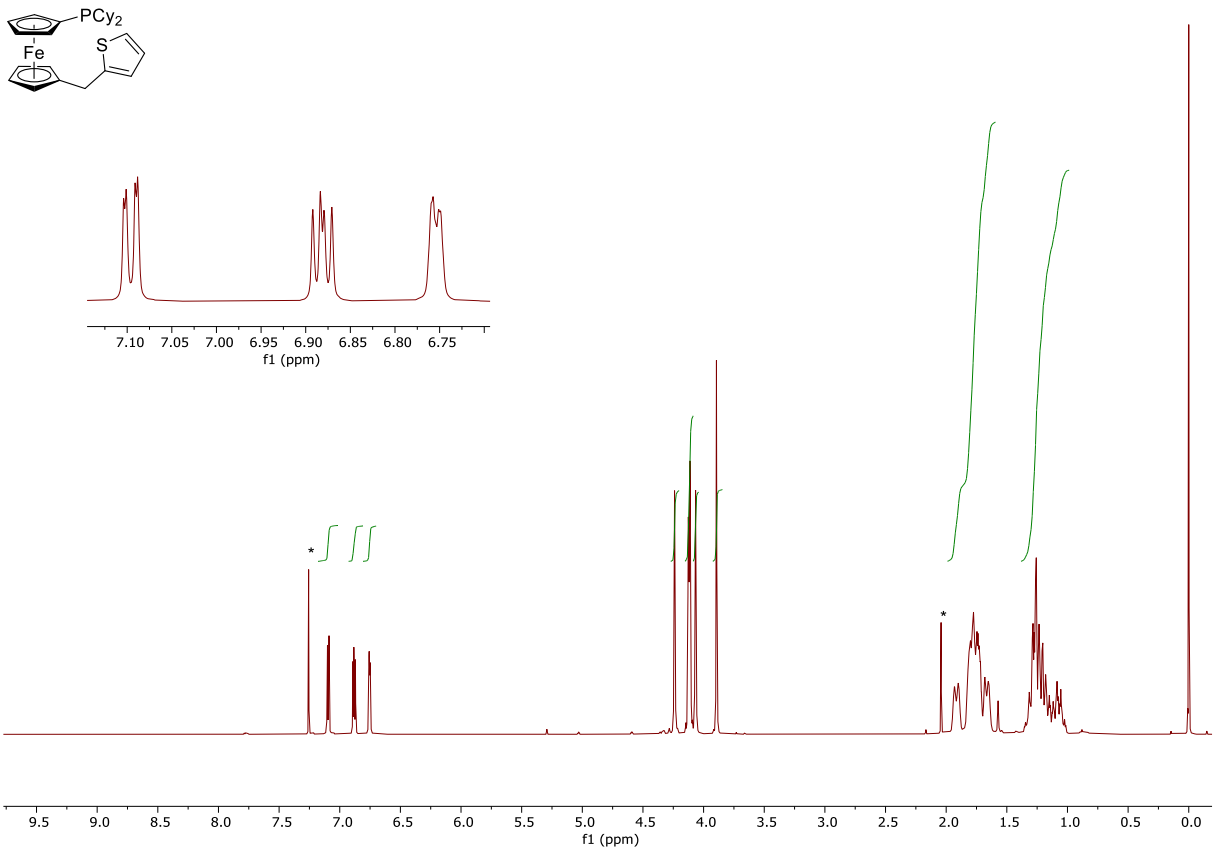

Figure S23. ^{1}H NMR spectrum (400 MHz, $CDCl_3$) of **2**.

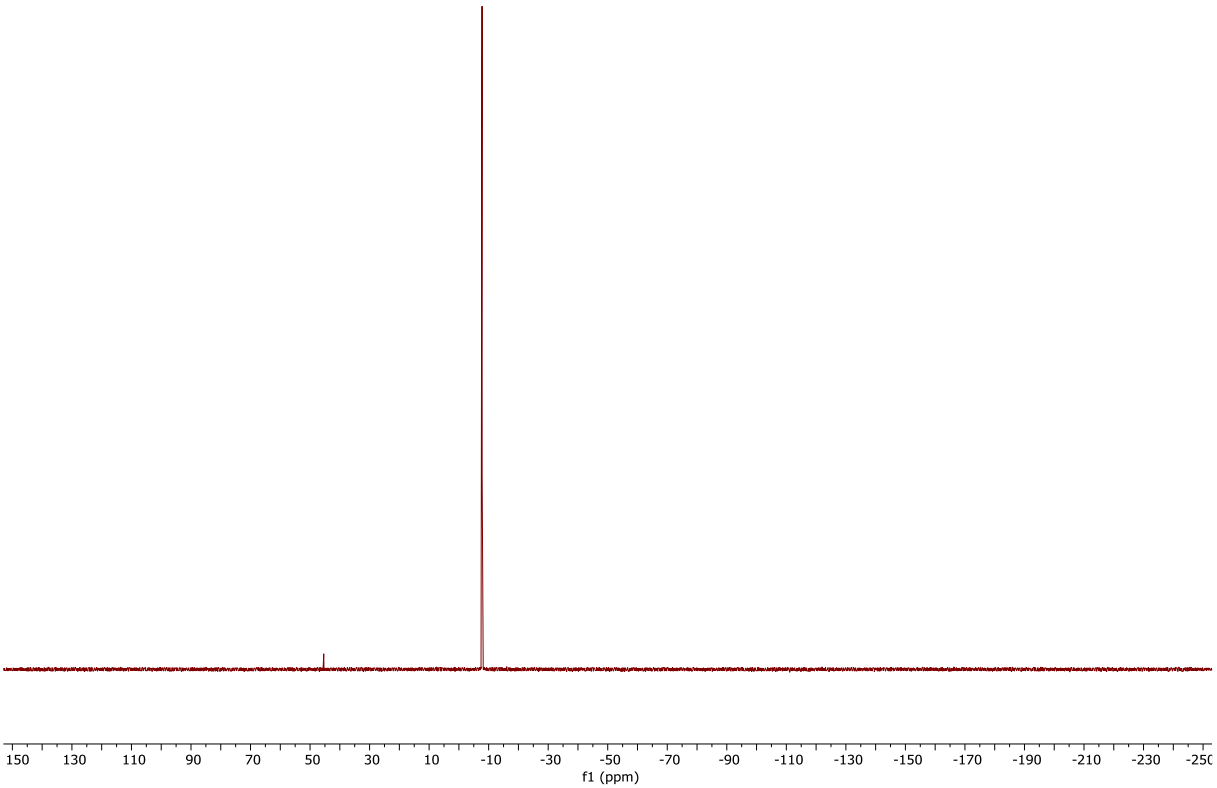

Figure S24. $^{31}P\{^{1}H\}$ NMR spectrum (162 MHz, $CDCl_3$) of **2**.

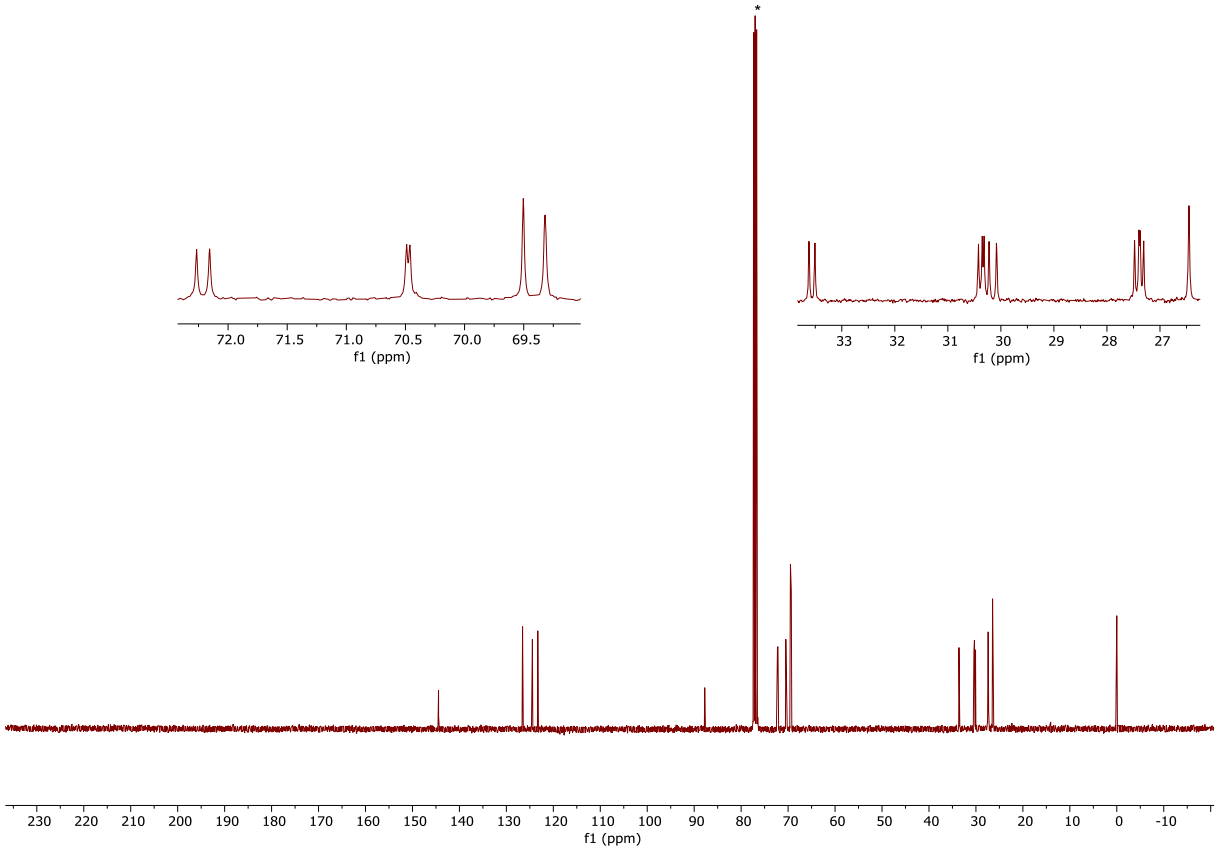

Figure S25. $^{13}C\{^{1}H\}$ NMR spectrum (101 MHz, $CDCl_3$) of **2**.

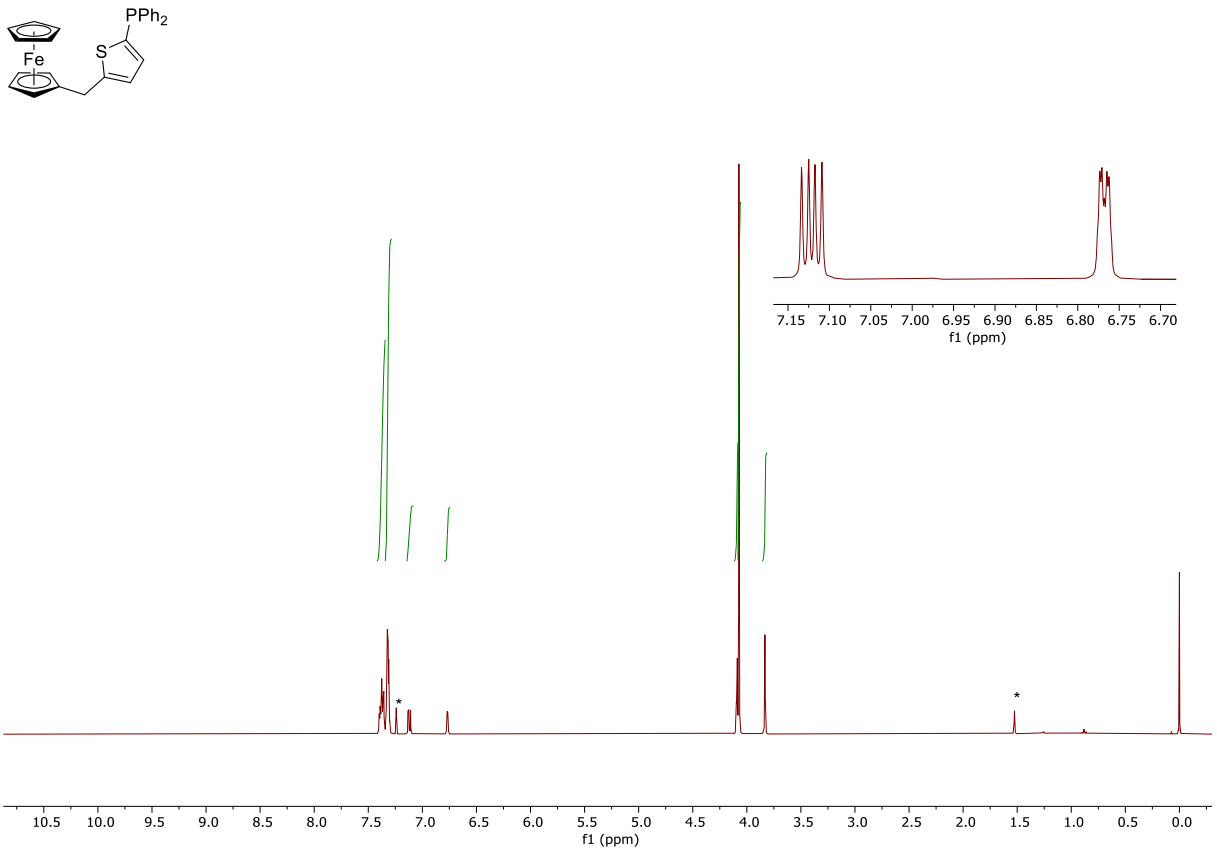

Figure S26. ^{1}H NMR spectrum (400 MHz, $CDCl_3$) of **13**.

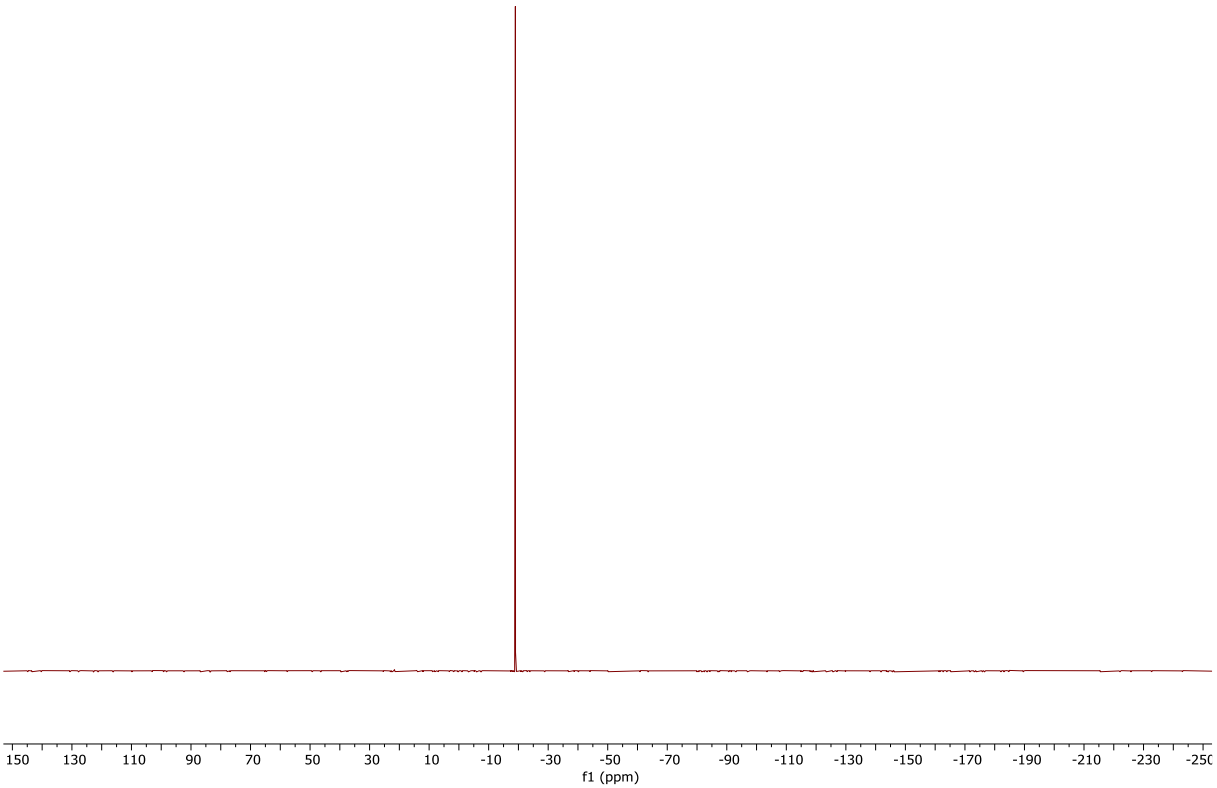

Figure S27. $^{31}P\{^{1}H\}$ NMR spectrum (162 MHz, $CDCl_3$) of **13**.

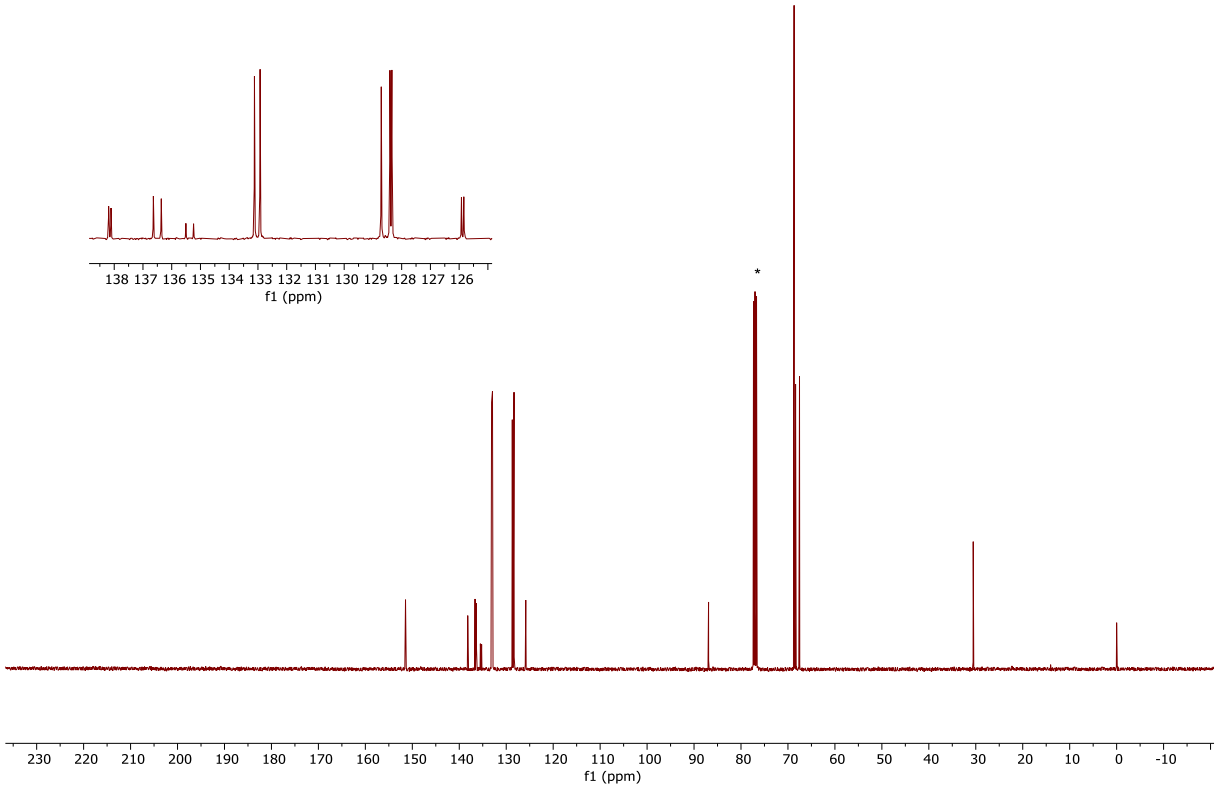

Figure S28. $^{13}C\{^{1}H\}$ NMR spectrum (101 MHz, $CDCl_3$) of **13**.

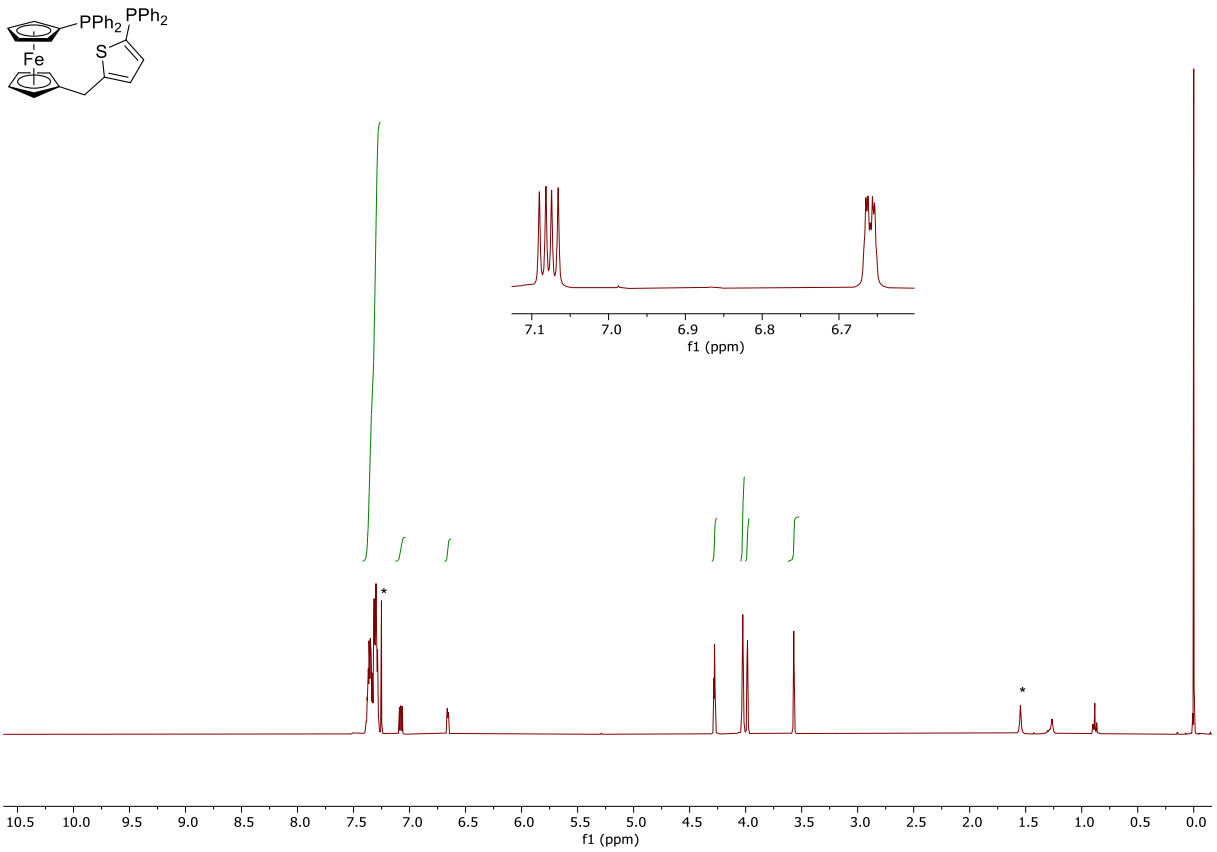

Figure S29. ^{1}H NMR spectrum (400 MHz, $CDCl_3$) of **14**.

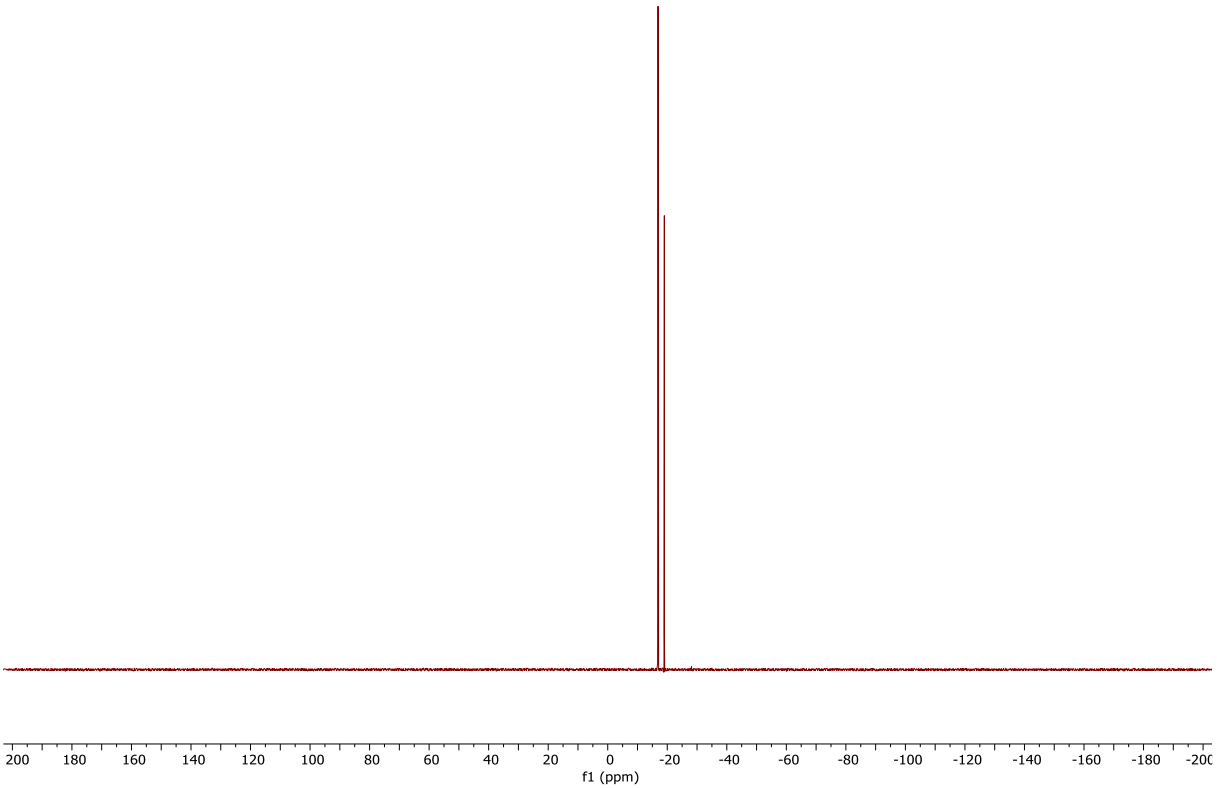

Figure S30. $^{31}P\{^{1}H\}$ NMR spectrum (162 MHz, $CDCl_3$) of **14**.

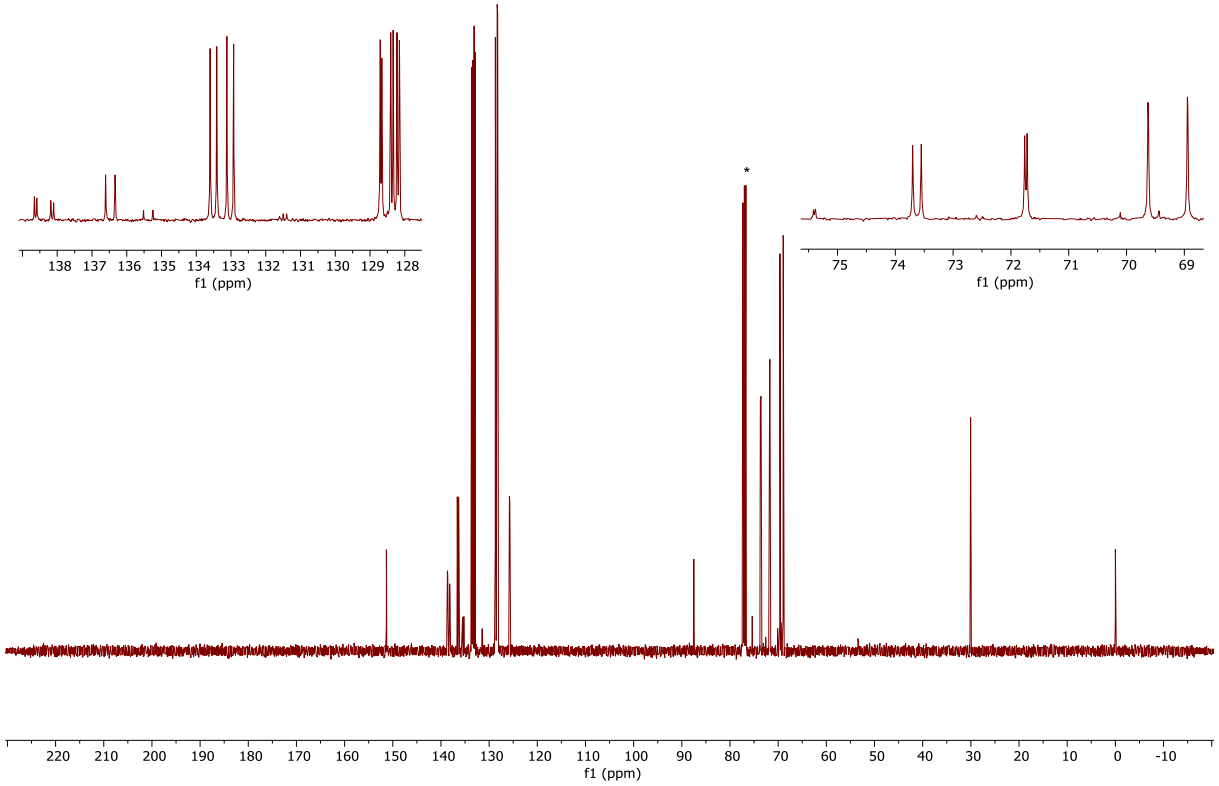

Figure S31. $^{13}C\{^{1}H\}$ NMR spectrum (101 MHz, $CDCl_3$) of **14**.

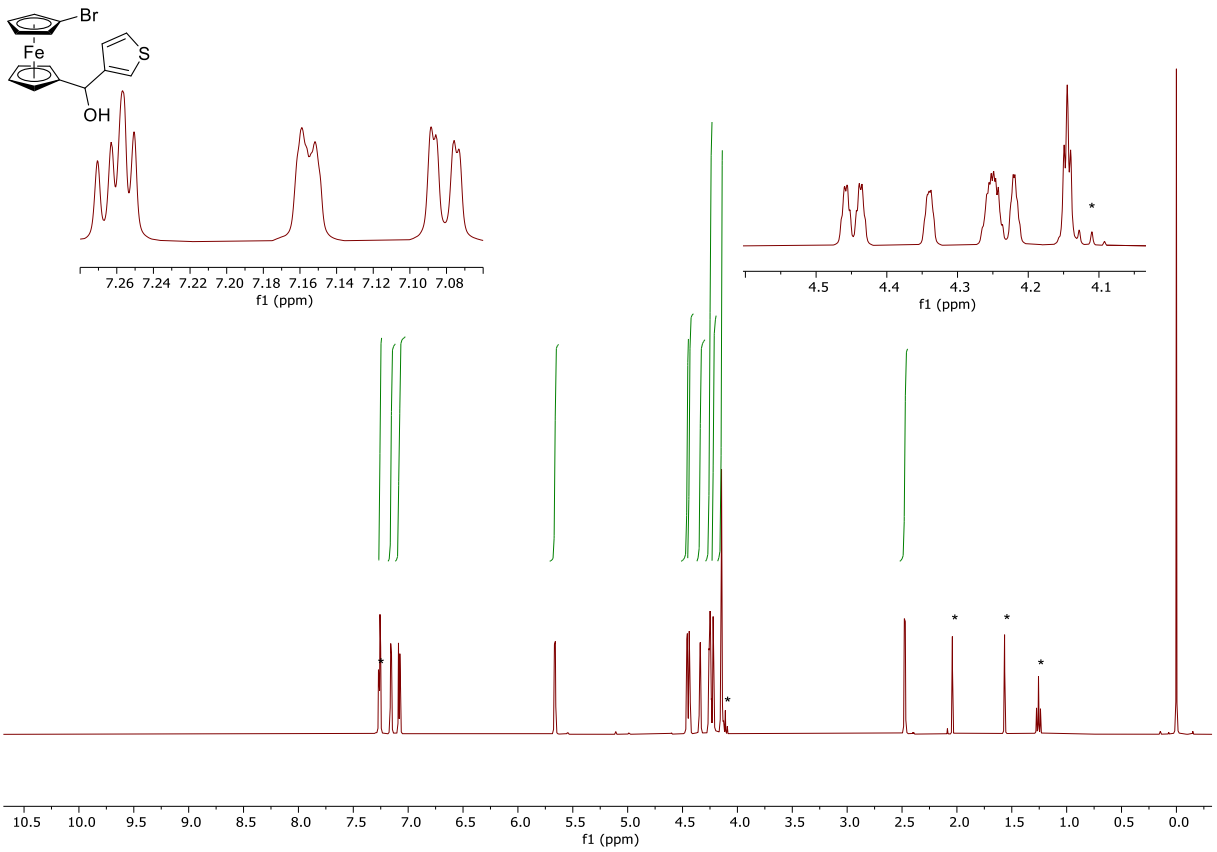

Figure S32. ^{1}H NMR spectrum (400 MHz, $CDCl_3$) of **15**.

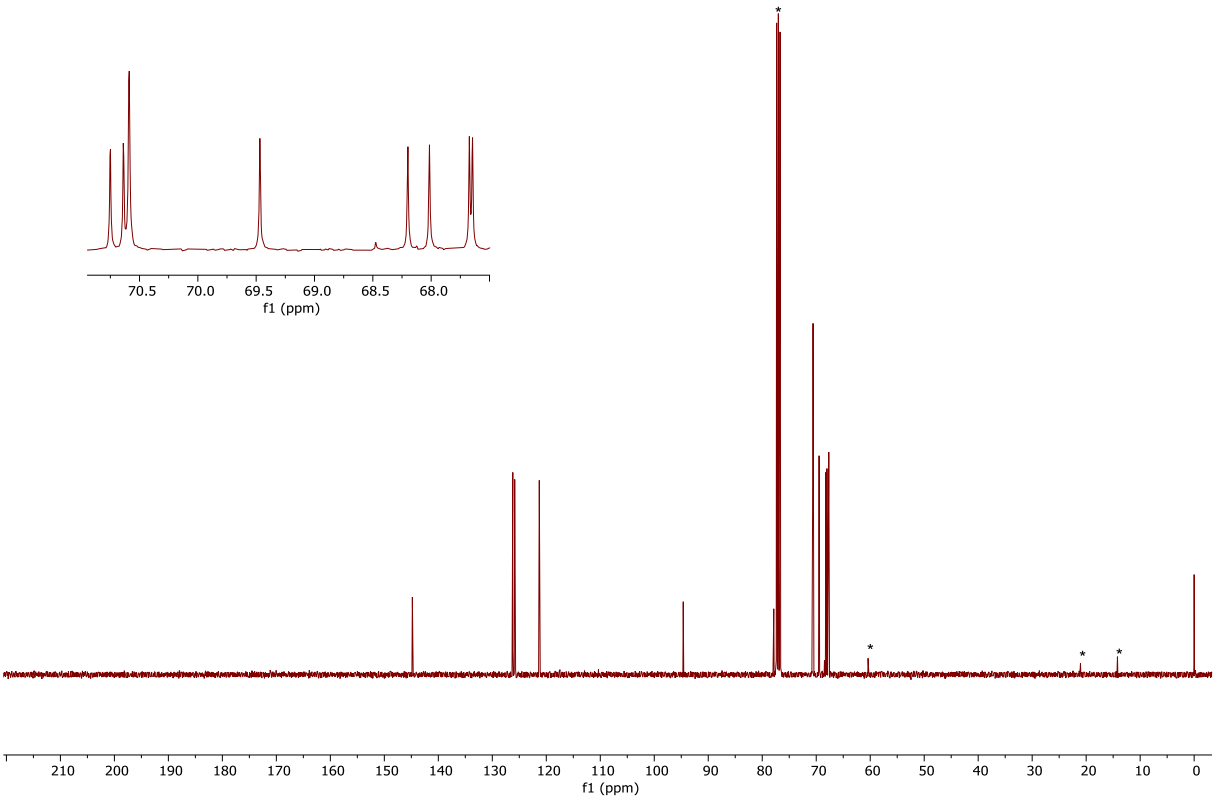

Figure S33. $^{13}C\{^{1}H\}$ NMR spectrum (101 MHz, $CDCl_3$) of **15**.

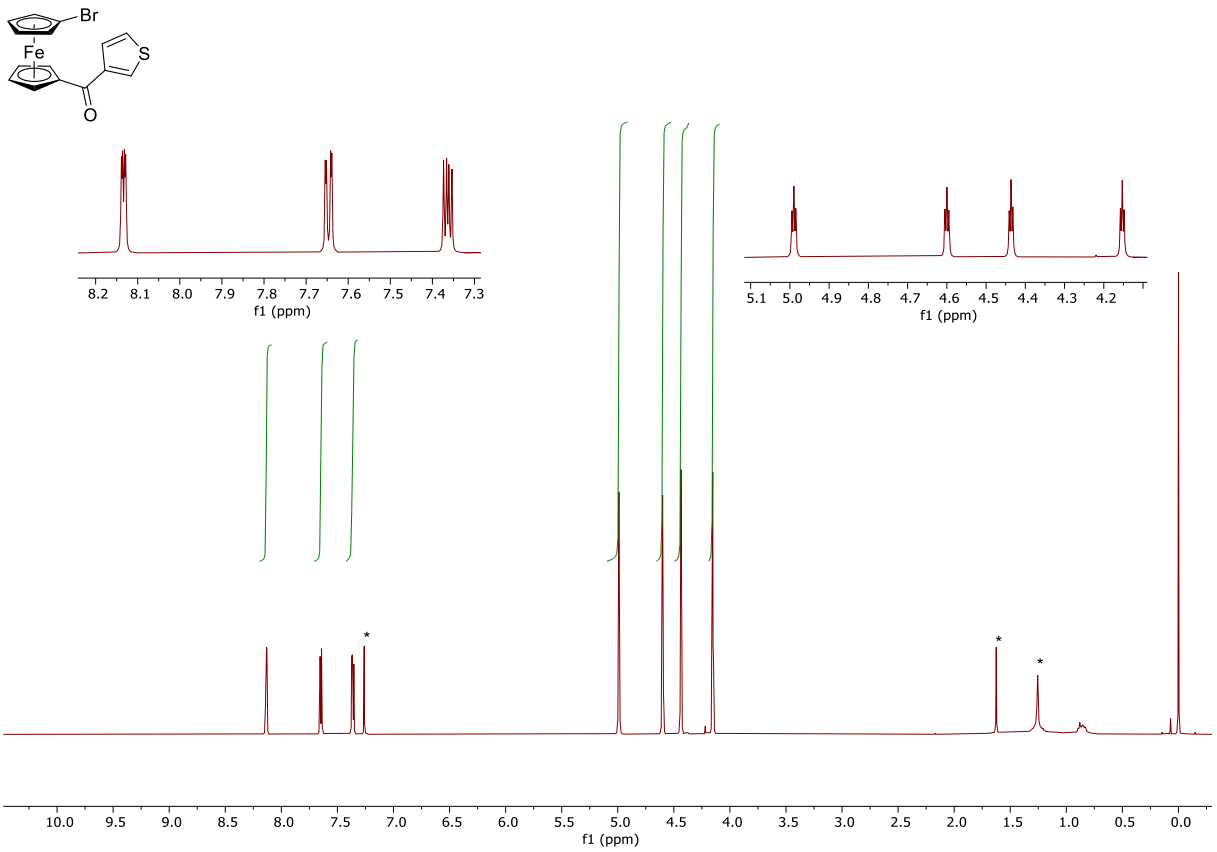

Figure S34. ^{1}H NMR spectrum (400 MHz, $CDCl_3$) of **16**.

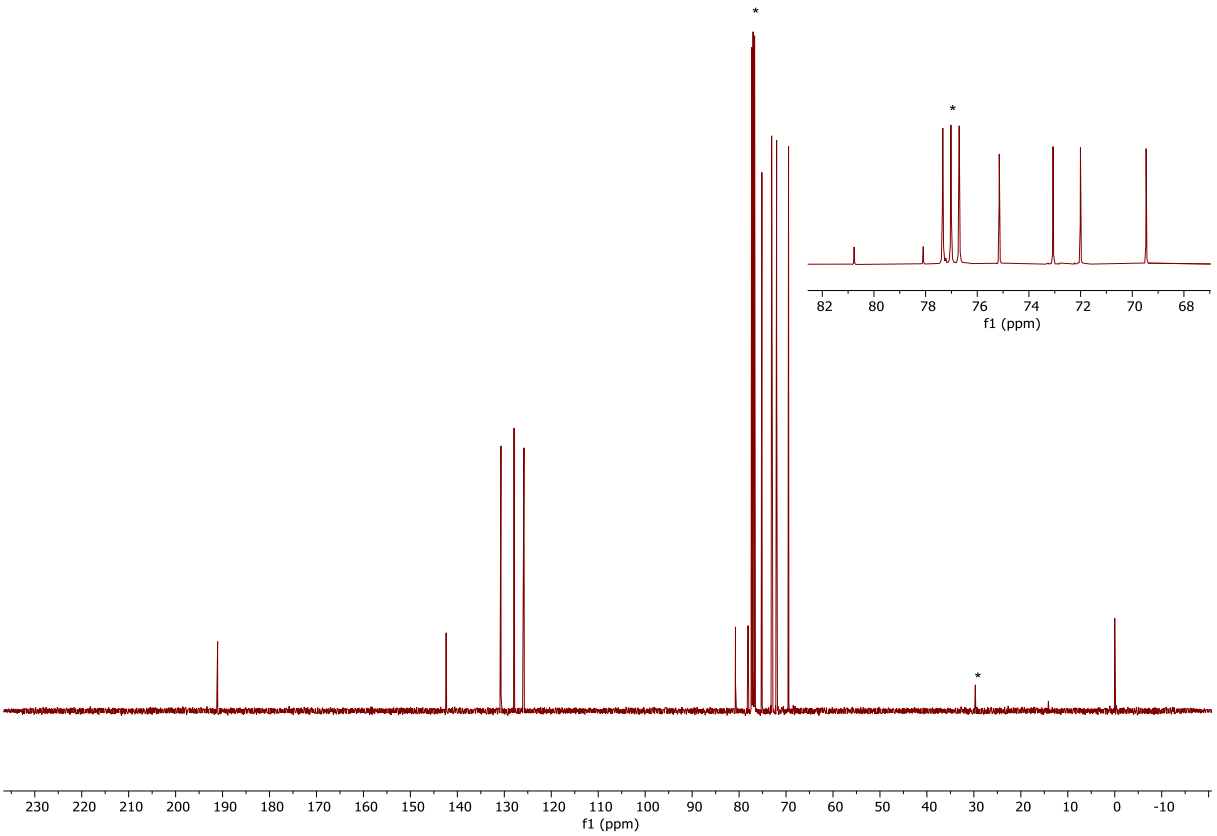

Figure S35. $^{13}C\{^{1}H\}$ NMR spectrum (101 MHz, $CDCl_3$) of **16**.

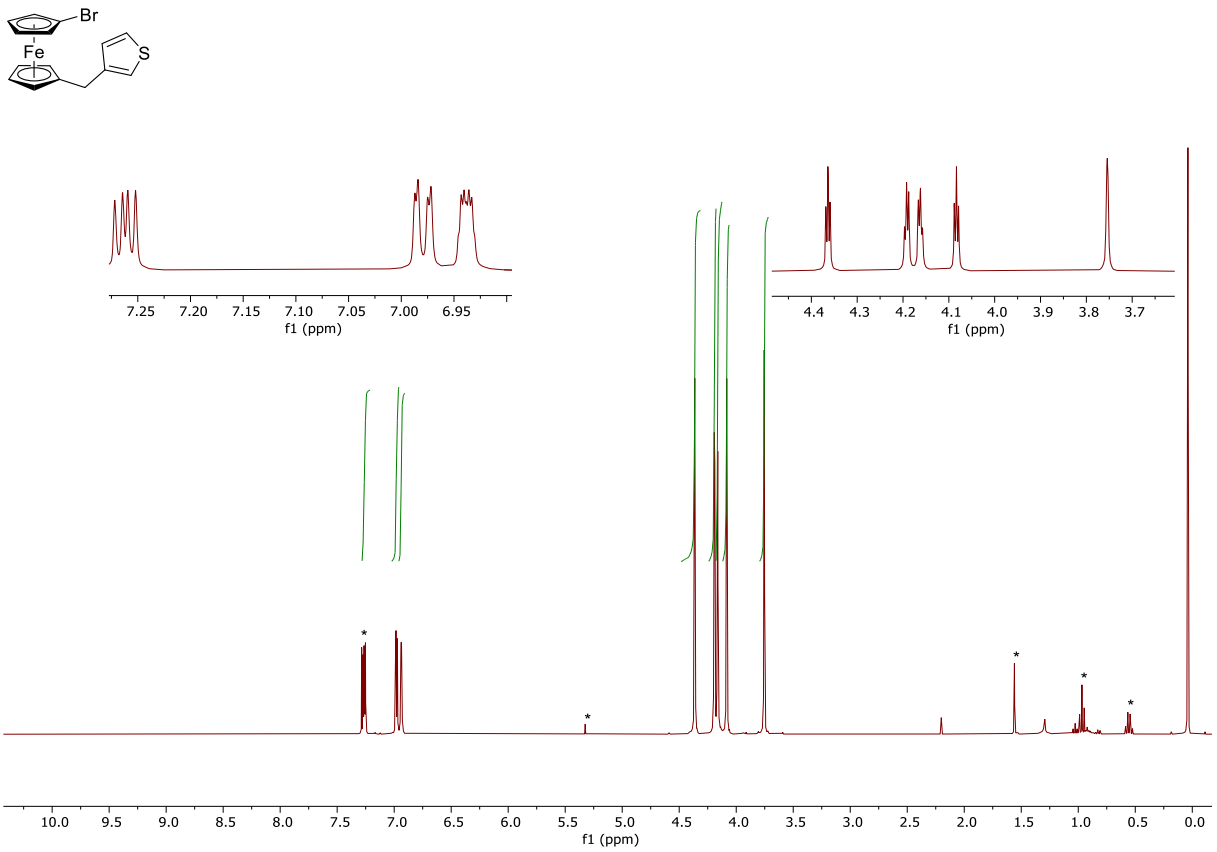

Figure S36. ^{1}H NMR spectrum (400 MHz, $CDCl_3$) of **17**.

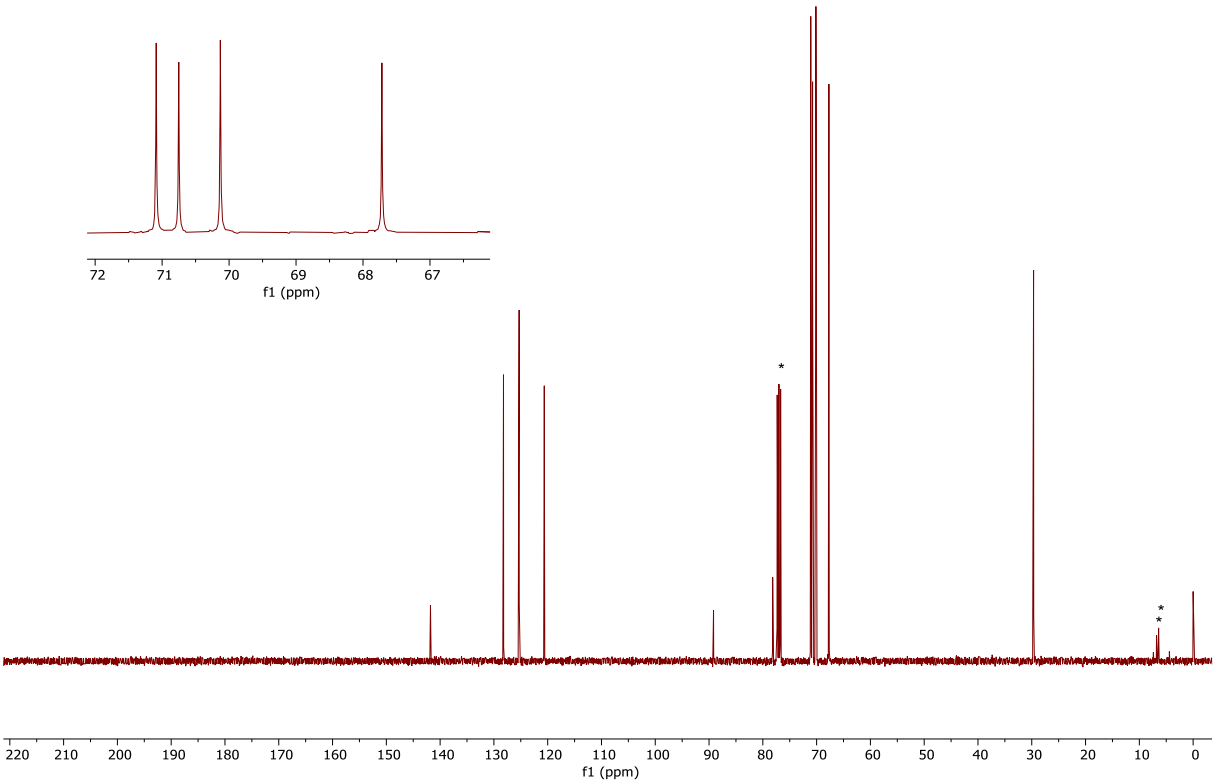

Figure S37. $^{13}C\{^{1}H\}$ NMR spectrum (101 MHz, $CDCl_3$) of **17**.

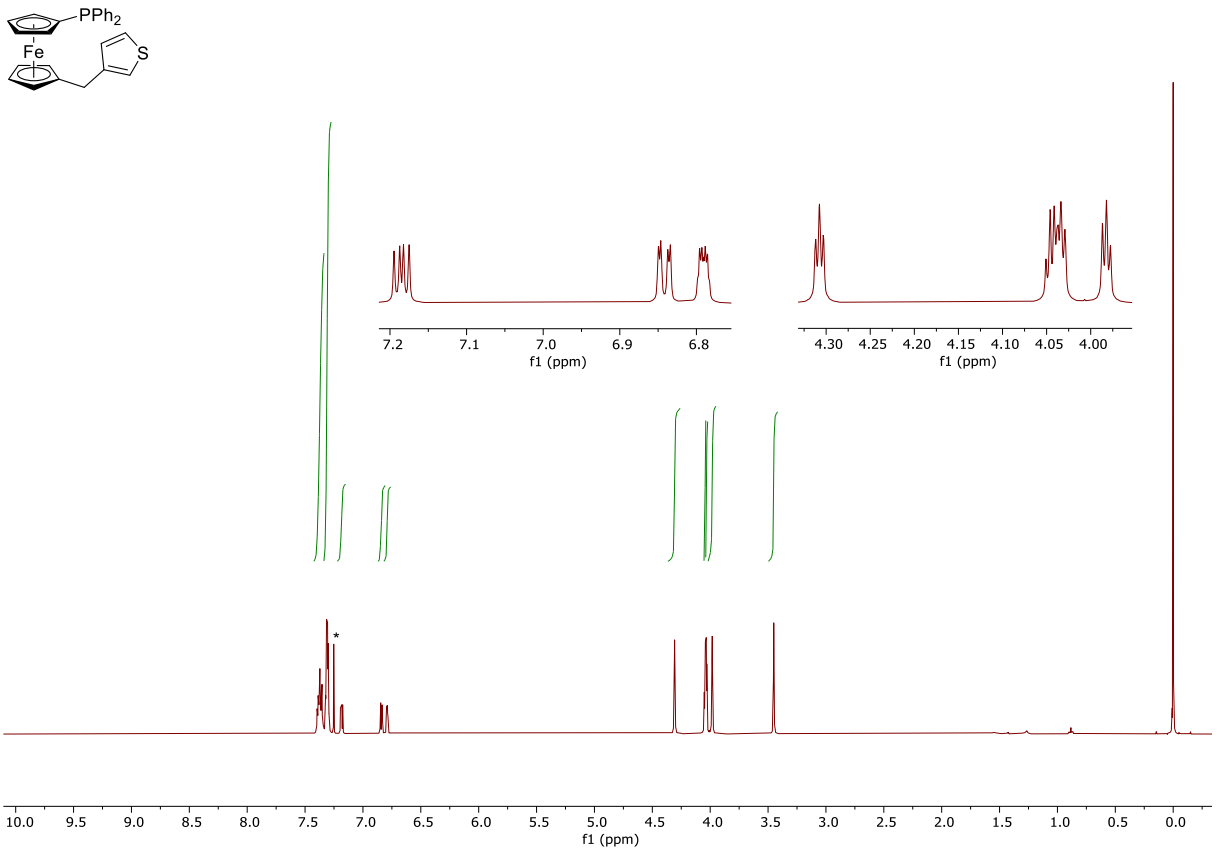

Figure S38. ^{1}H NMR spectrum (400 MHz, $CDCl_3$) of **3**.

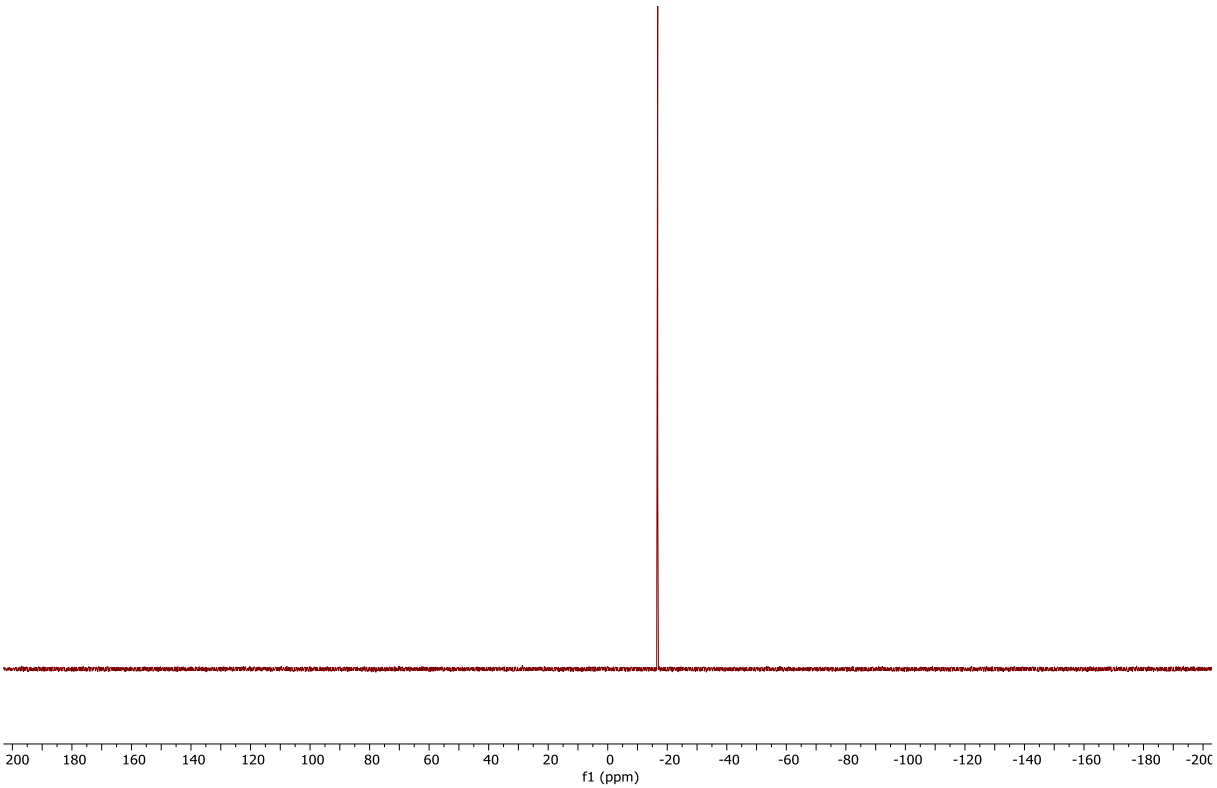

Figure S39. $^{31}P\{^{1}H\}$ NMR spectrum (162 MHz, $CDCl_3$) of **3**.

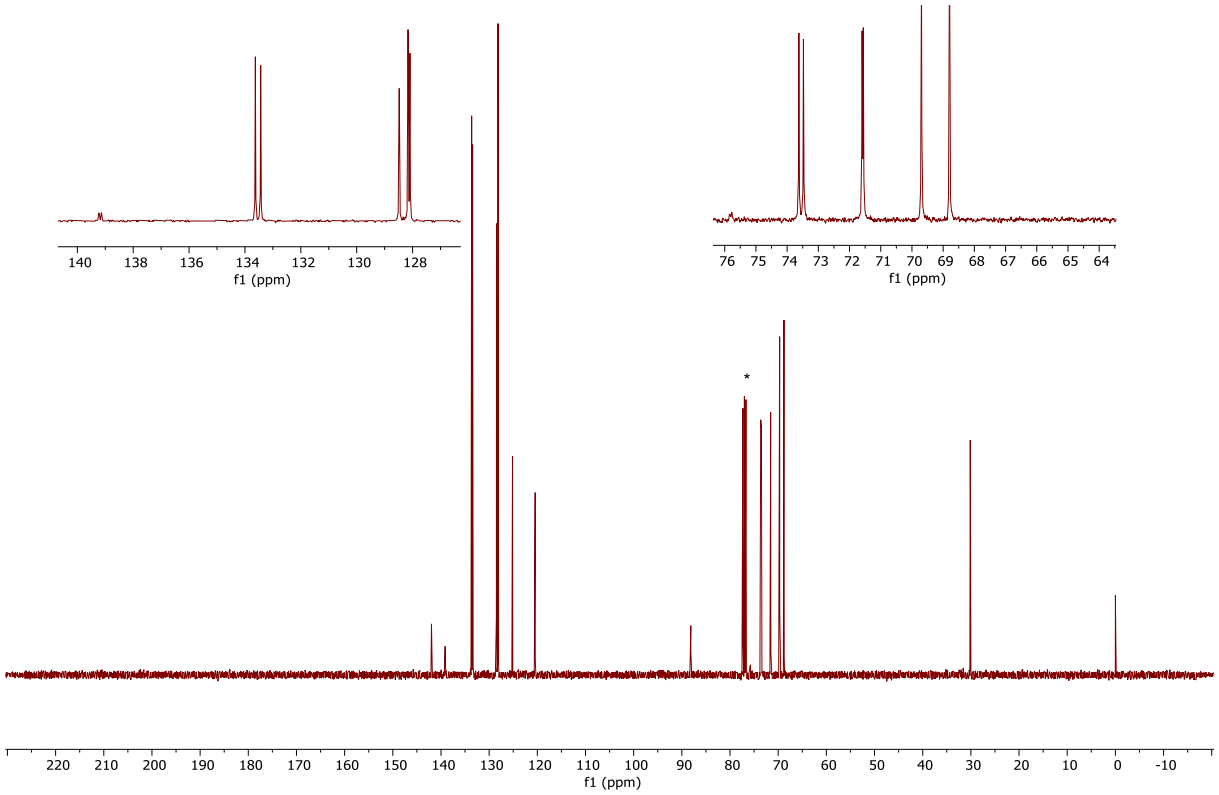

Figure S40. $^{13}C\{^{1}H\}$ NMR spectrum (101 MHz, $CDCl_3$) of **3**.

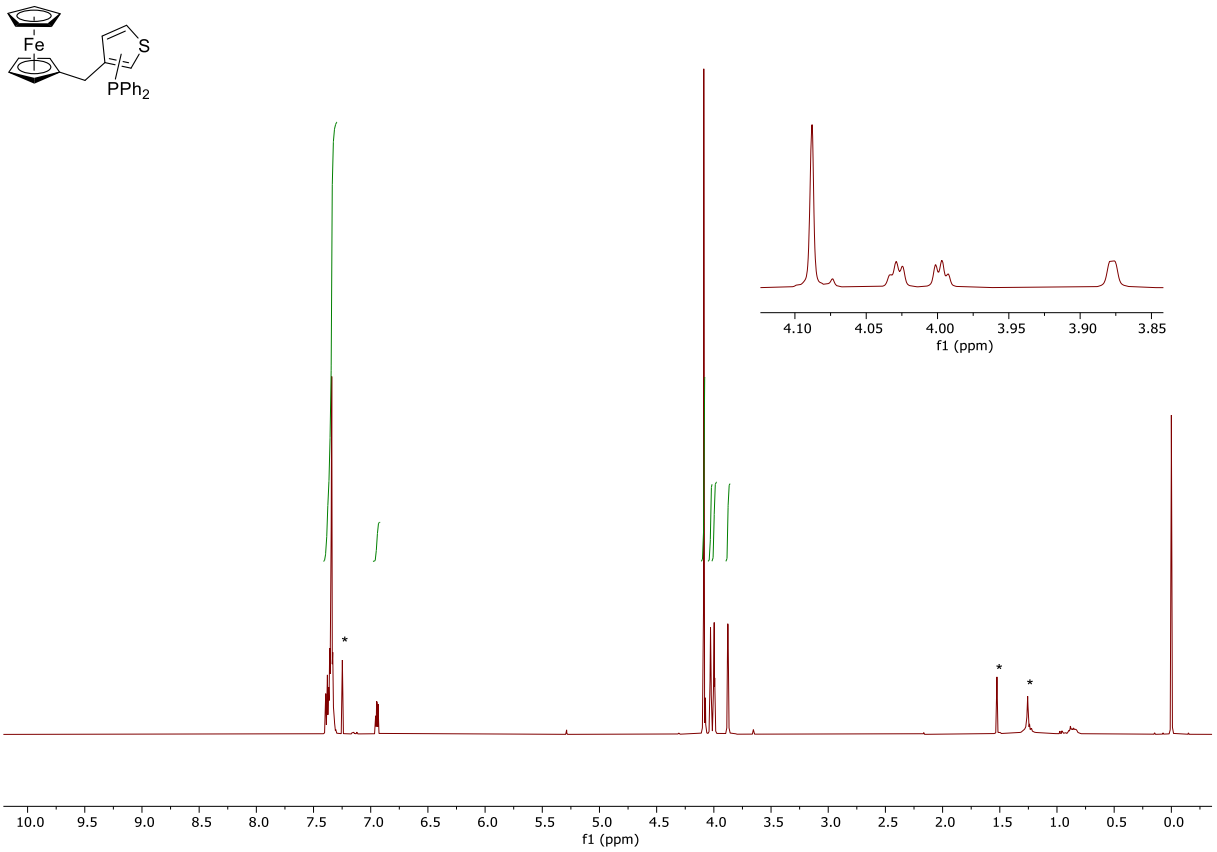

Figure S41. ^{1}H NMR spectrum (400 MHz, $CDCl_3$) of **19**.

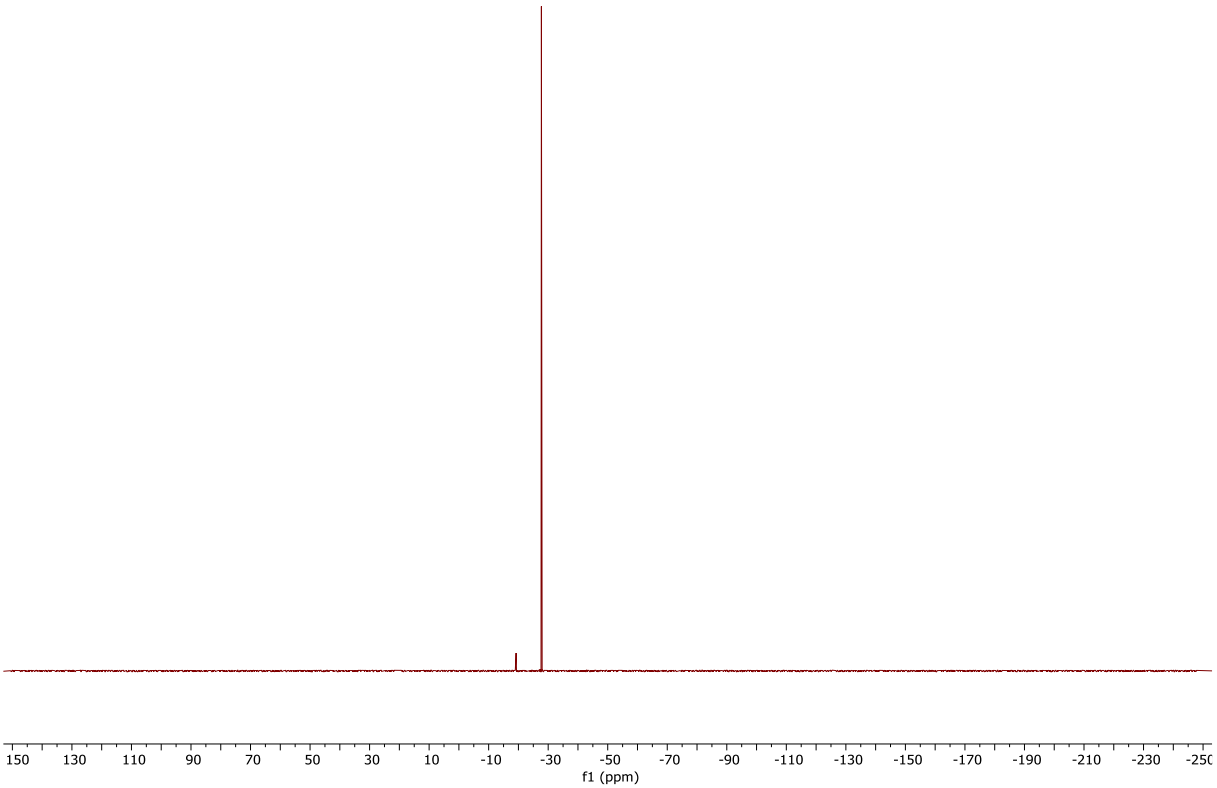

Figure S42. $^{31}P\{^{1}H\}$ NMR spectrum (162 MHz, $CDCl_3$) of **19**.

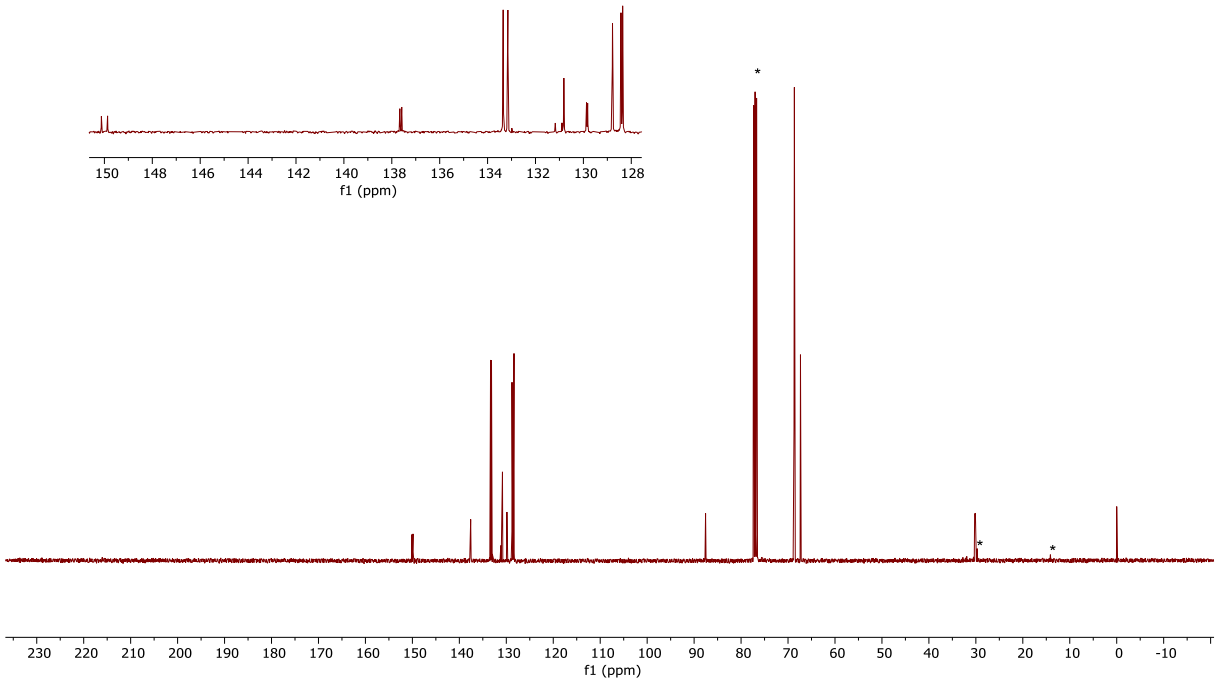

Figure S43. $^{13}C\{^{1}H\}$ NMR spectrum (101 MHz, $CDCl_3$) of **19**.

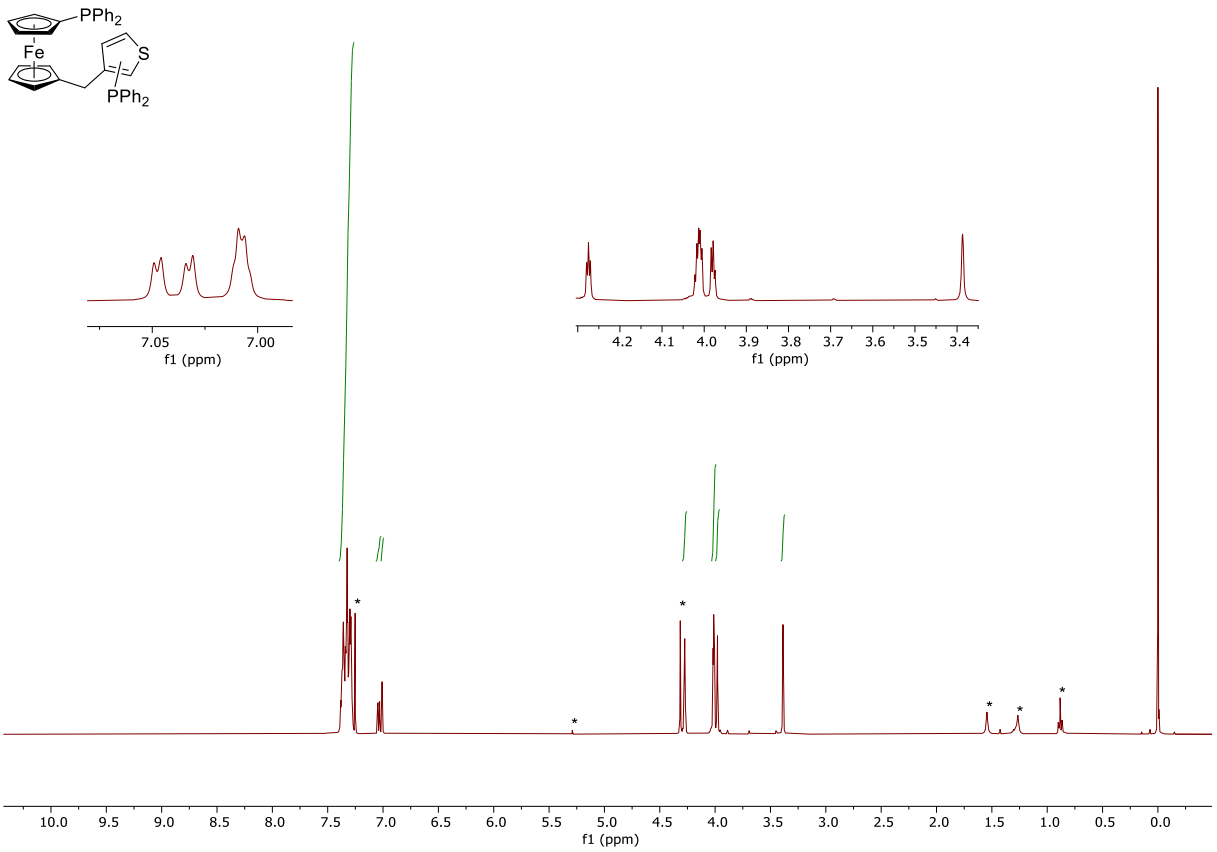

Figure S44. ^{1}H NMR spectrum (400 MHz, $CDCl_3$) of **20**.

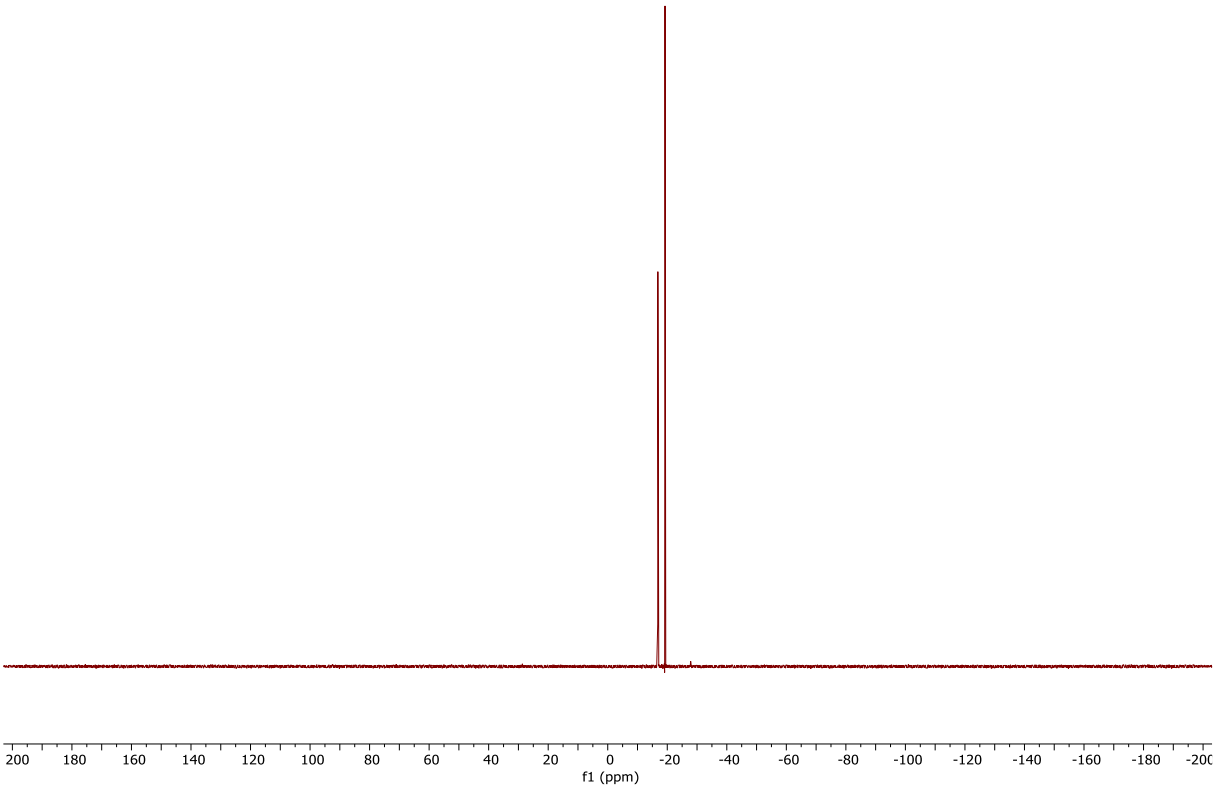

Figure S45. $^{31}P\{^{1}H\}$ NMR spectrum (162 MHz, $CDCl_3$) of **20**.

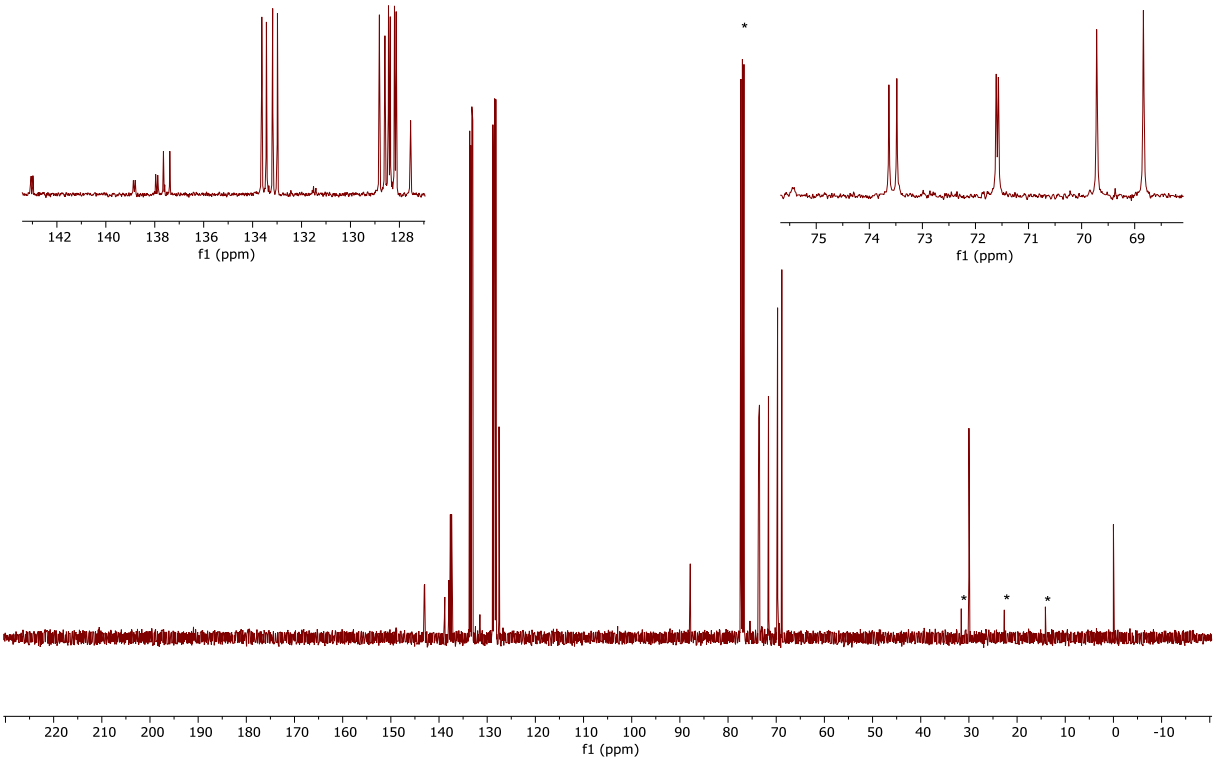

Figure S45. $^{13}C\{^{1}H\}$ NMR spectrum (101 MHz, $CDCl_3$) of **20**.

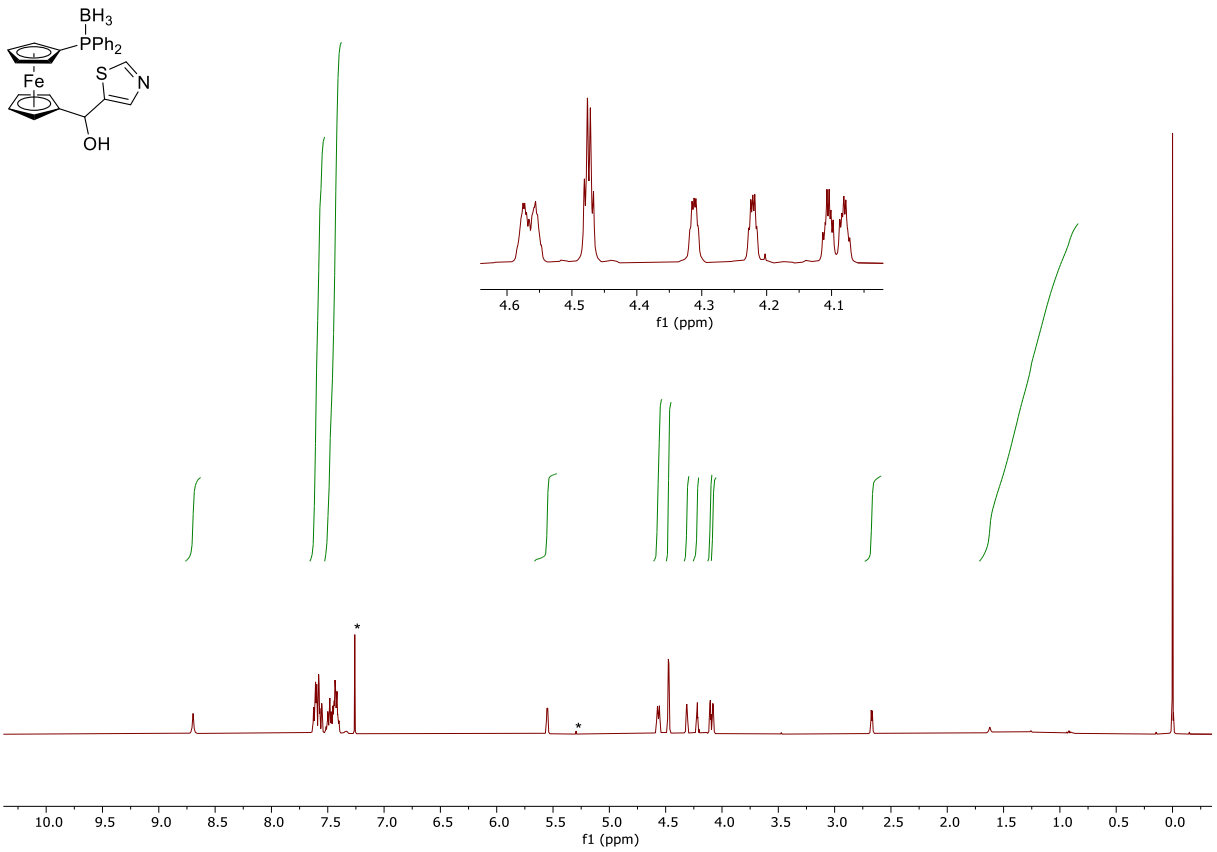

Figure S46. ^{1}H NMR spectrum (400 MHz, $CDCl_3$) of **21**·BH_3.

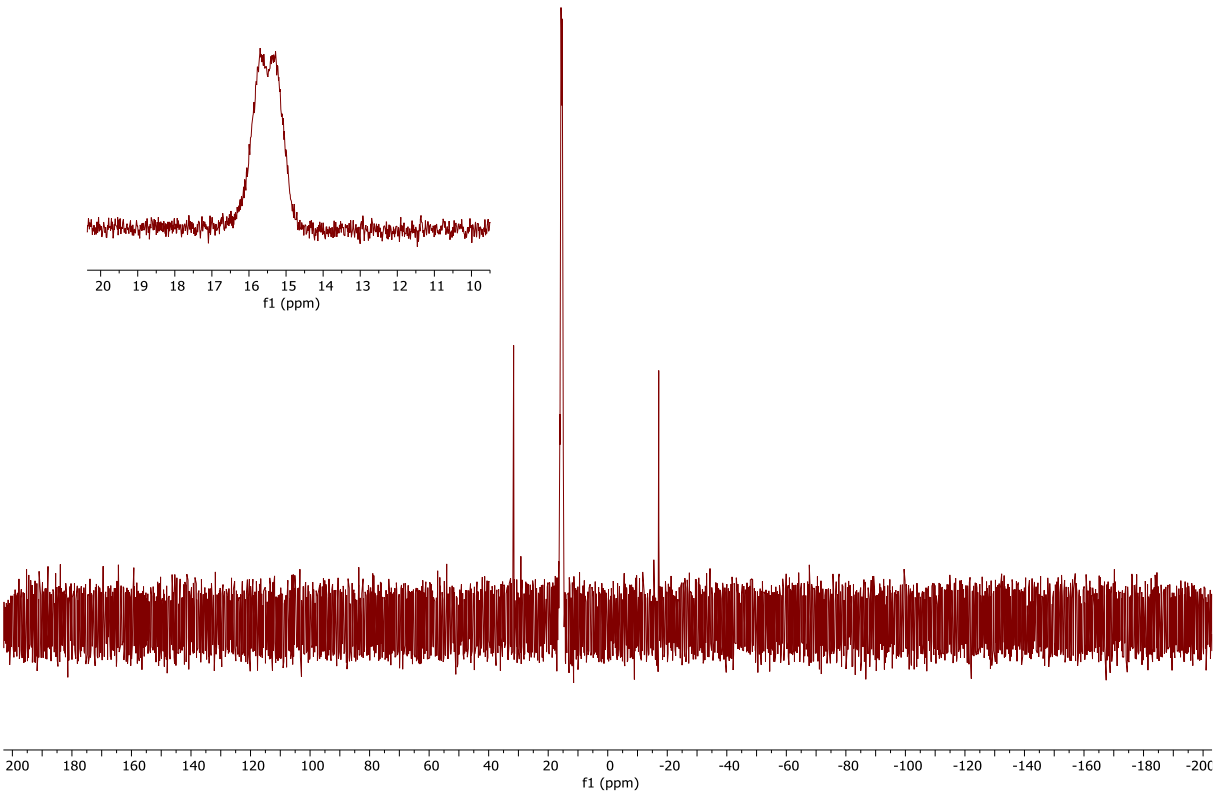

Figure S47. $^{31}P\{^{1}H\}$ NMR spectrum (162 MHz, $CDCl_3$) of **21**·BH_3.

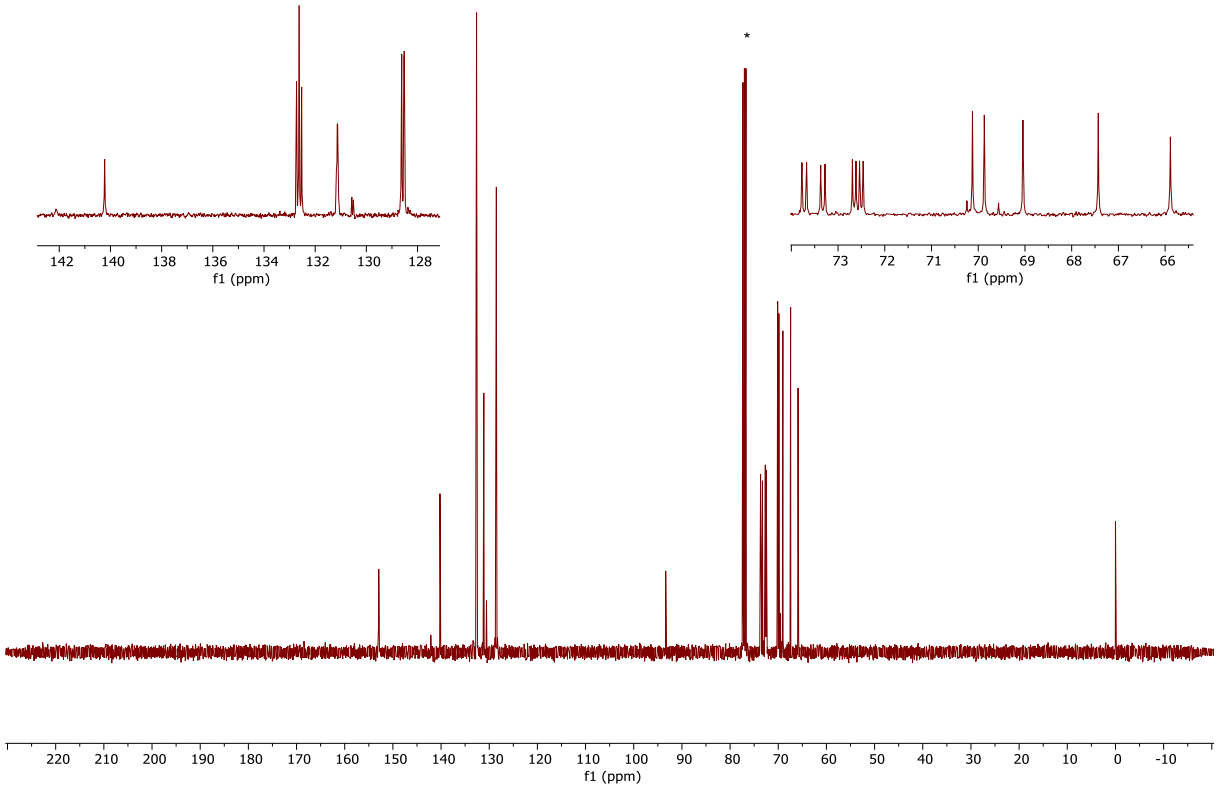

Figure S48. $^{13}C\{^{1}H\}$ NMR spectrum (101 MHz, $CDCl_3$) of **21**·BH_3.

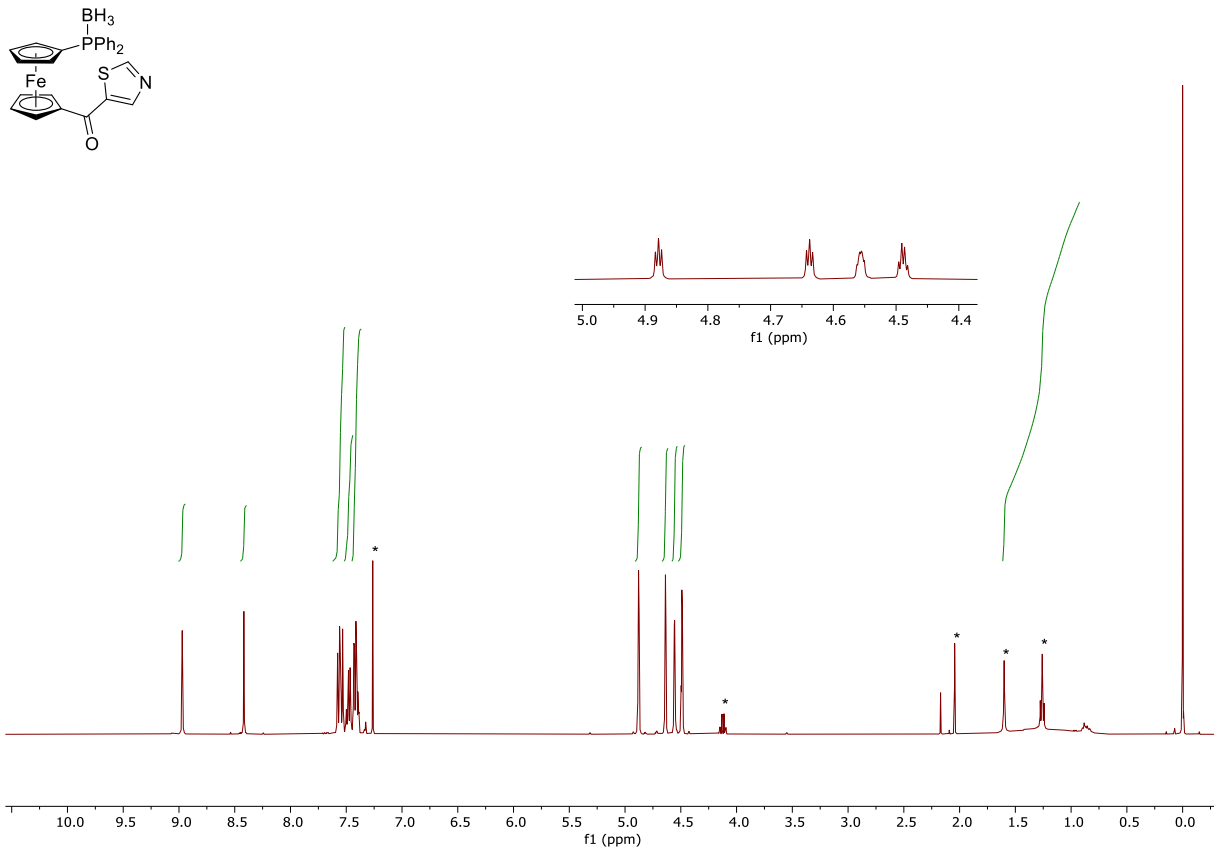

Figure S49. ^{1}H NMR spectrum (400 MHz, $CDCl_3$) of **22**·BH_3.

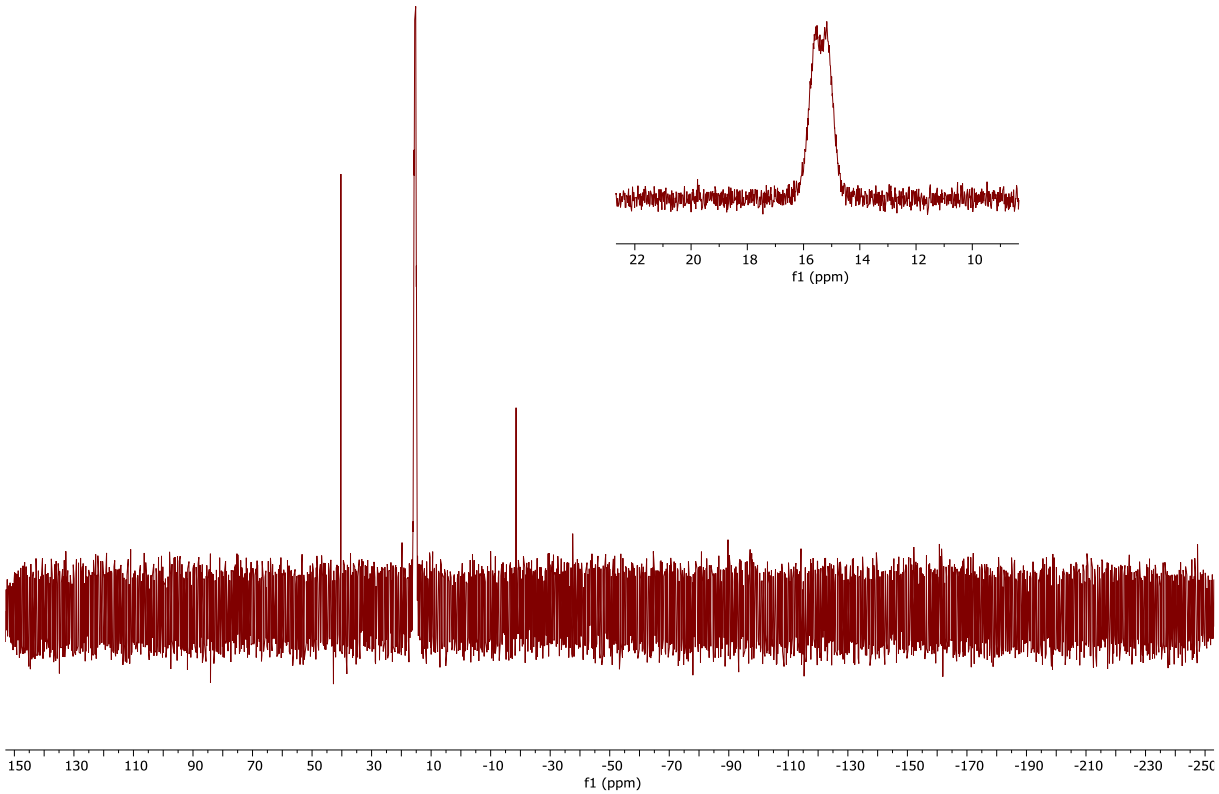

Figure S50. $^{31}P\{^{1}H\}$ NMR spectrum (162 MHz, $CDCl_3$) of **22**·BH_3.

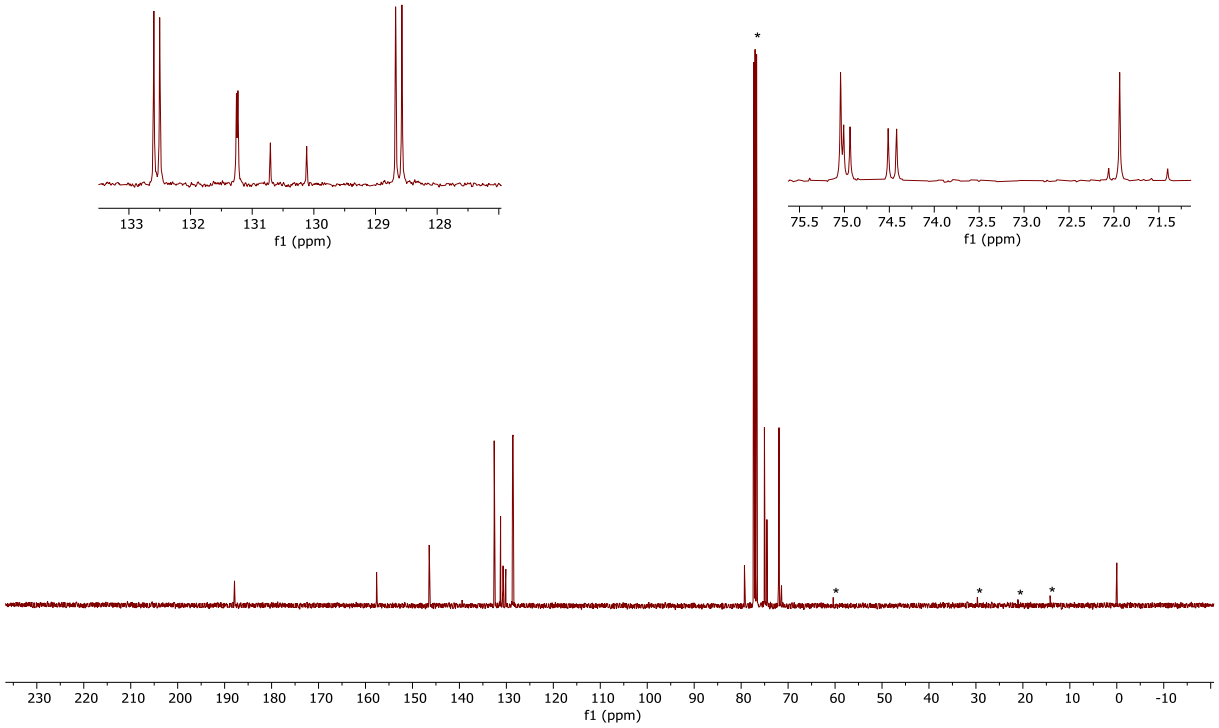

Figure S51. $^{13}C\{^{1}H\}$ NMR spectrum (101 MHz, $CDCl_3$) of **22**·BH_3.

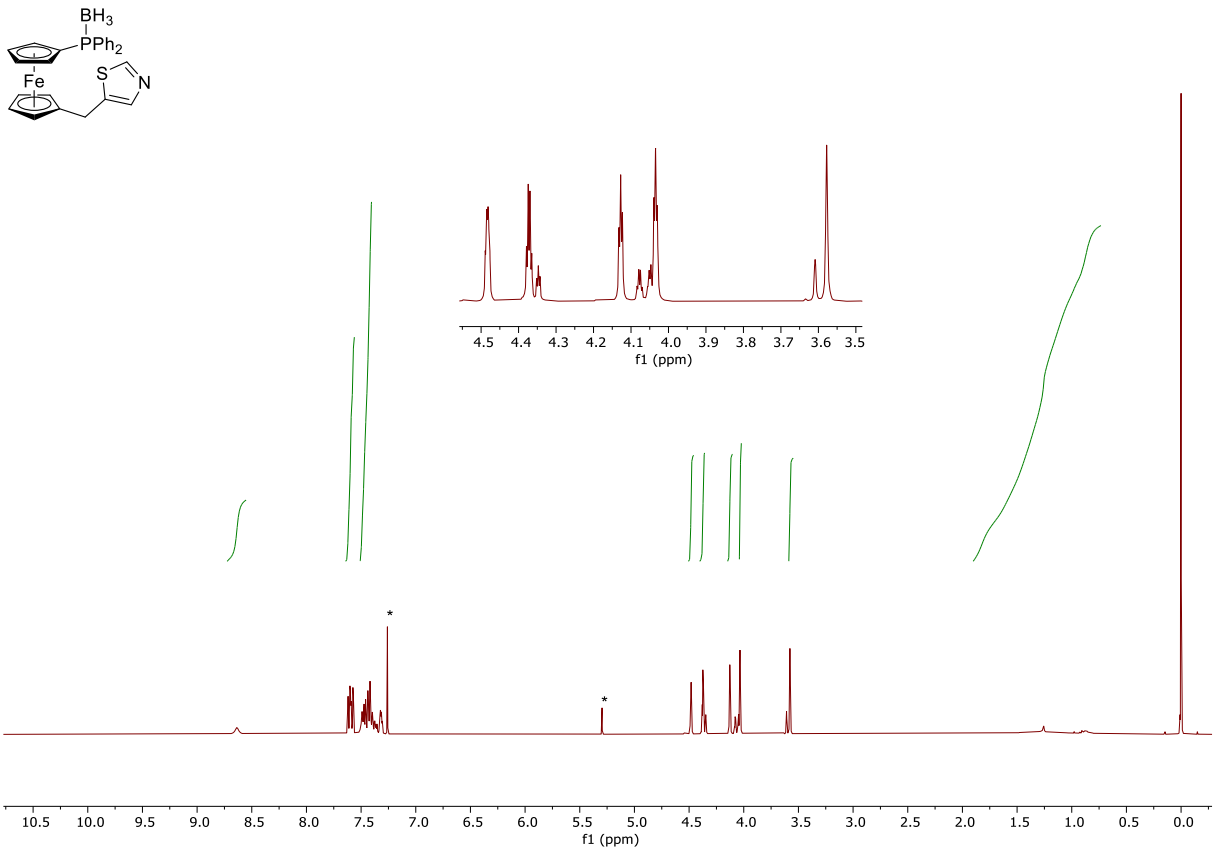

Figure S52. ^{1}H NMR spectrum (400 MHz, $CDCl_3$) of **4**·BH_3.

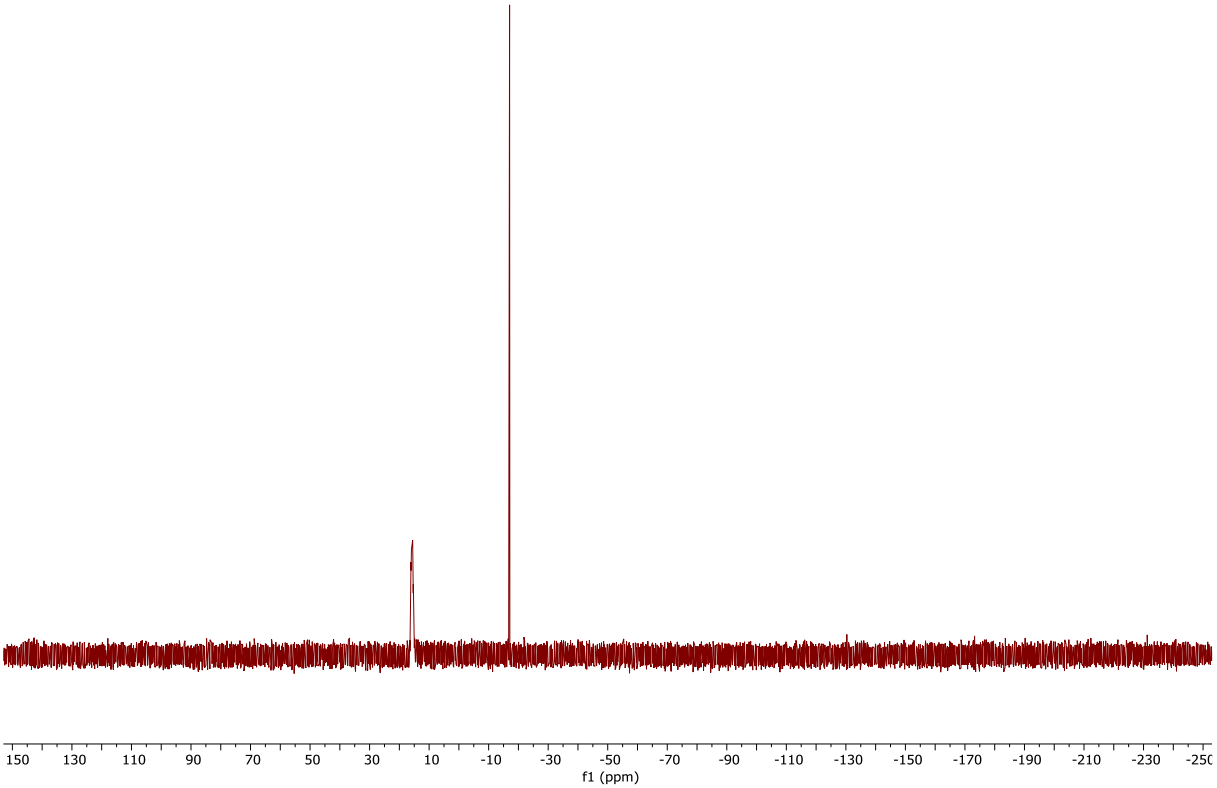

Figure S53. $^{31}P\{^{1}H\}$ NMR spectrum (162 MHz, $CDCl_3$) of **4**·BH_3.

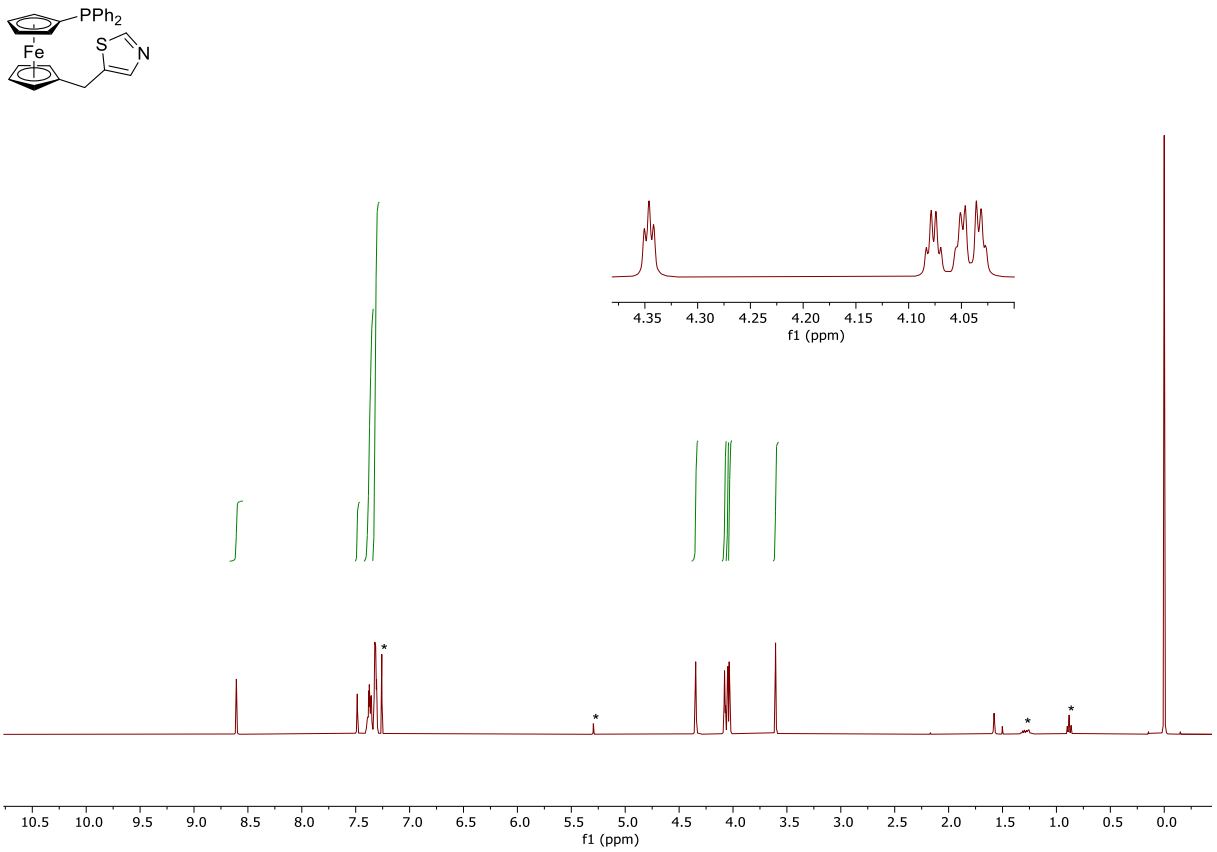

Figure S54. ^{1}H NMR spectrum (400 MHz, $CDCl_3$) of **4**.

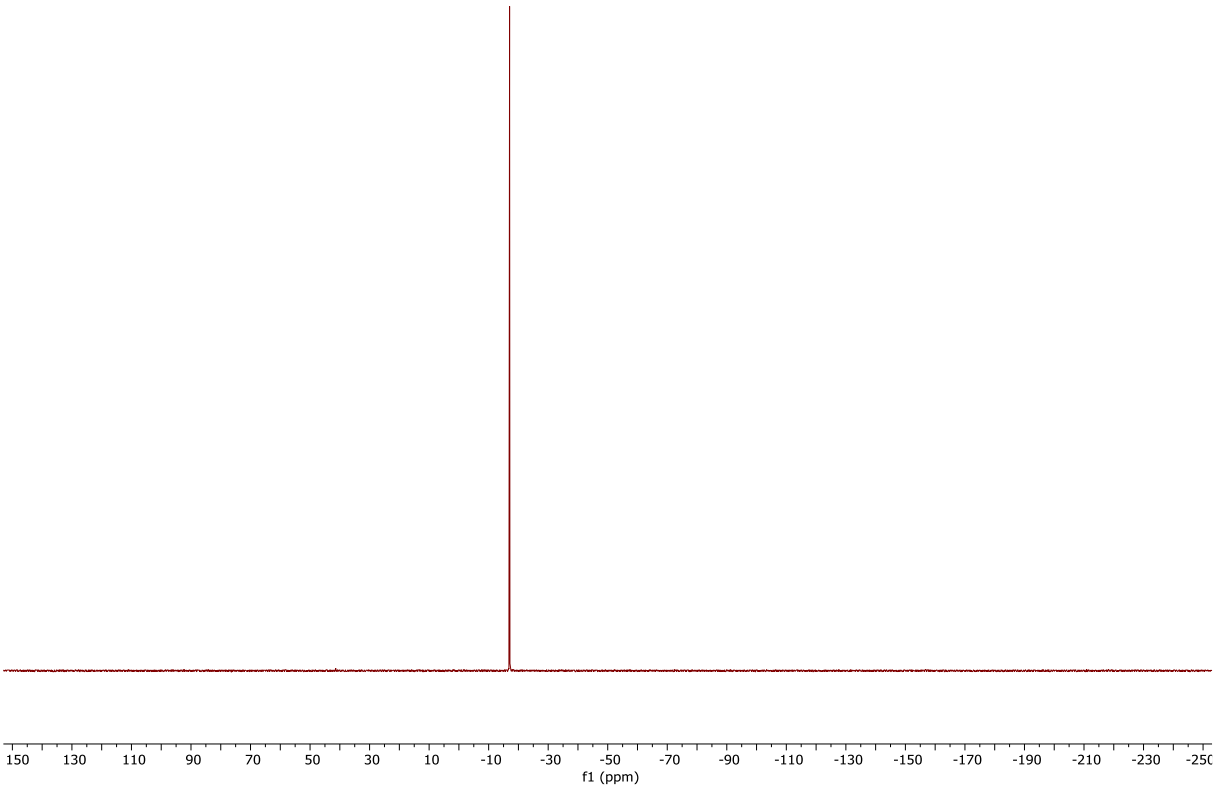

Figure S55. $^{31}P\{^{1}H\}$ NMR spectrum (162 MHz, $CDCl_3$) of **4**.

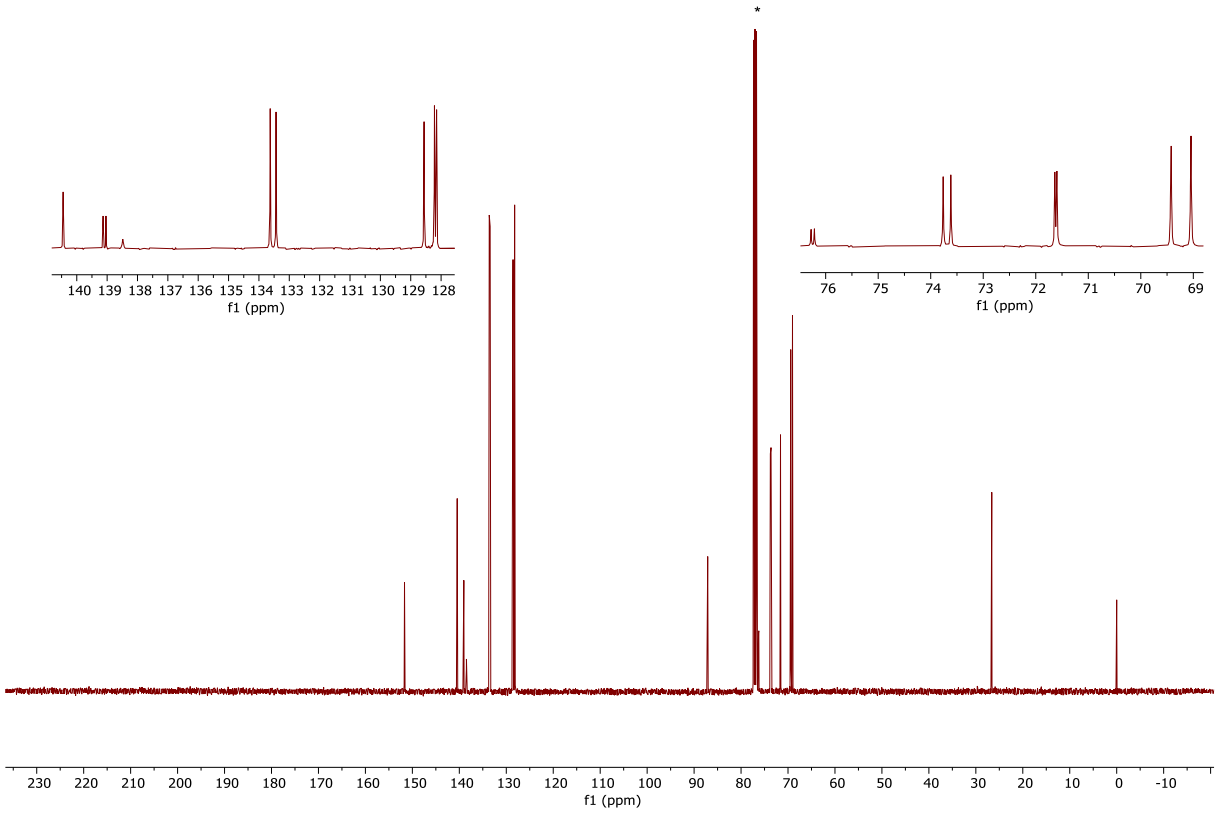

Figure S56. $^{13}C\{^{1}H\}$ NMR spectrum (101 MHz, $CDCl_3$) of **4**.

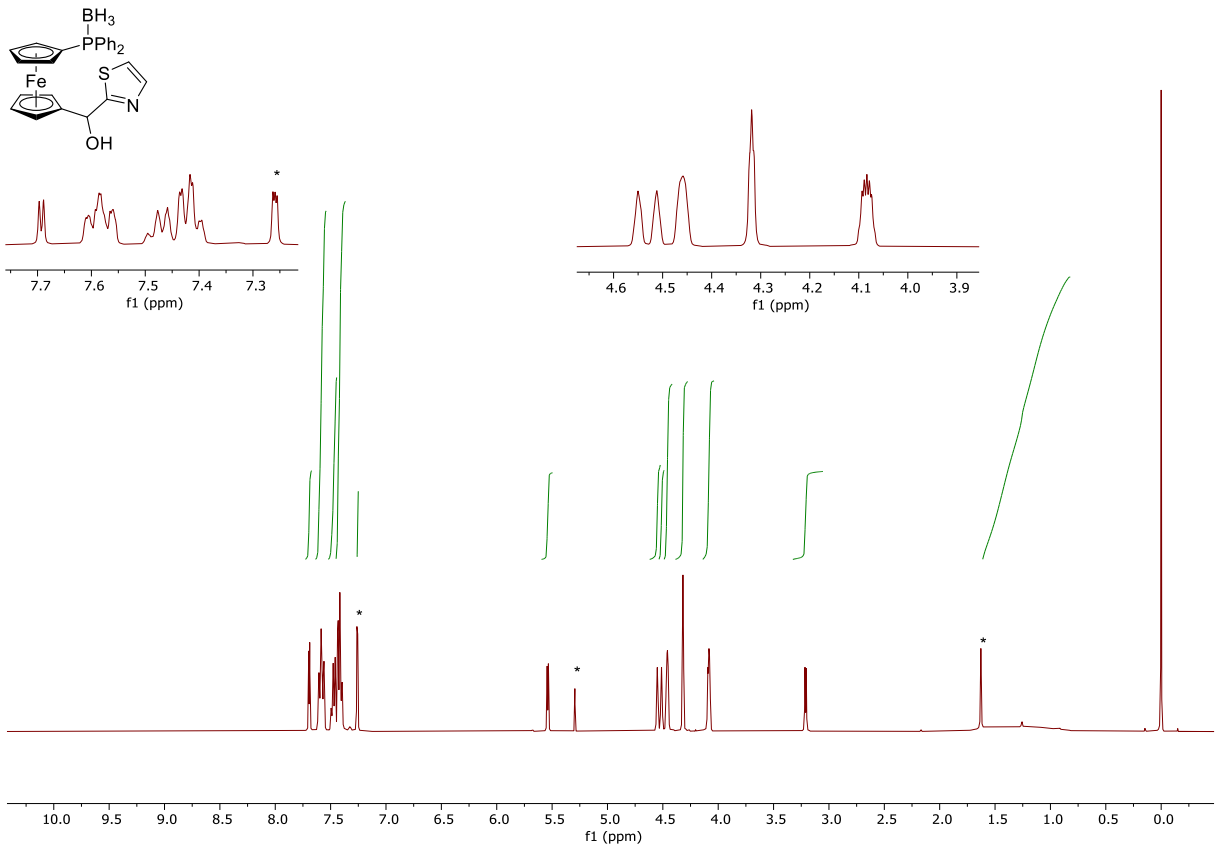

Figure S57. ^{1}H NMR spectrum (400 MHz, $CDCl_3$) of **23**·BH_3.

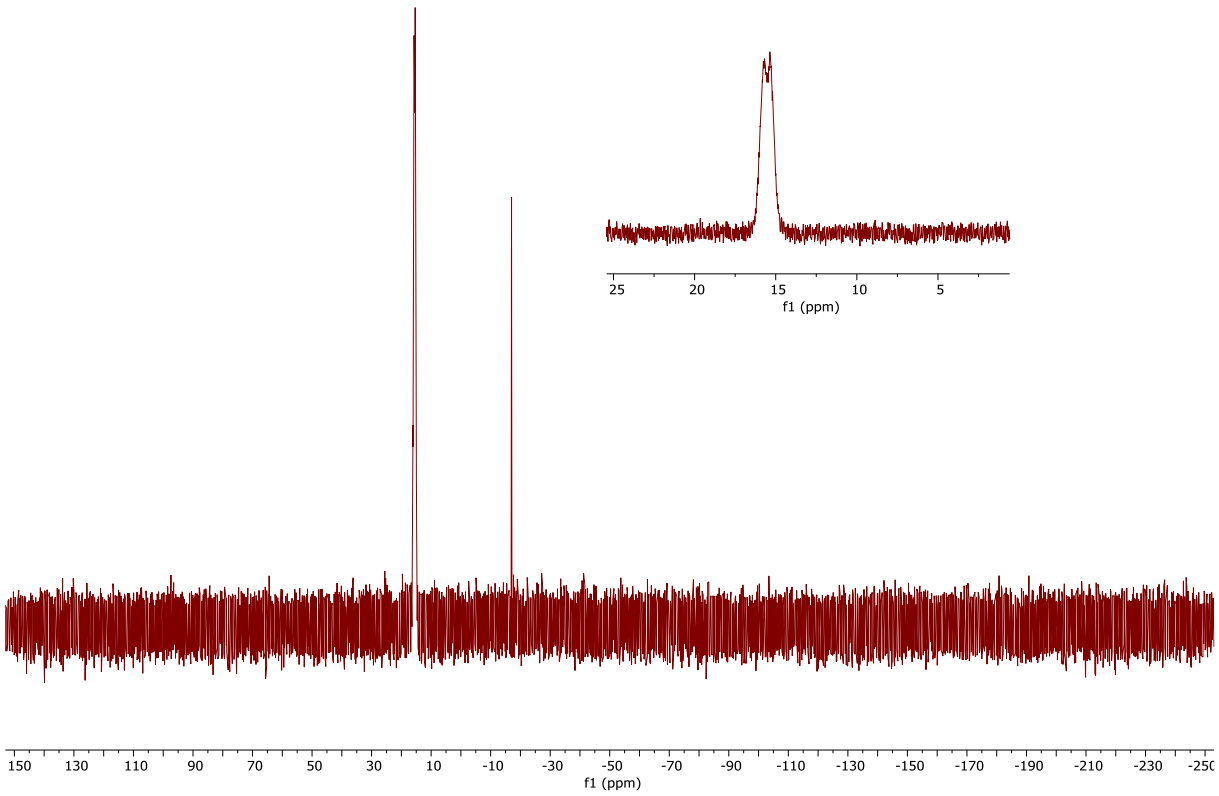

Figure S58. $^{31}P\{^{1}H\}$ NMR spectrum (162 MHz, $CDCl_3$) of **23**·BH_3.

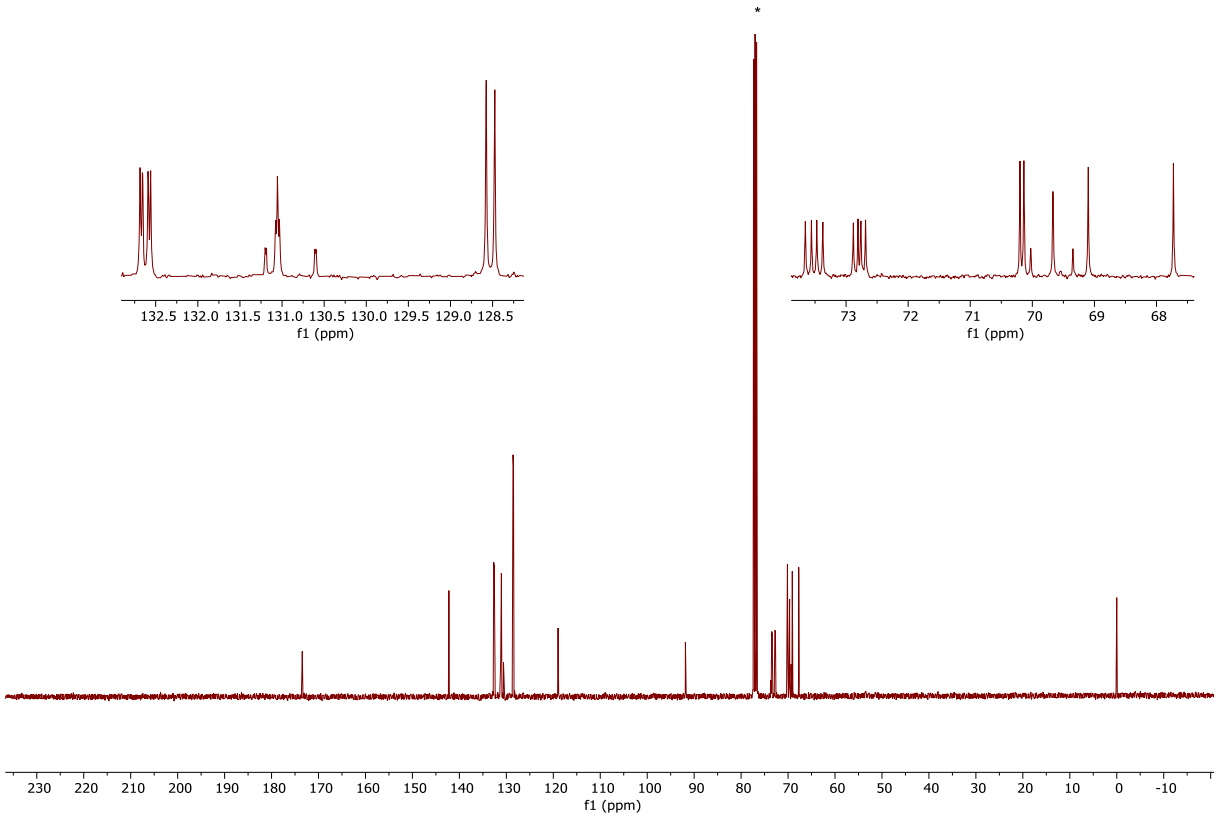

Figure S59. $^{13}C\{^{1}H\}$ NMR spectrum (101 MHz, $CDCl_3$) of **23**·BH_3.

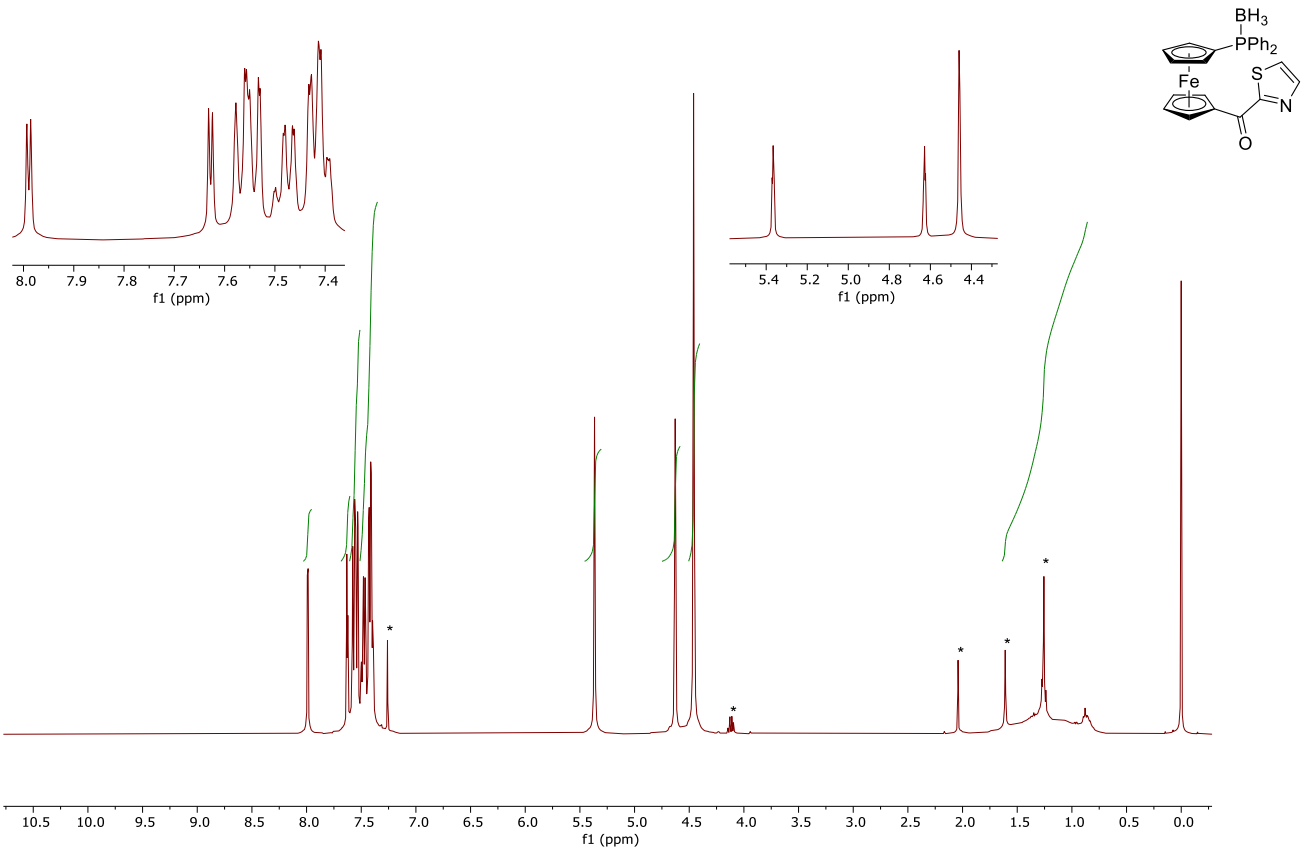

Figure S60. ^{1}H NMR spectrum (400 MHz, $CDCl_3$) of **24**·BH_3.

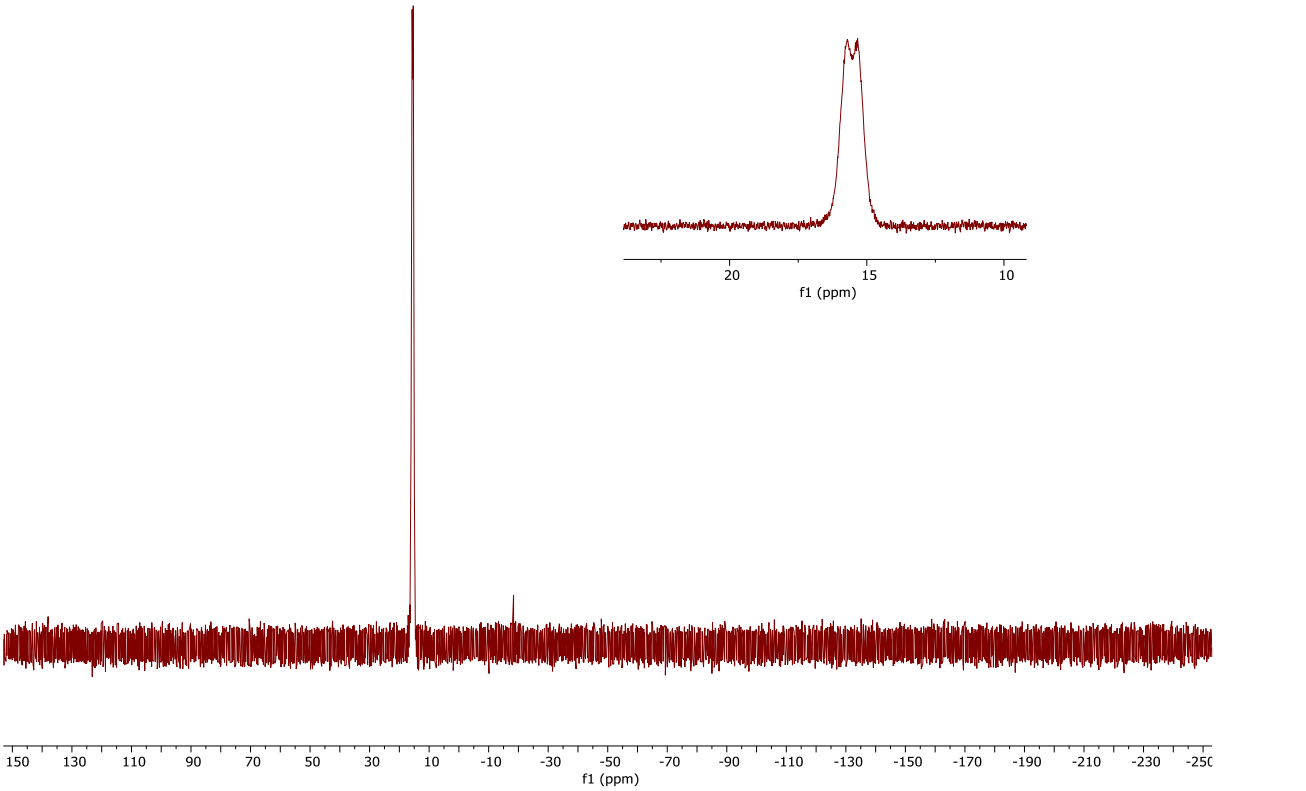

Figure S61. $^{31}P\{^{1}H\}$ NMR spectrum (162 MHz, $CDCl_3$) of **24**·BH_3.

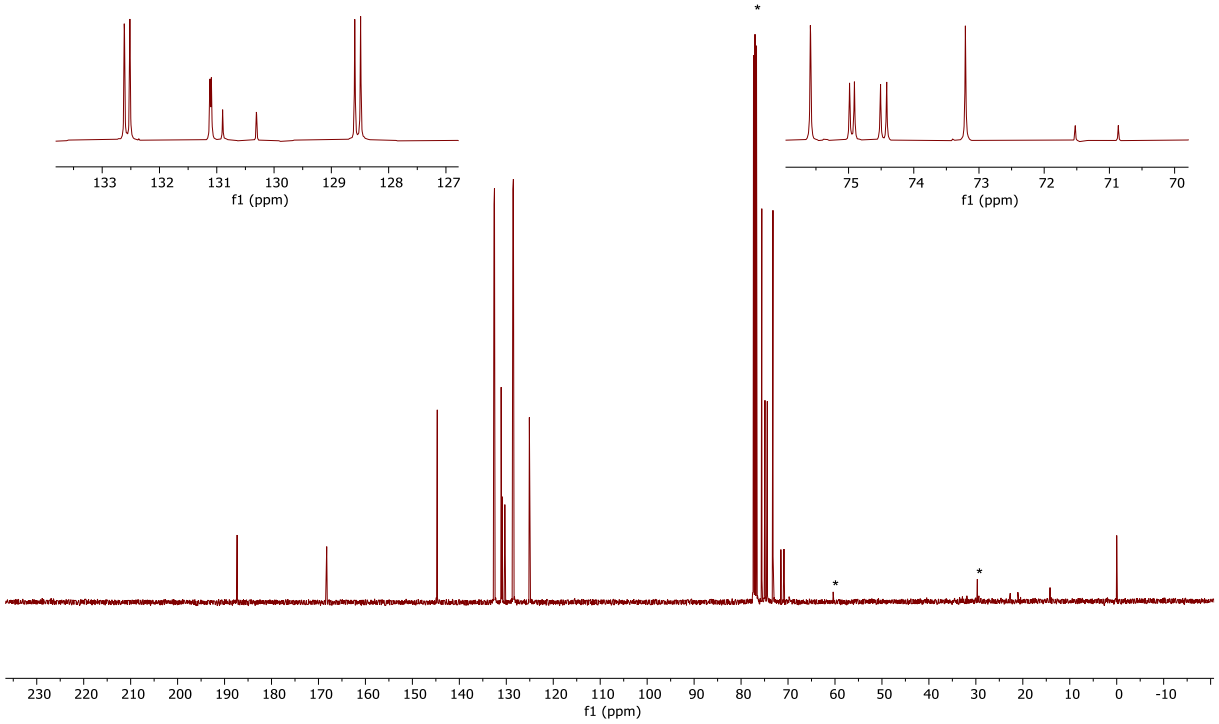

Figure S62. $^{13}C\{^{1}H\}$ NMR spectrum (101 MHz, $CDCl_3$) of **24**·BH_3.

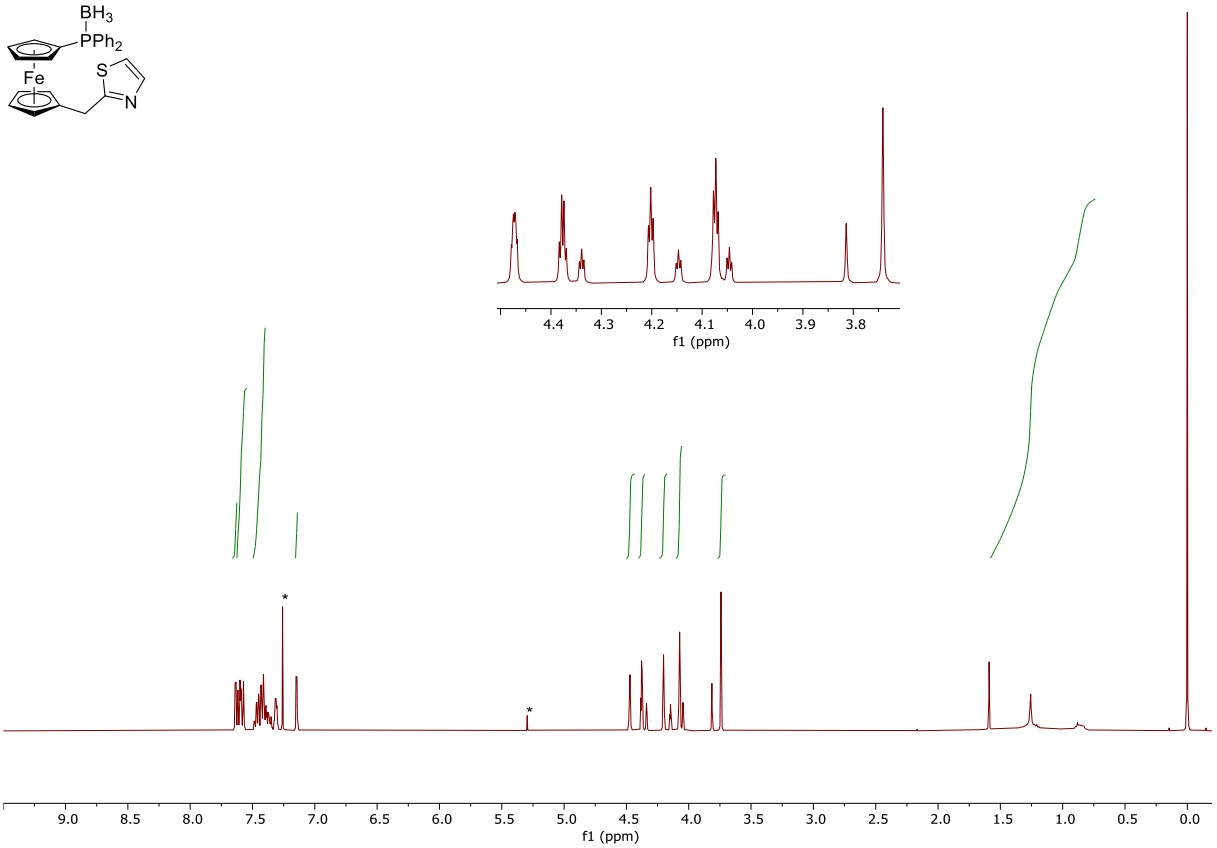

Figure S63. ^{1}H NMR spectrum (400 MHz, $CDCl_3$) of **5**·BH_3.

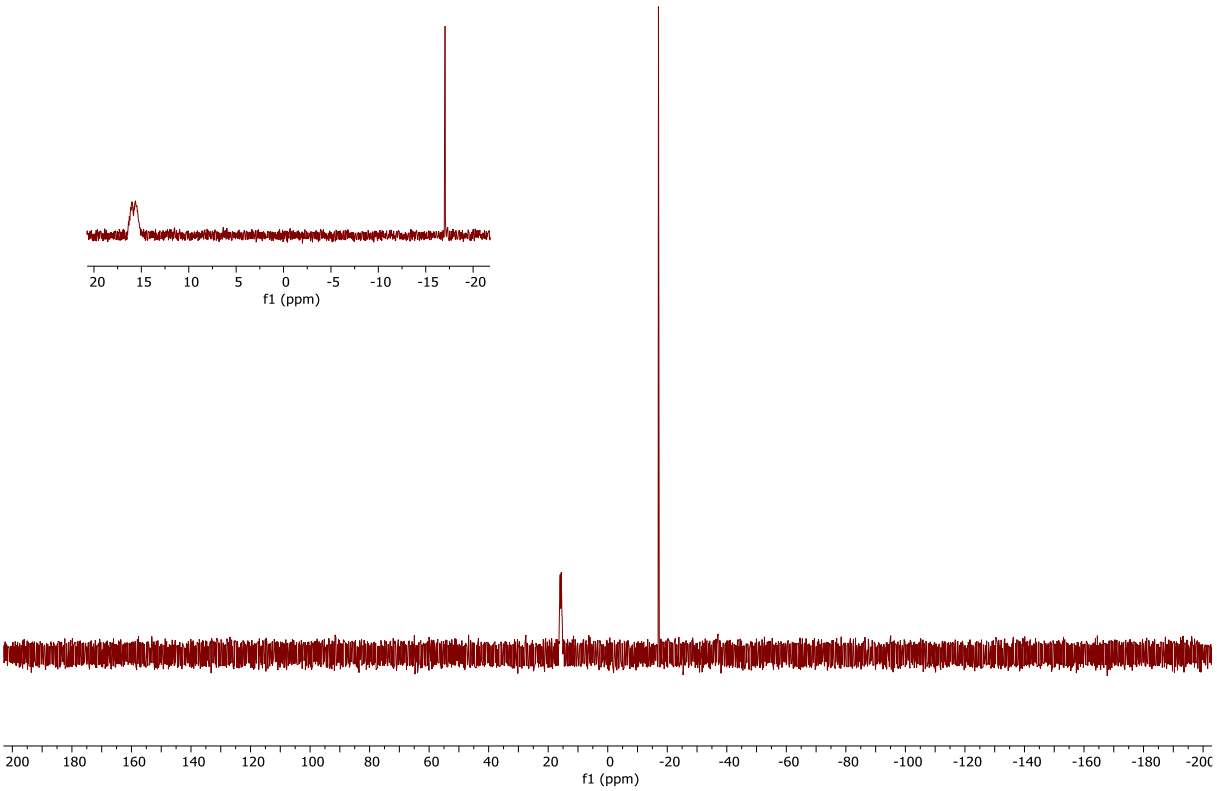

Figure S64. $^{31}P\{^{1}H\}$ NMR spectrum (162 MHz, $CDCl_3$) of **5**·BH_3.

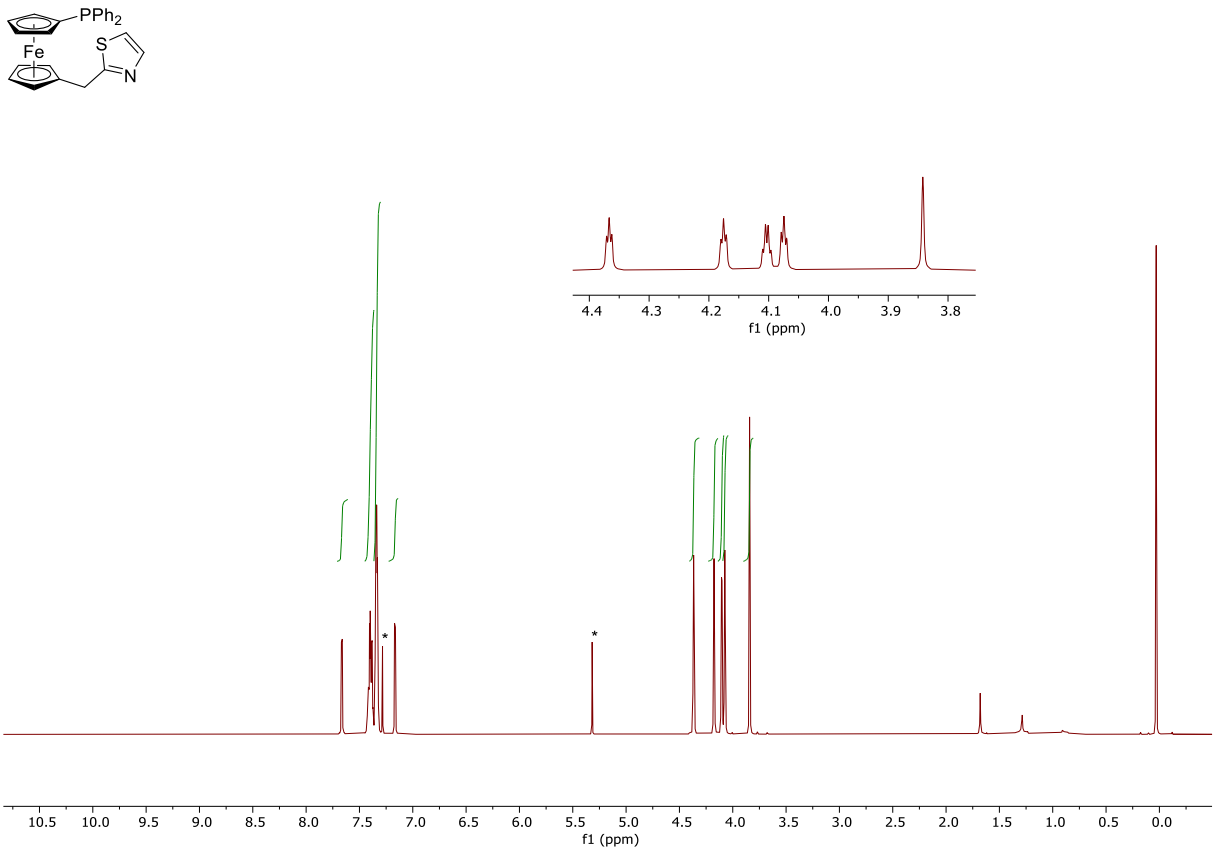

Figure S65. ^{1}H NMR spectrum (400 MHz, $CDCl_3$) of **5**.

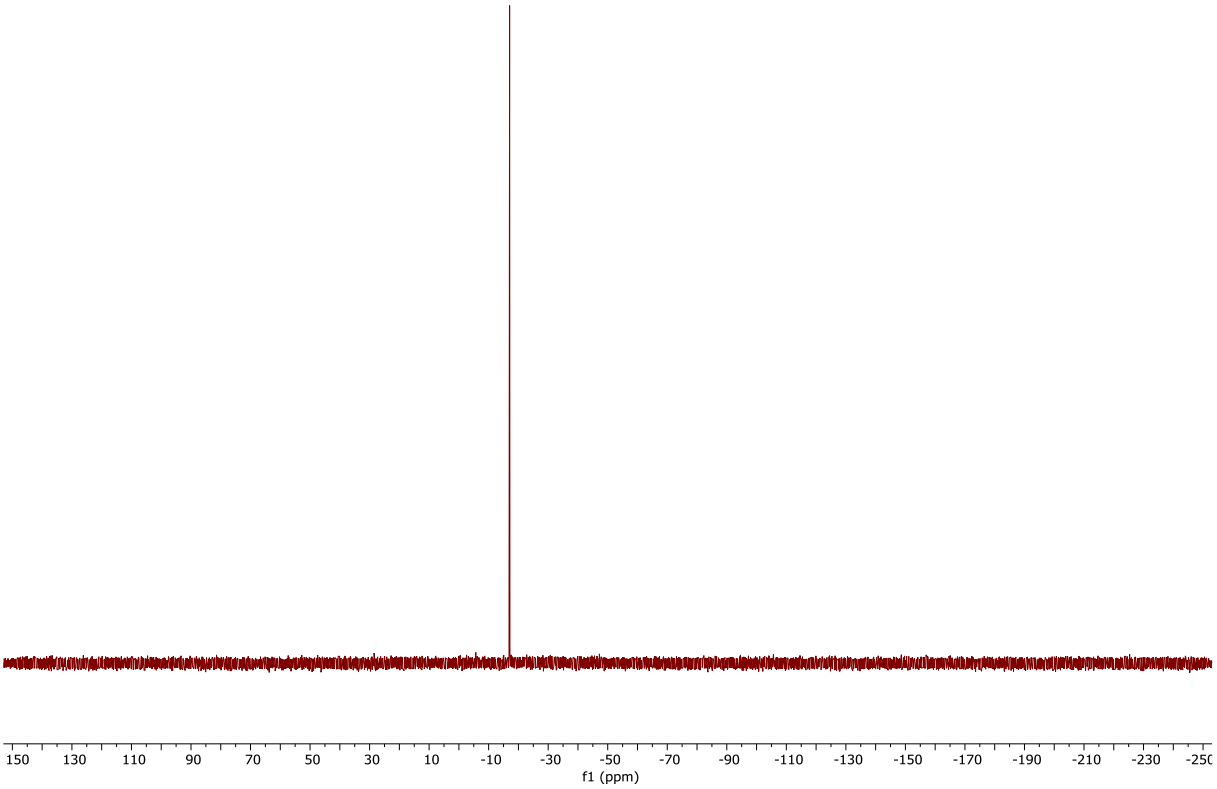

Figure S66. $^{31}P\{^{1}H\}$ NMR spectrum (162 MHz, $CDCl_3$) of **5**.

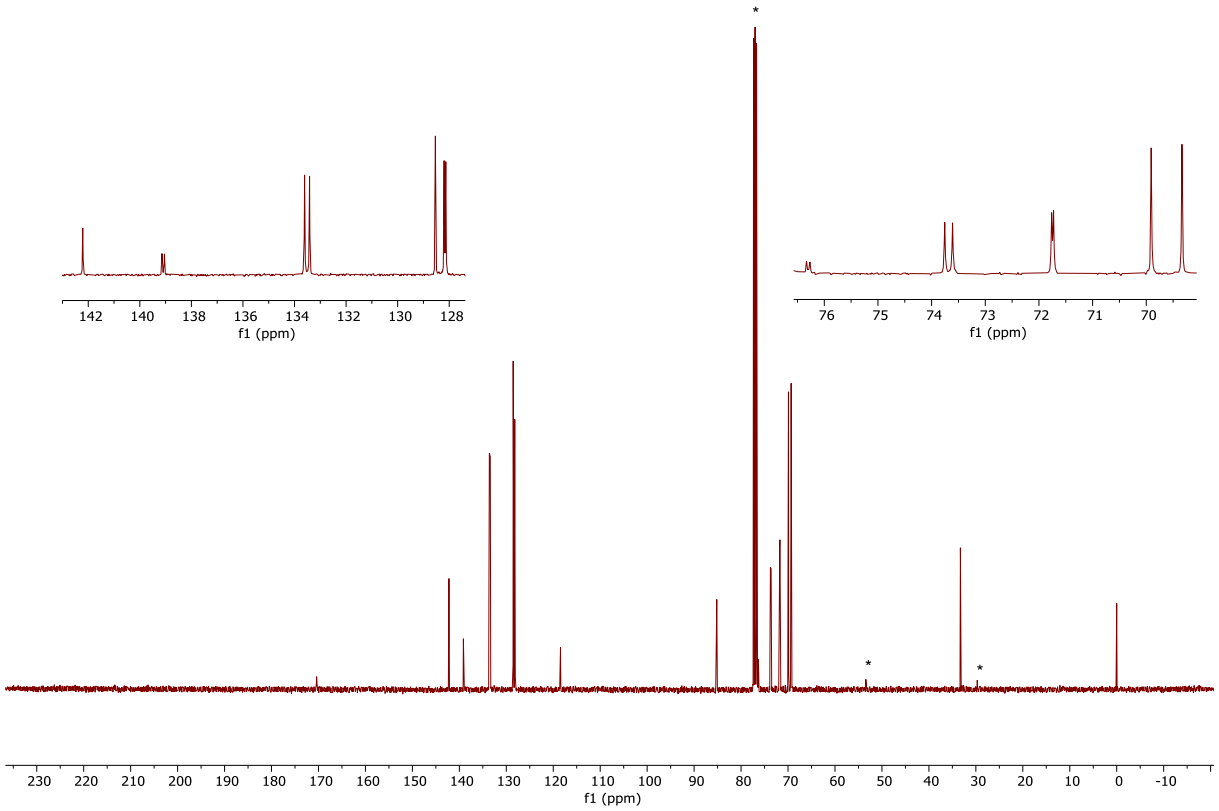

Figure S67. $^{13}C\{^{1}H\}$ NMR spectrum (101 MHz, $CDCl_3$) of **5**.

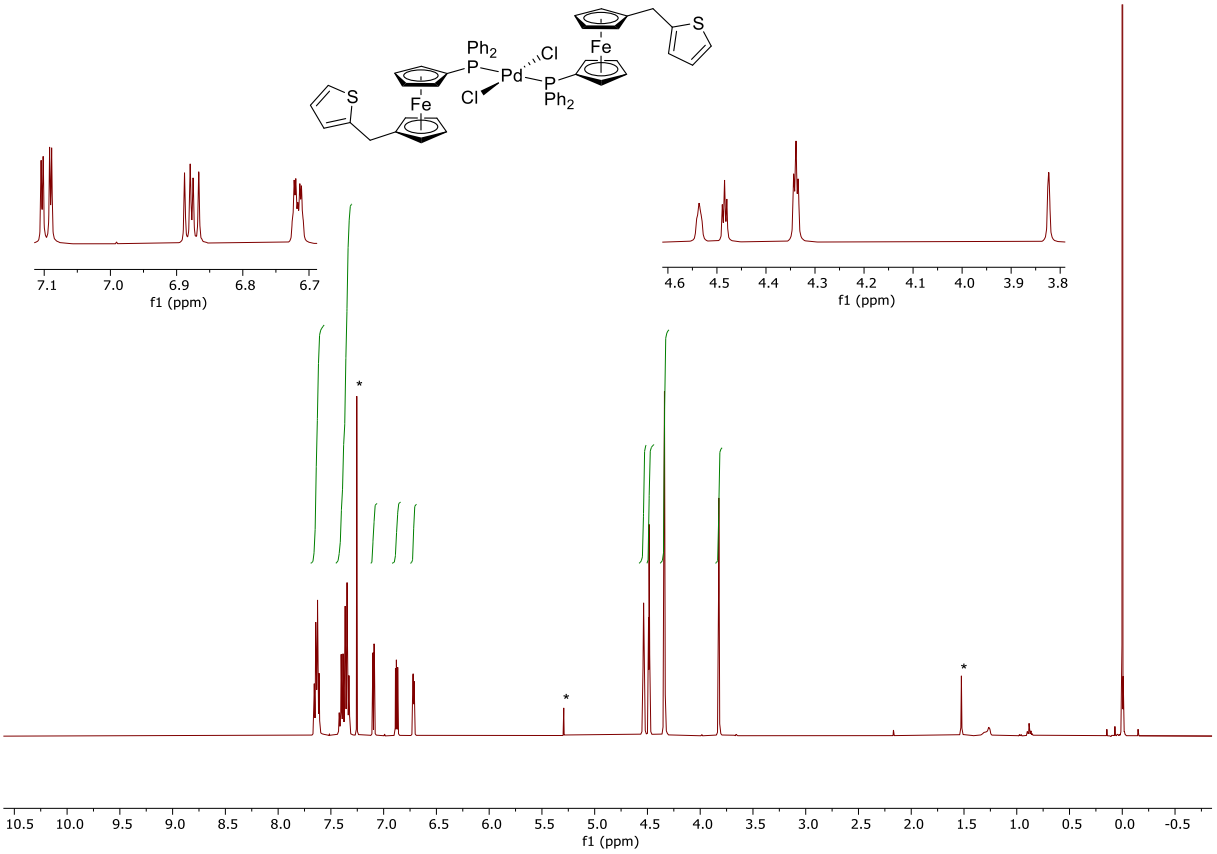

Figure S68. ^{1}H NMR spectrum (400 MHz, $CDCl_3$) of **25**.

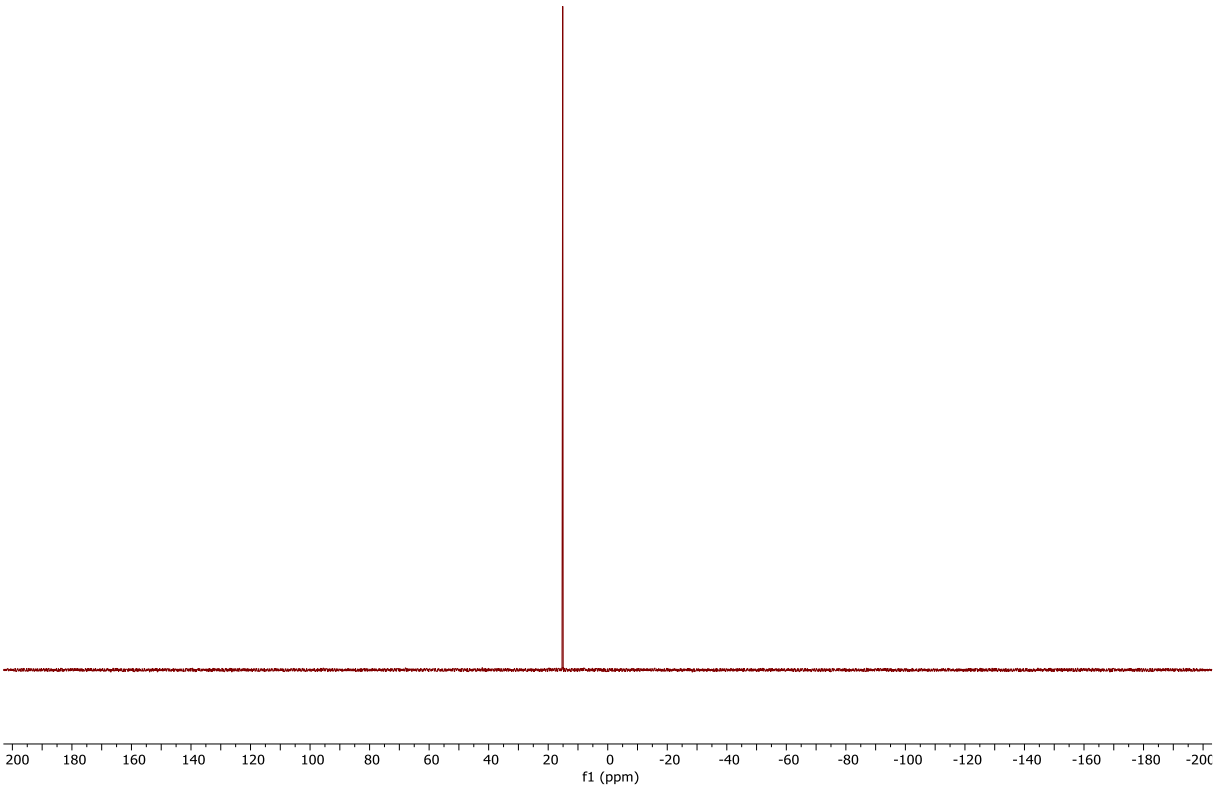

Figure S69. $^{31}P\{^{1}H\}$ NMR spectrum (162 MHz, $CDCl_3$) of **25**.

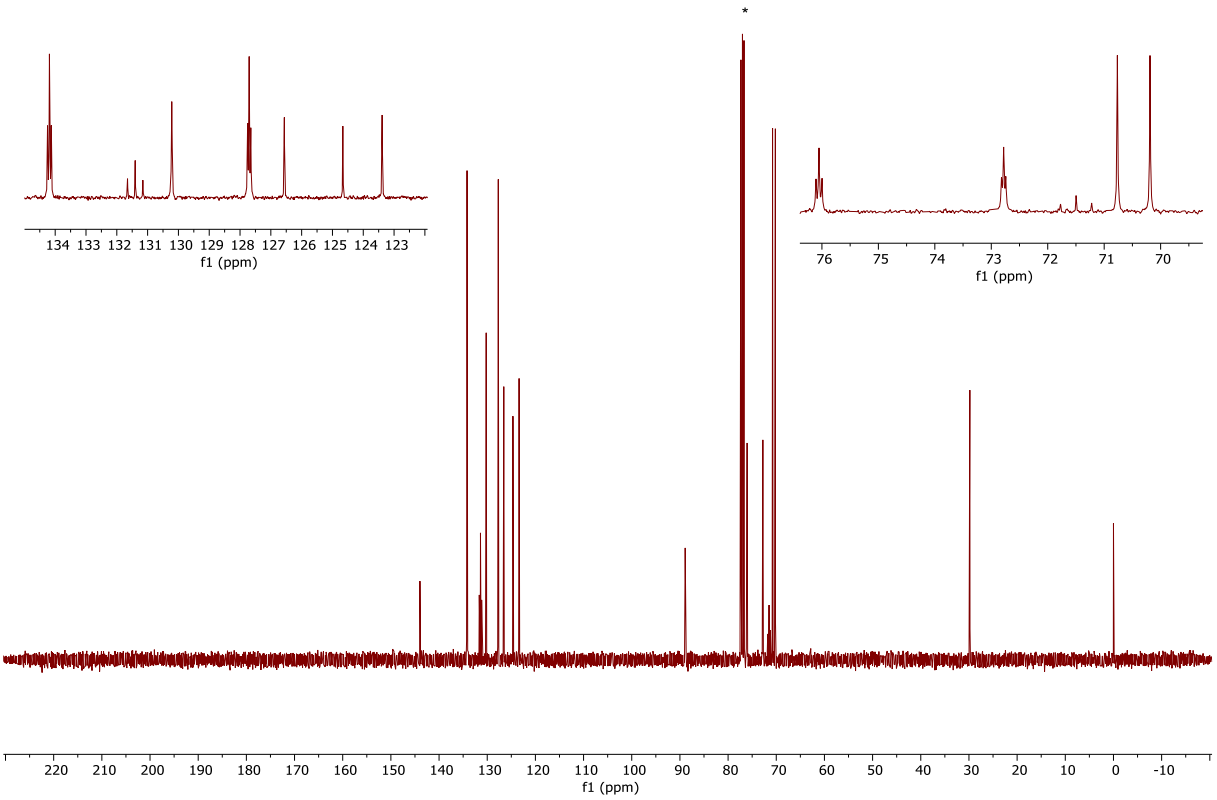

Figure S70. $^{13}C\{^{1}H\}$ NMR spectrum (101 MHz, $CDCl_3$) of **25**.

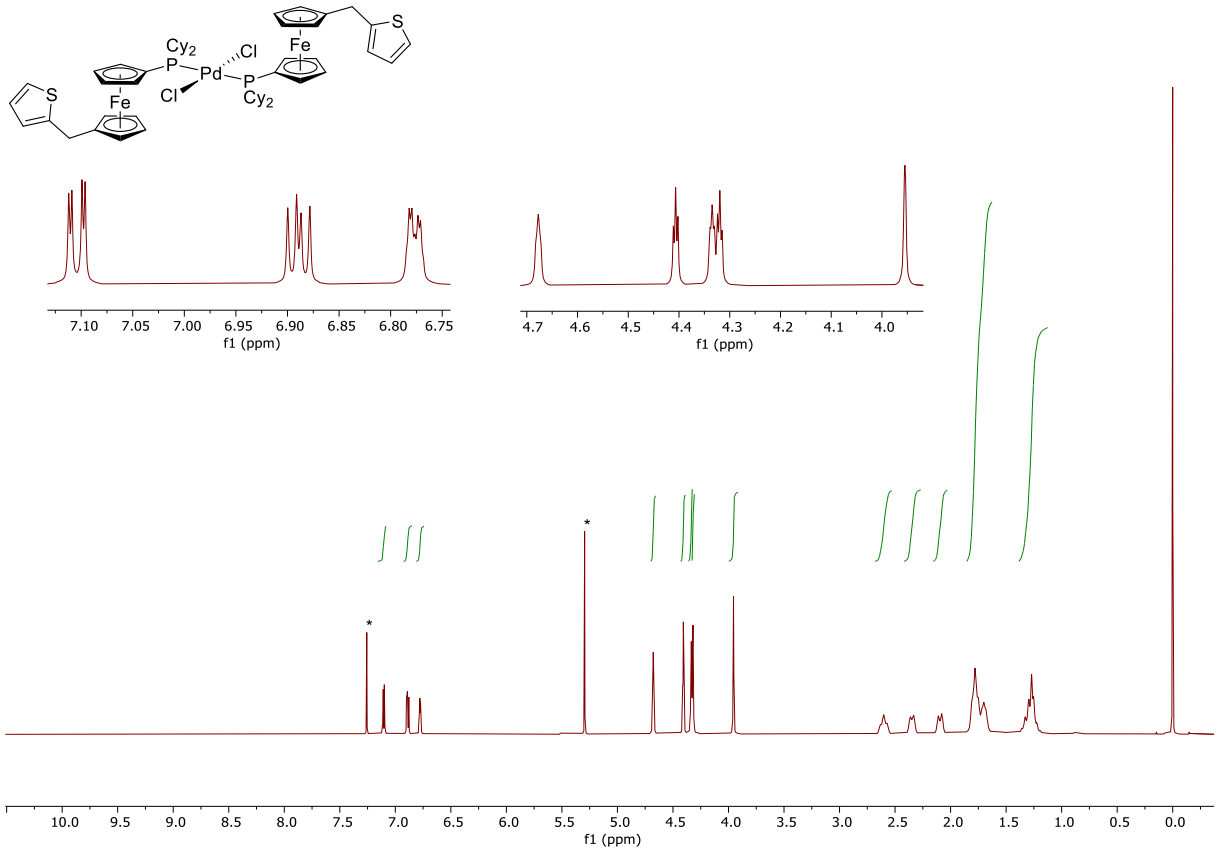

Figure S71. ^{1}H NMR spectrum (400 MHz, $CDCl_3$) of **26**.

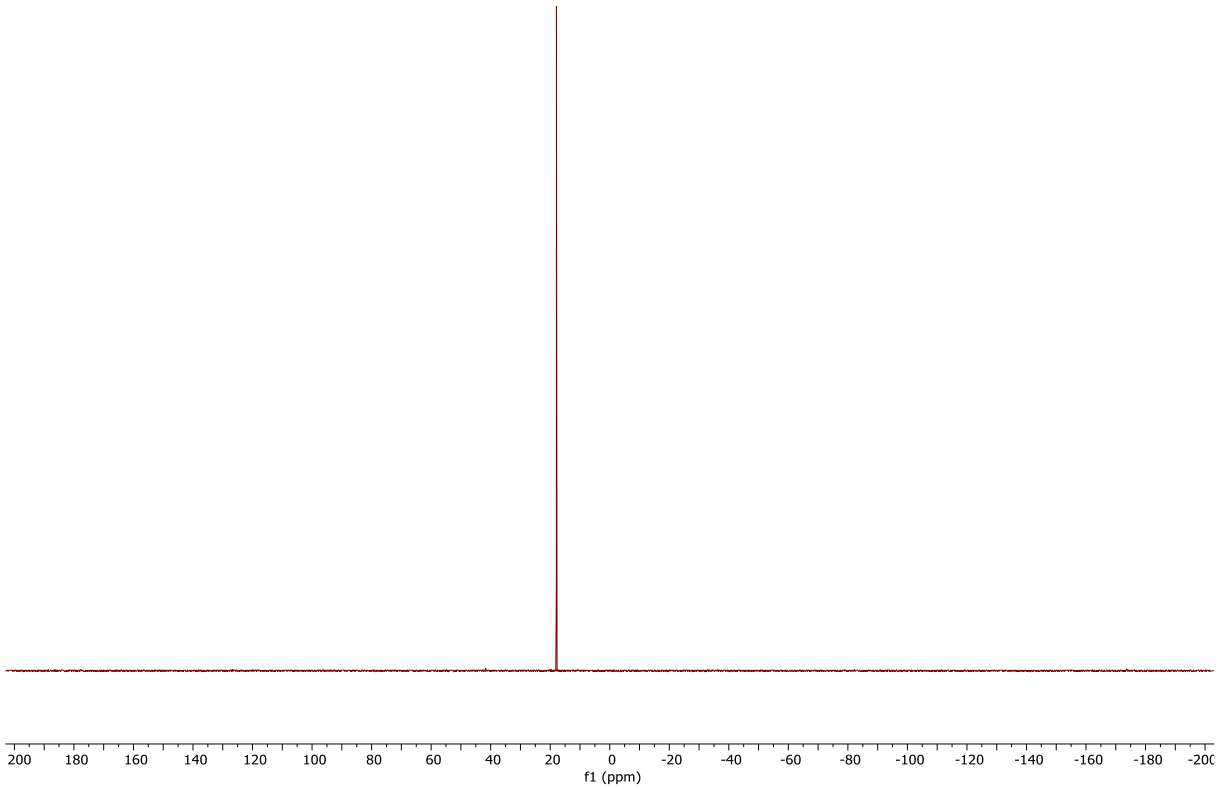

Figure S72. $^{31}P\{^{1}H\}$ NMR spectrum (162 MHz, $CDCl_3$) of **26**.

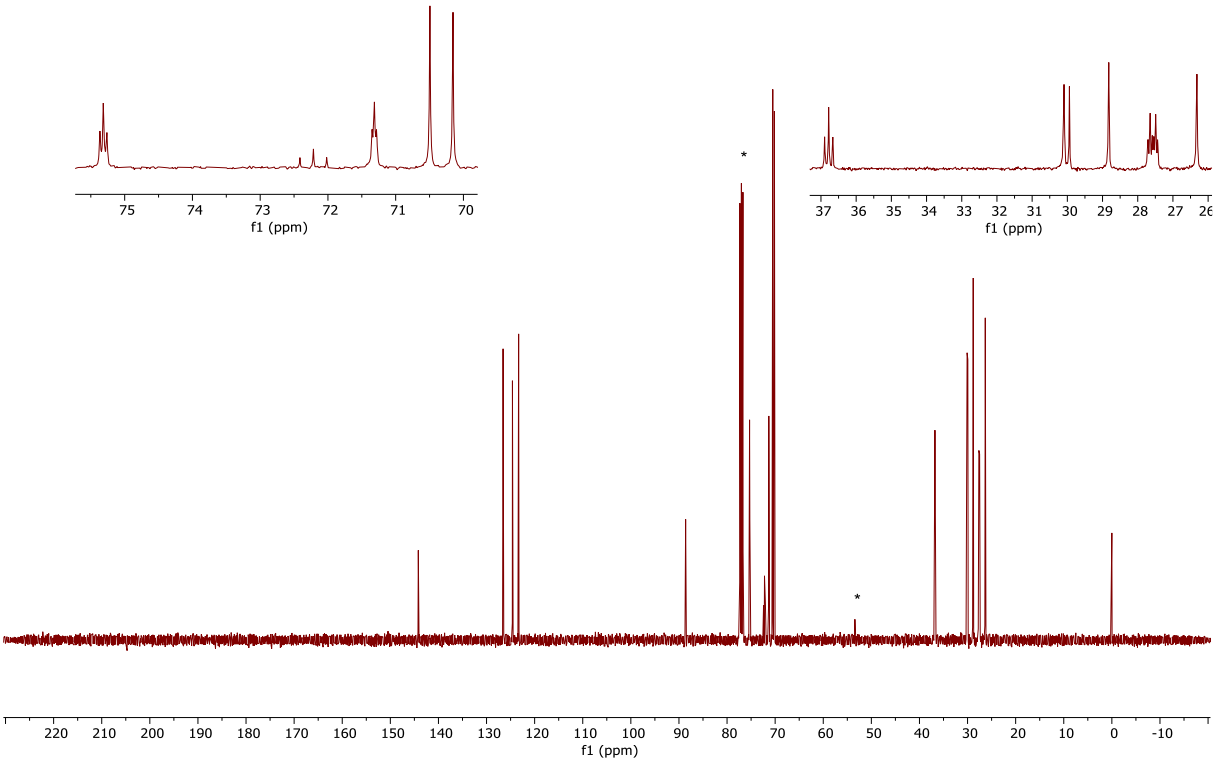

Figure S73. $^{13}C\{^{1}H\}$ NMR spectrum (101 MHz, $CDCl_3$) of **26**.

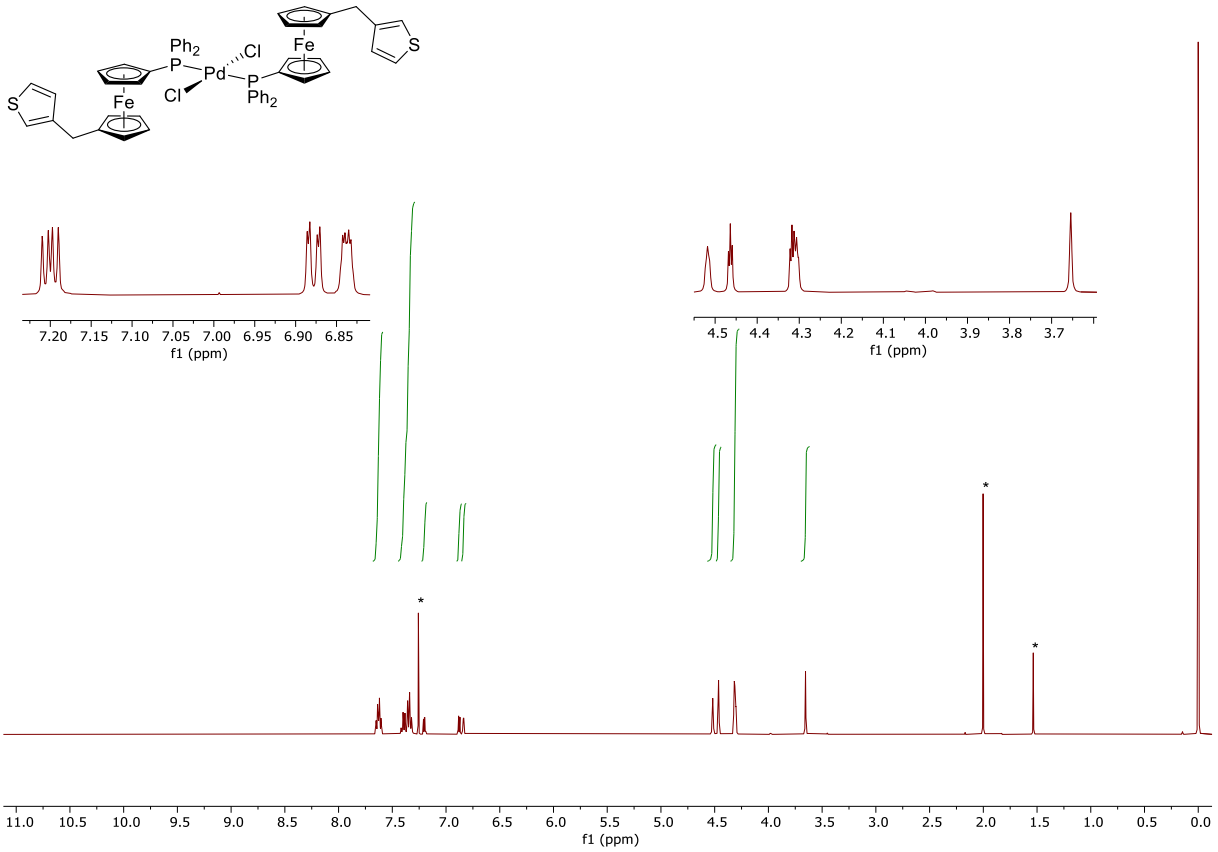

Figure S74. ^{1}H NMR spectrum (400 MHz, $CDCl_3$) of **27**.

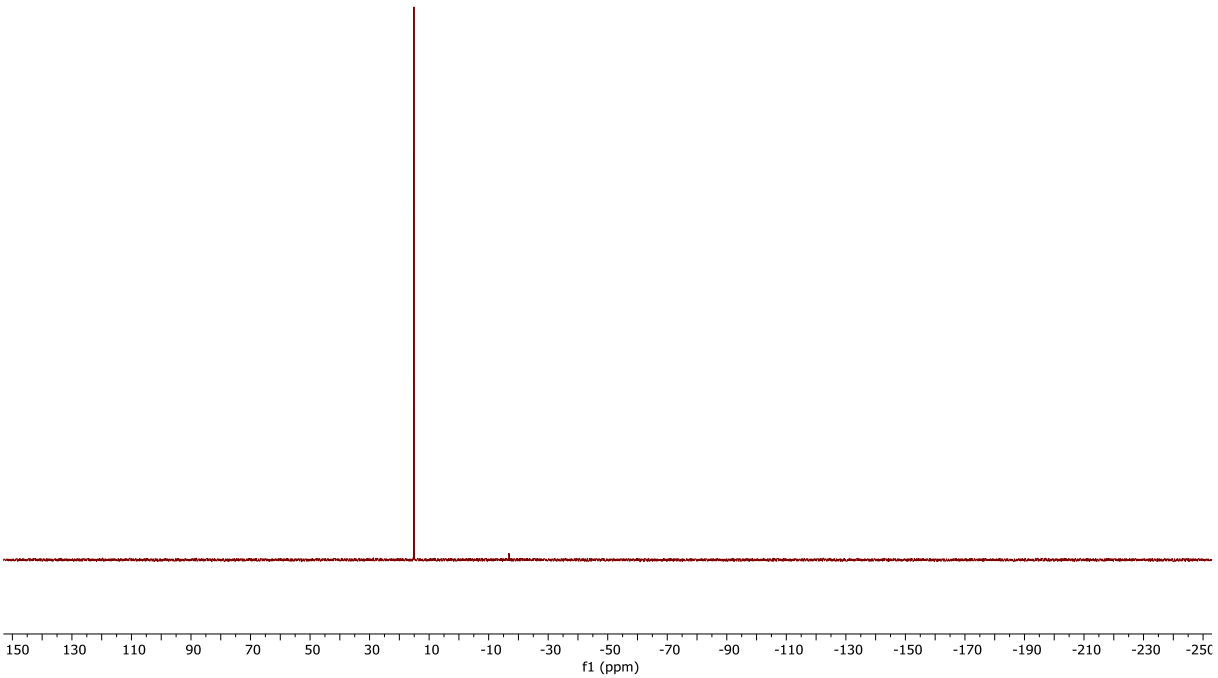

Figure S75. $^{31}P\{^{1}H\}$ NMR spectrum (162 MHz, $CDCl_3$) of **27**.

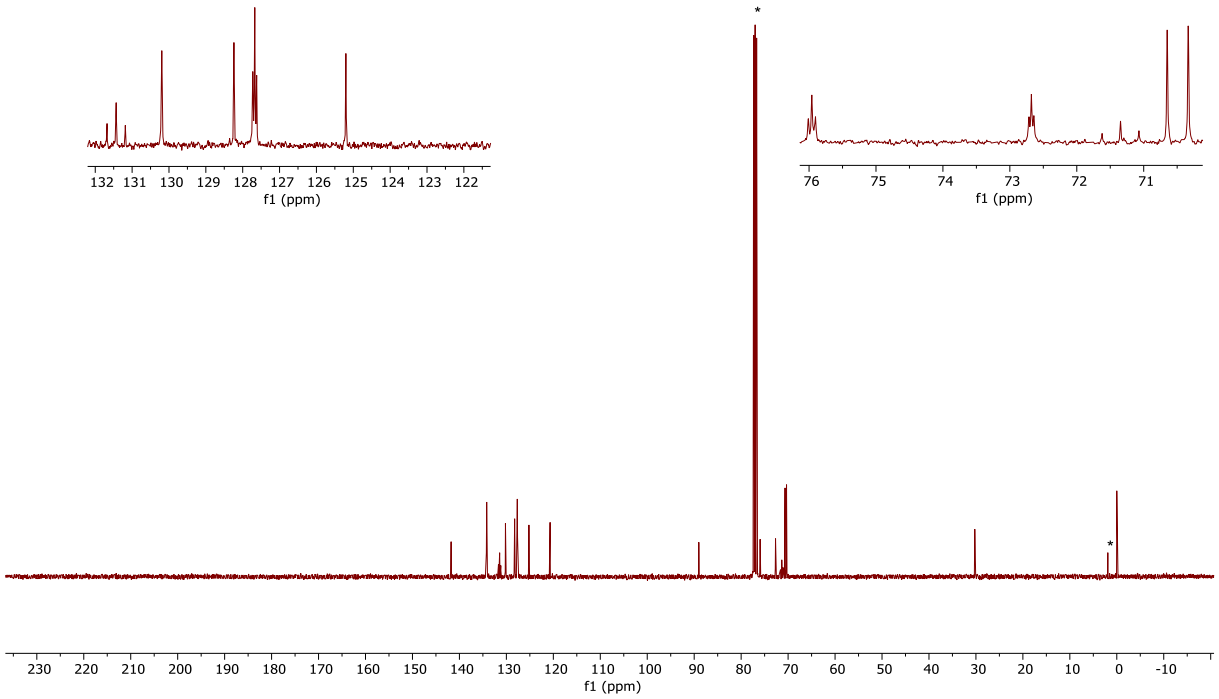

Figure S76. $^{13}C\{^{1}H\}$ NMR spectrum (101 MHz, $CDCl_3$) of **27**.

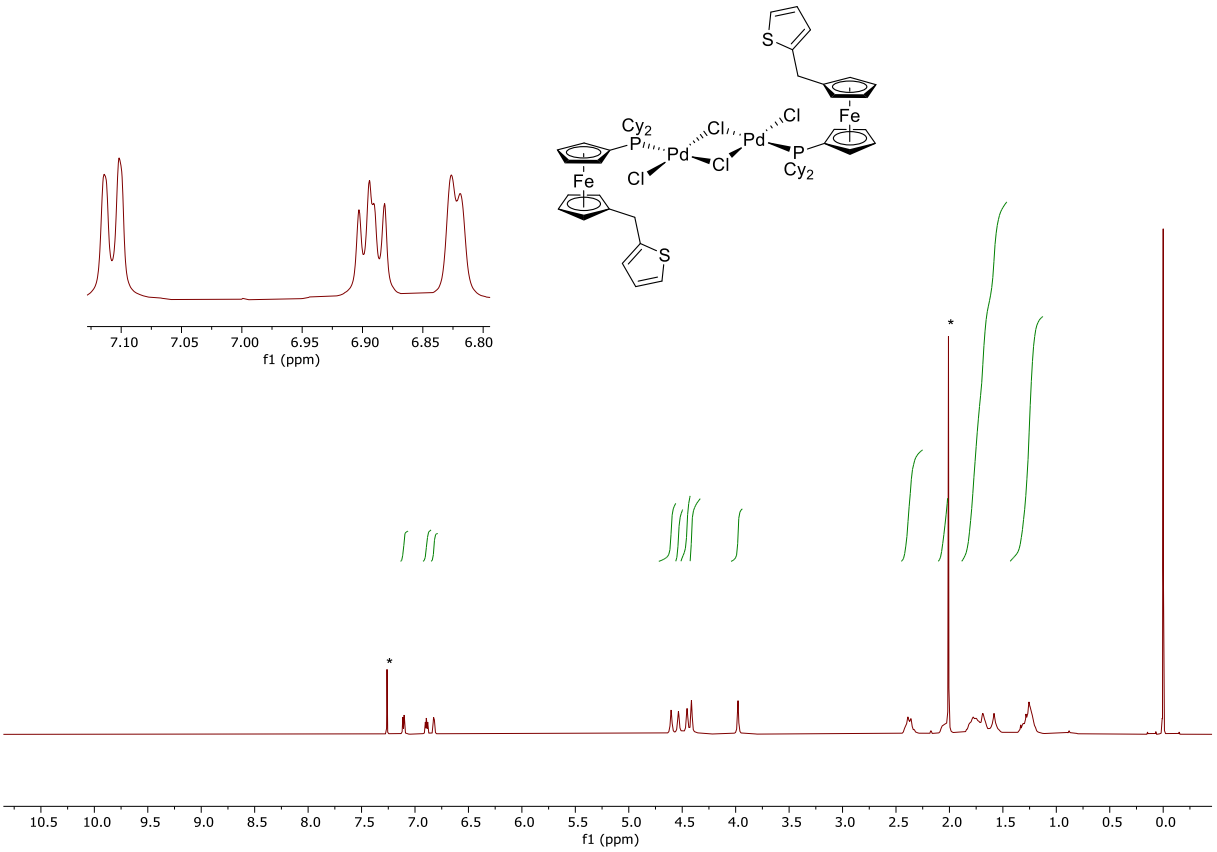

Figure S77. ^{1}H NMR spectrum (400 MHz, $CDCl_3$) of **28**.

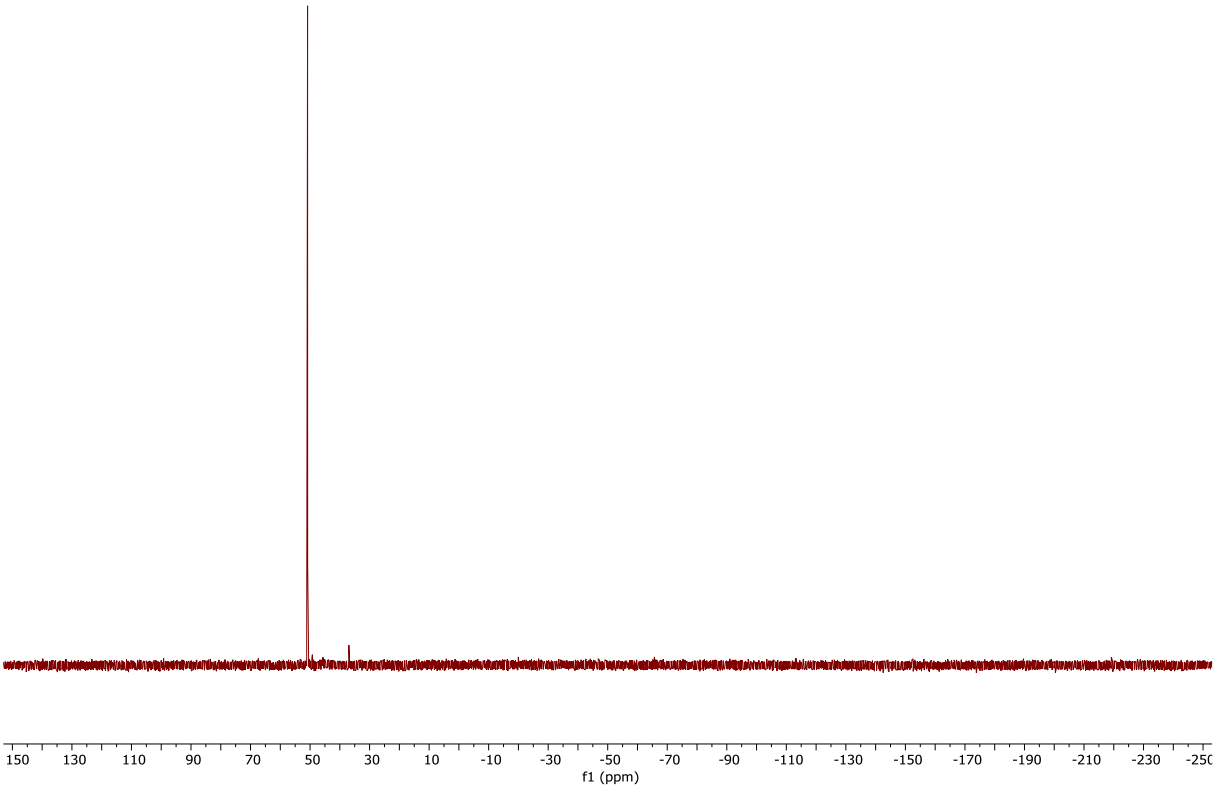

Figure S78. $^{31}P\{^{1}H\}$ NMR spectrum (162 MHz, $CDCl_3$) of **28**.

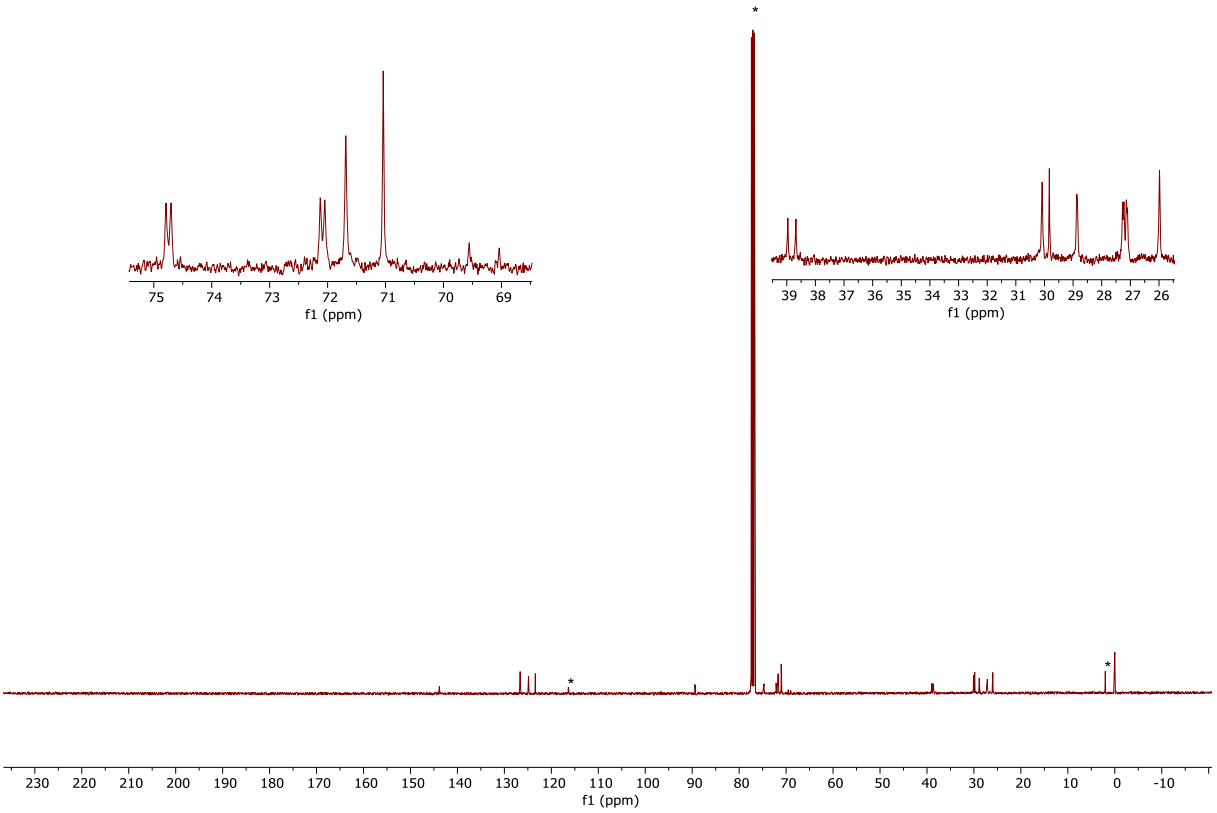

Figure S79. $^{13}C\{^{1}H\}$ NMR spectrum (101 MHz, $CDCl_3$) of **28**.

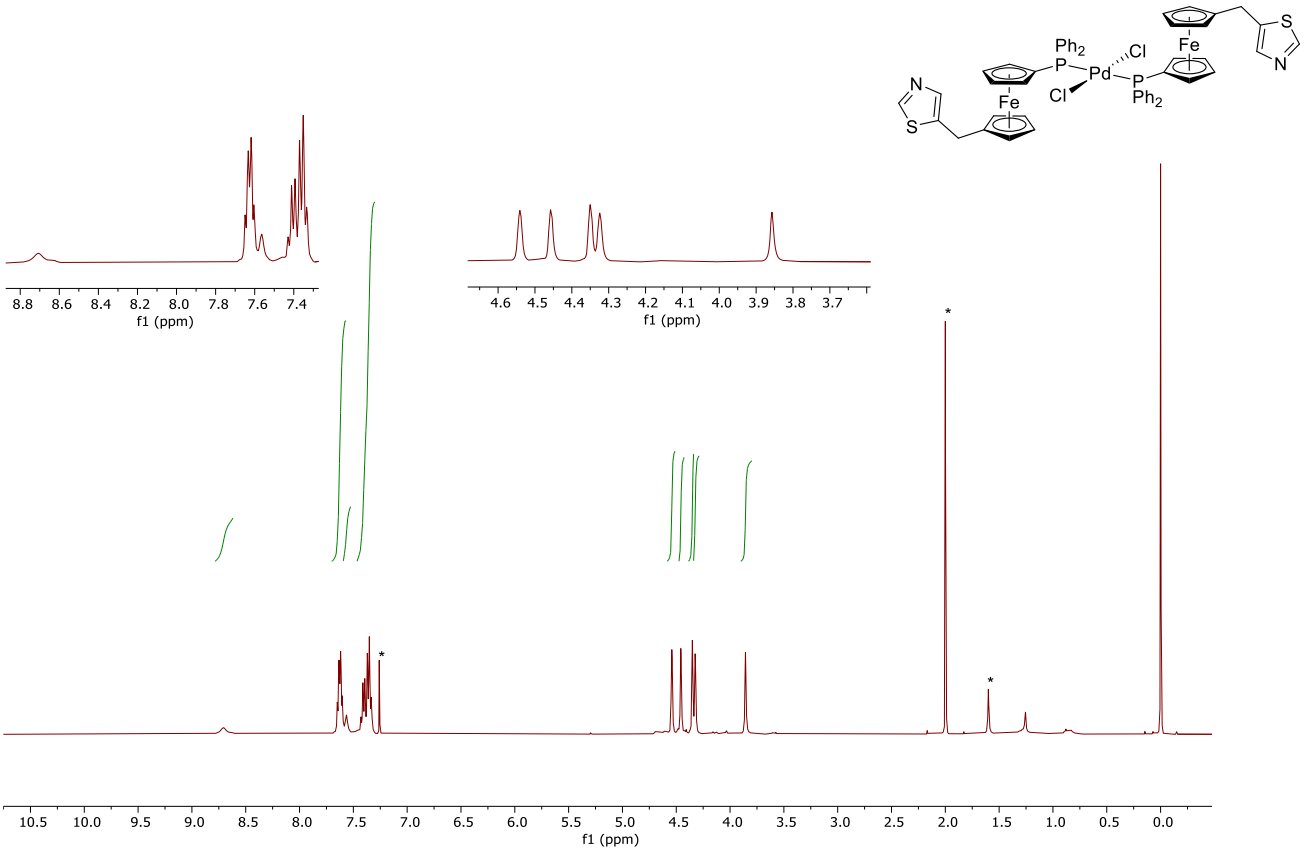

Figure S80. ^{1}H NMR spectrum (400 MHz, $CDCl_3$) of **29**.

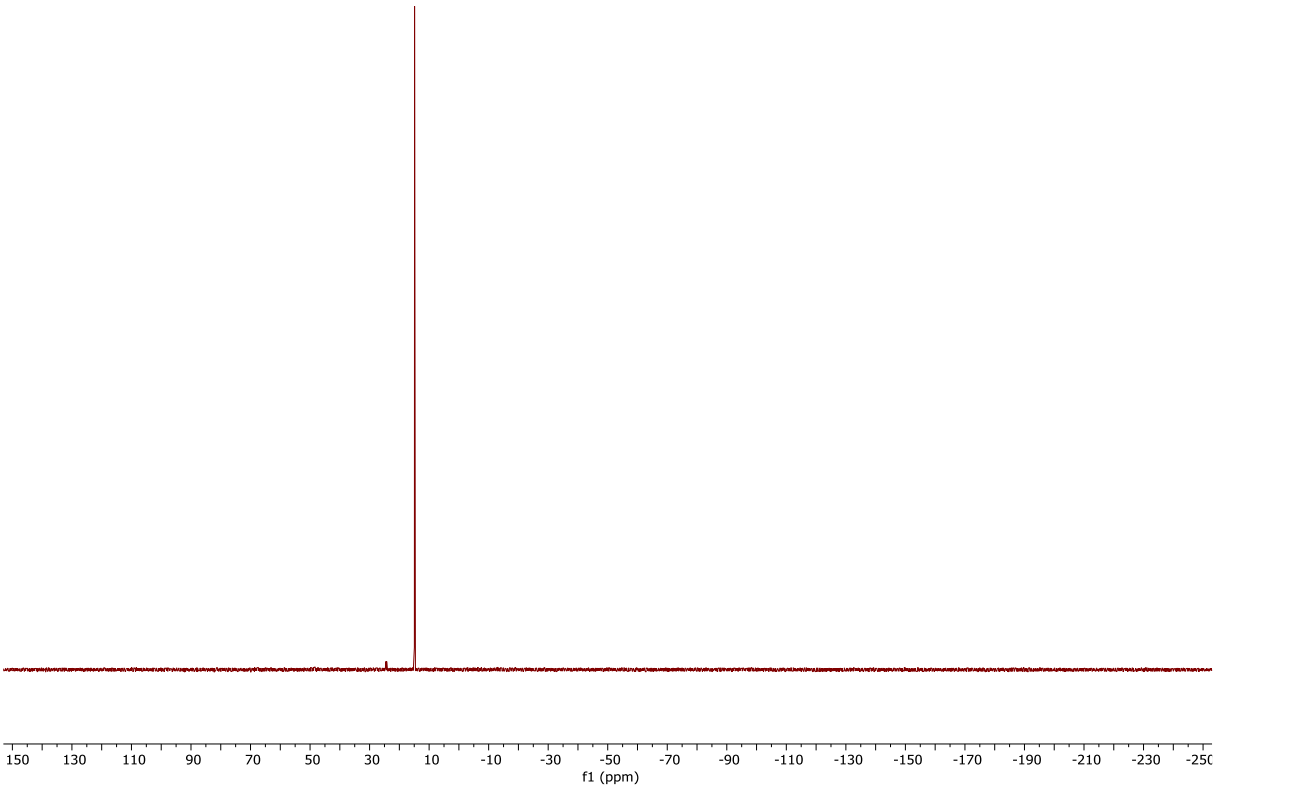

Figure S81. $^{31}P\{^{1}H\}$ NMR spectrum (162 MHz, $CDCl_3$) of **29**.

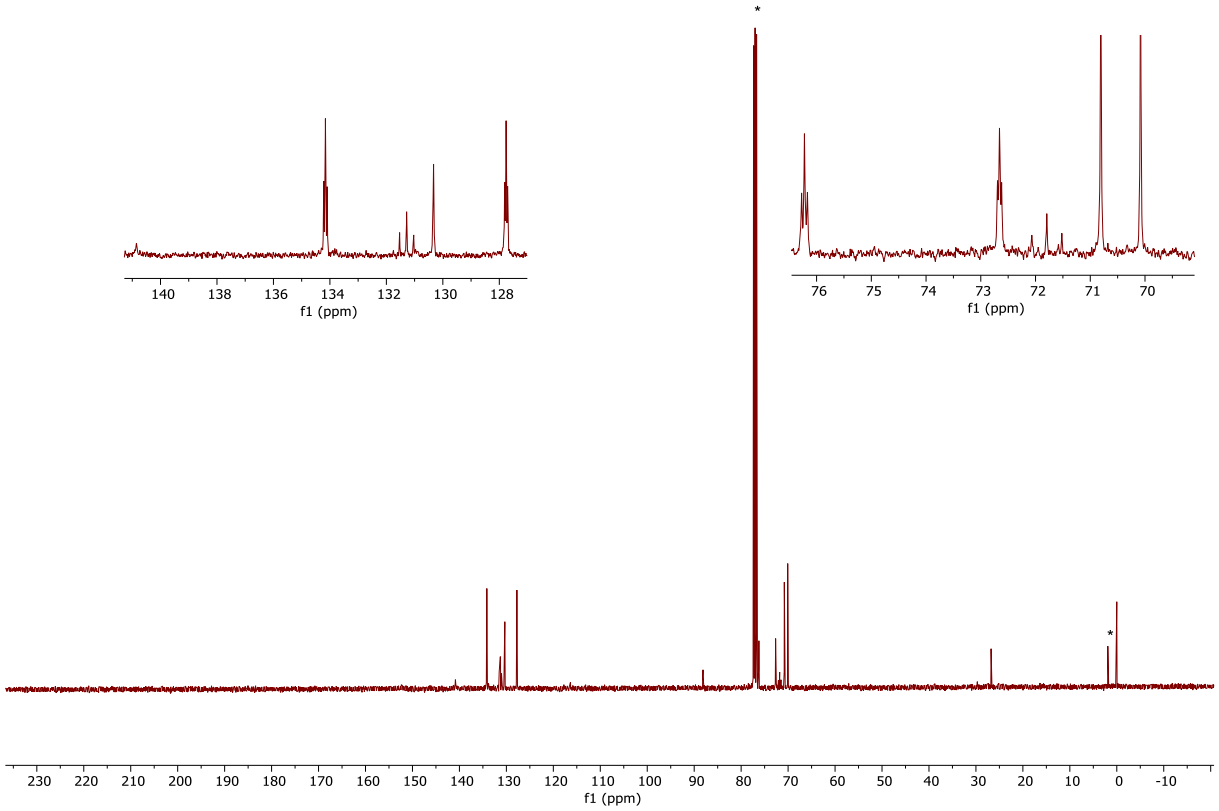

Figure S82. $^{13}C\{^{1}H\}$ NMR spectrum (101 MHz, $CDCl_3$) of **29**.

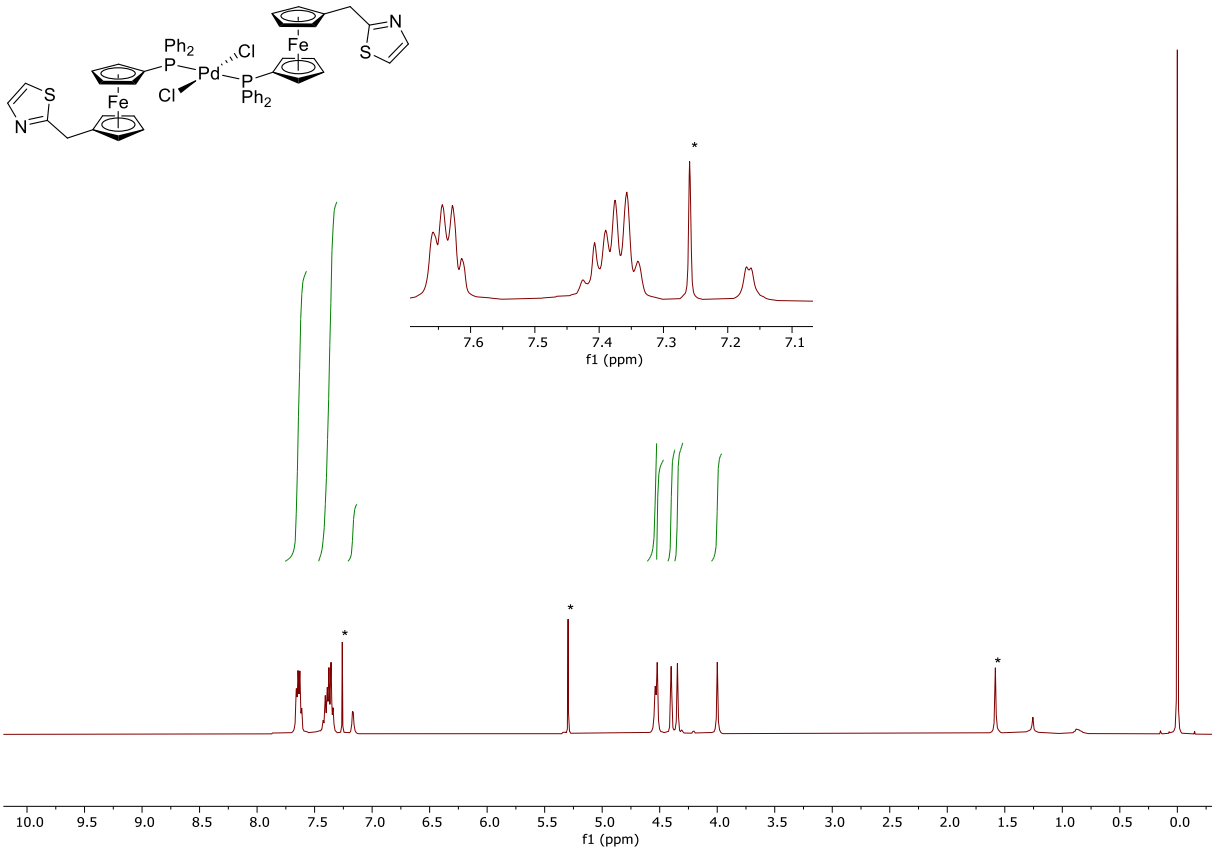

Figure S83. ^{1}H NMR spectrum (400 MHz, $CDCl_3$) of **30**.

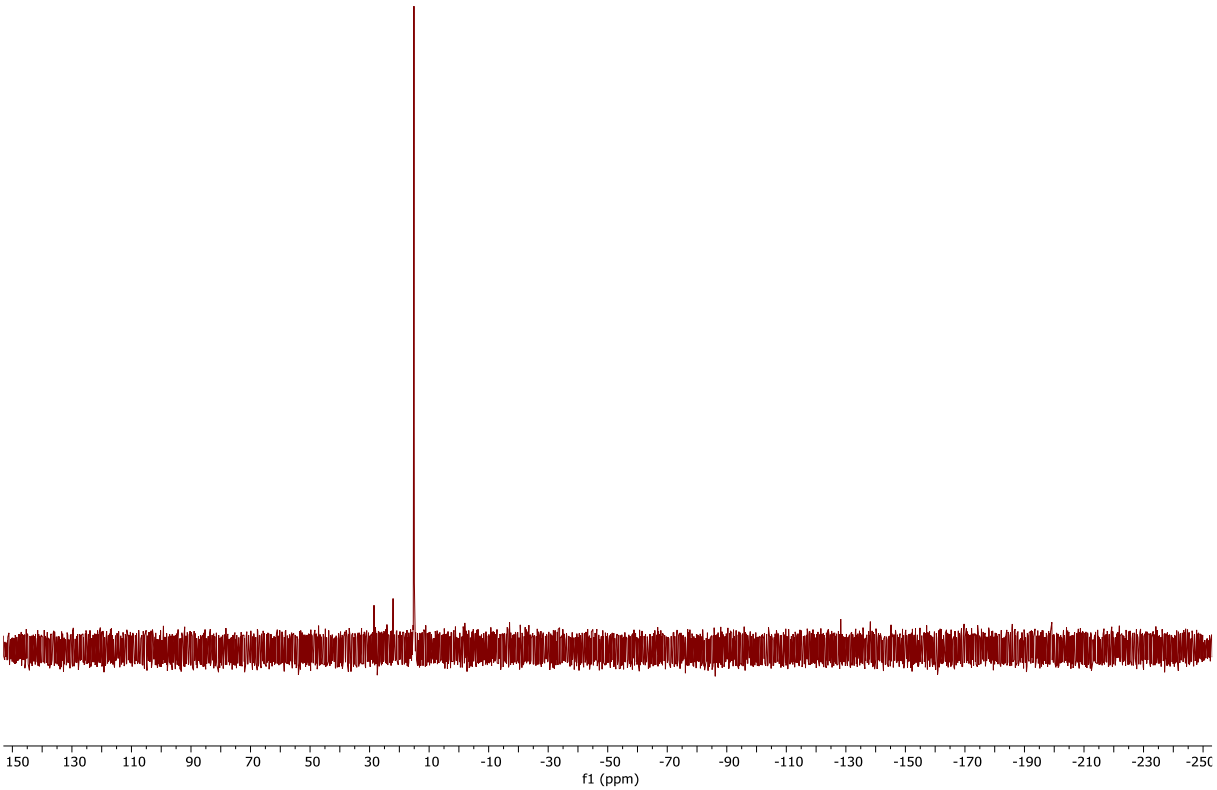

Figure S84. $^{31}P\{^{1}H\}$ NMR spectrum (162 MHz, $CDCl_3$) of **30**.

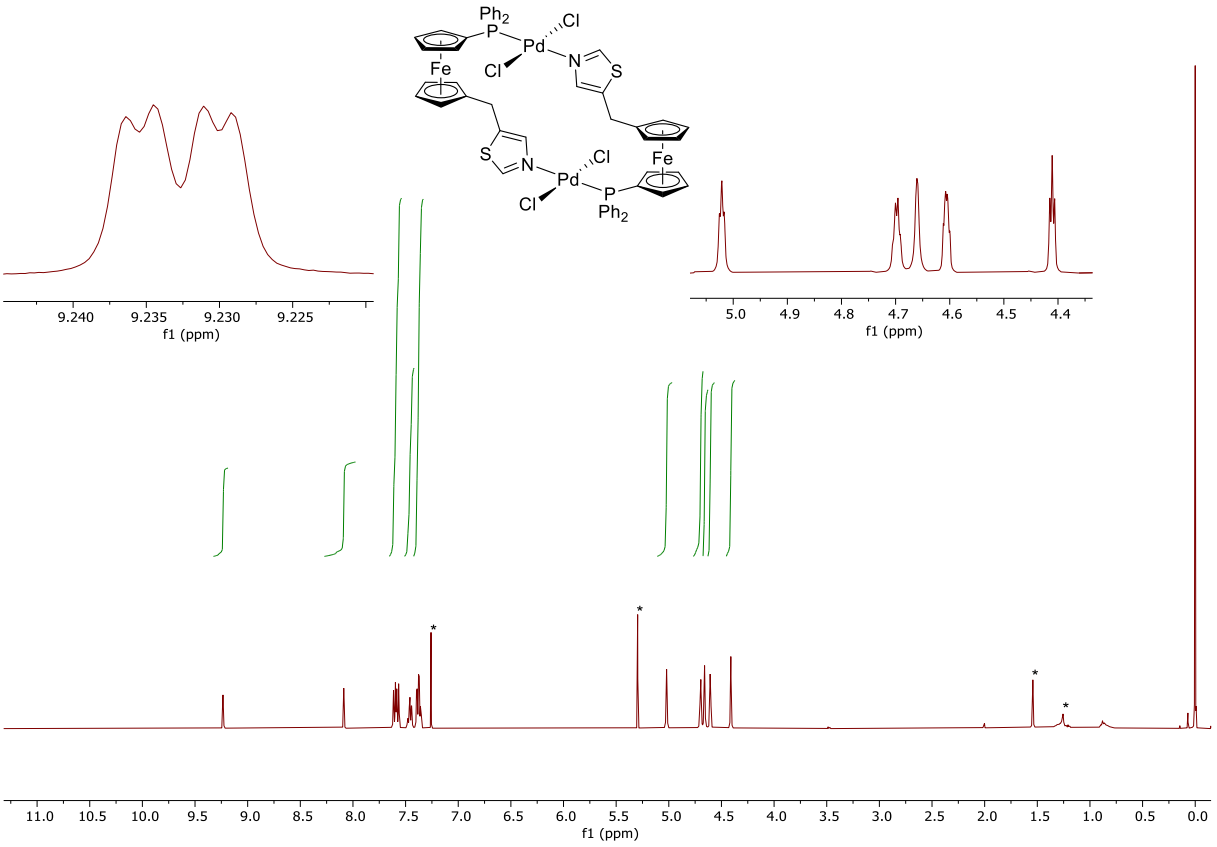

Figure S85. ^{1}H NMR spectrum (400 MHz, $CDCl_3$) of **31**.

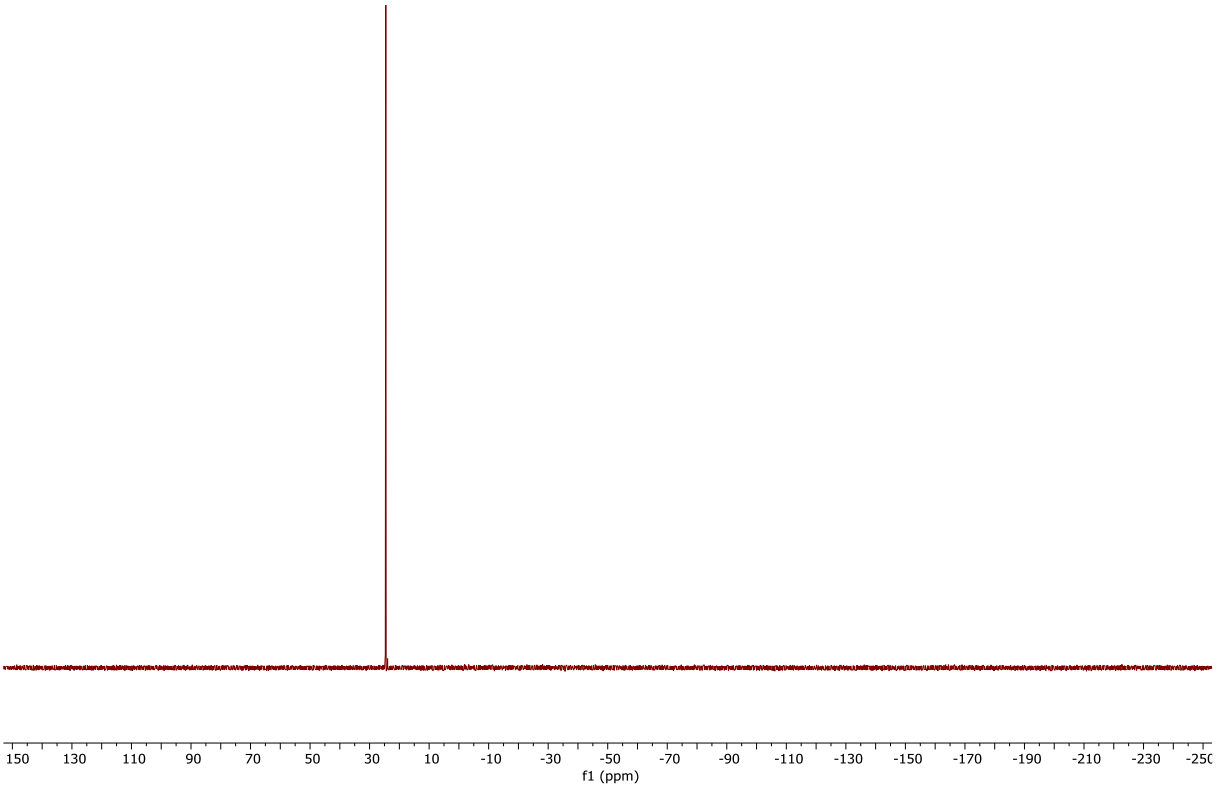

Figure S86. $^{31}P\{^{1}H\}$ NMR spectrum (162 MHz, $CDCl_3$) of **31**.

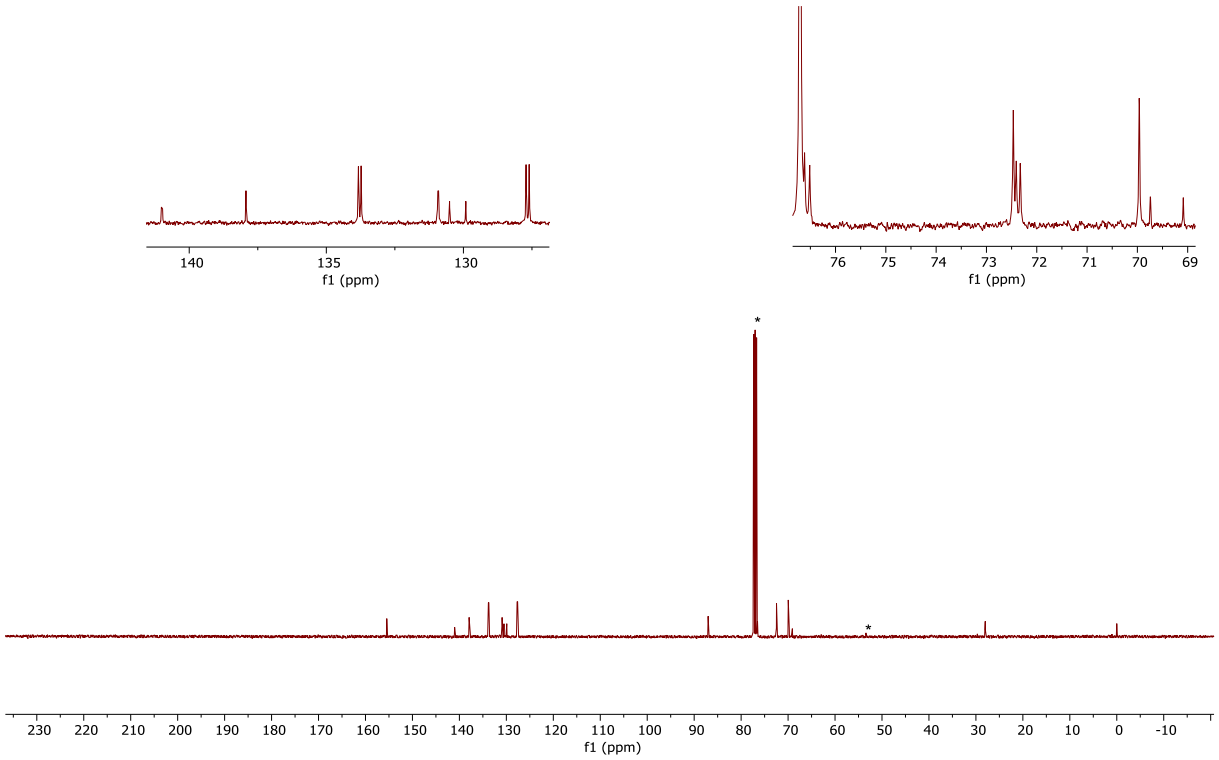

Figure S87. $^{13}C\{^{1}H\}$ NMR spectrum (101 MHz, $CDCl_3$) of **31**.

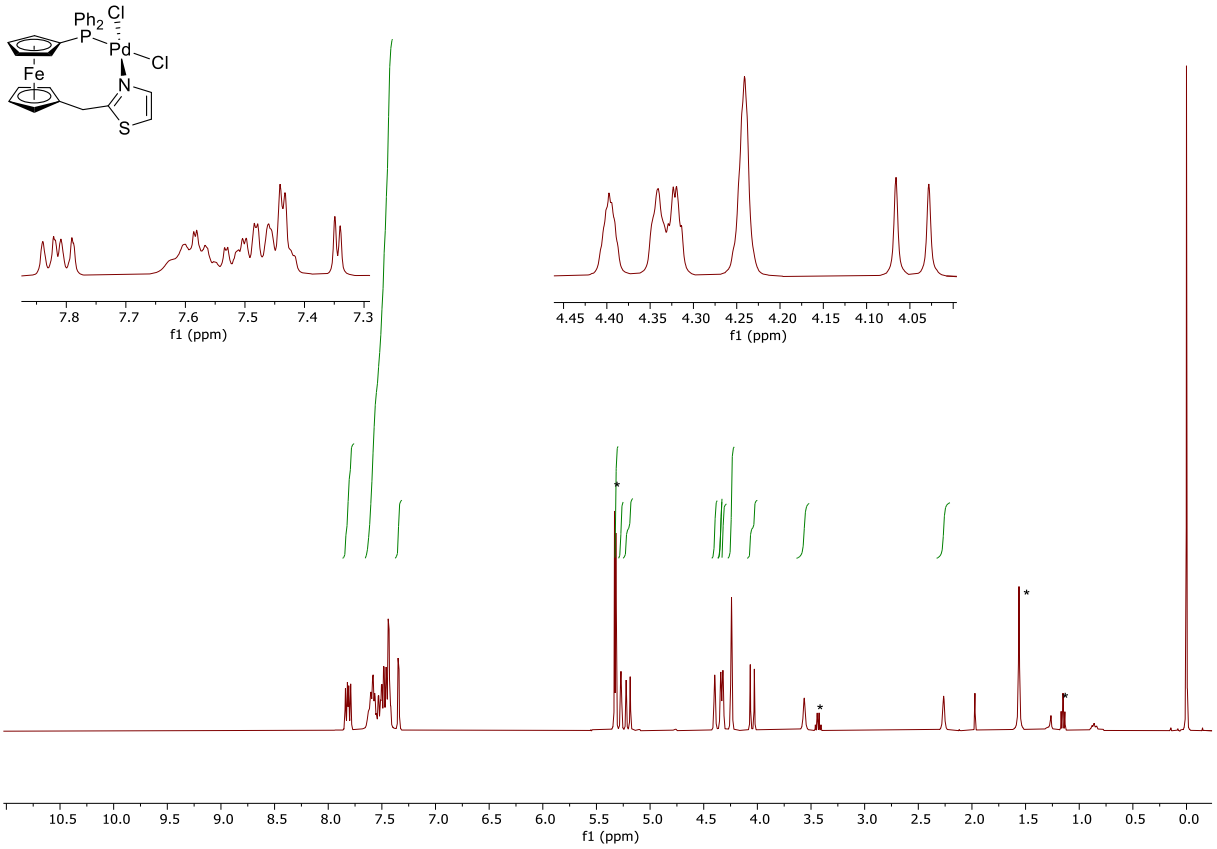

Figure S88. ^{1}H NMR spectrum (400 MHz, CD_2Cl_2) of **32**.

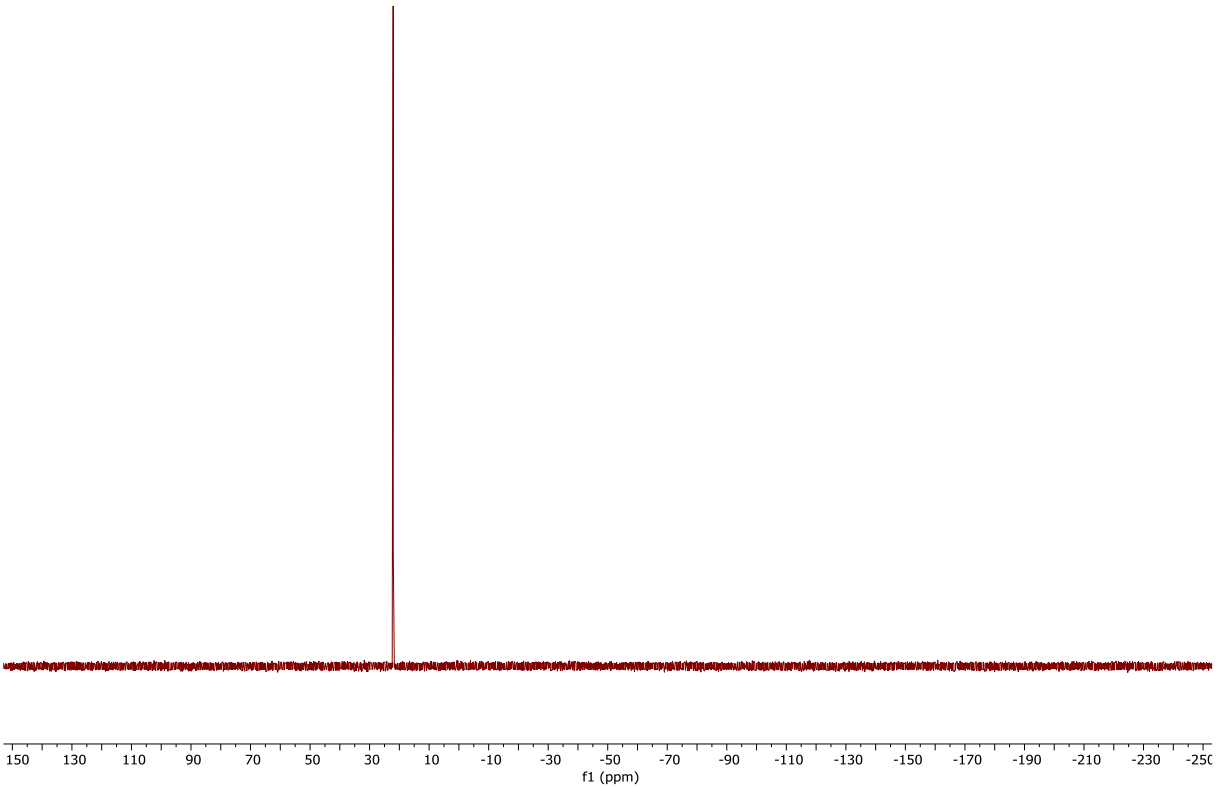

Figure S89. $^{31}P\{^{1}H\}$ NMR spectrum (162 MHz, CD_2Cl_2) of **32**.

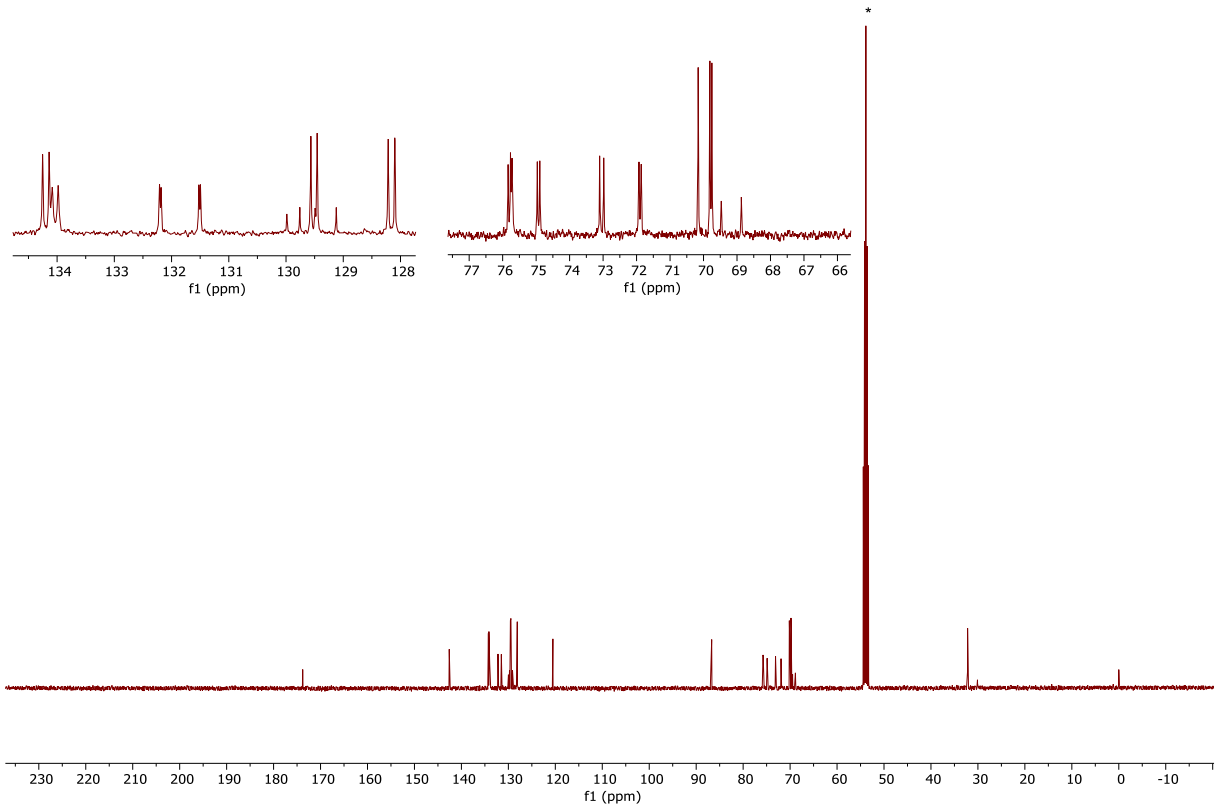

Figure S90. $^{13}C\{^{1}H\}$ NMR spectrum (101 MHz, CD_2Cl_2) of **32**.

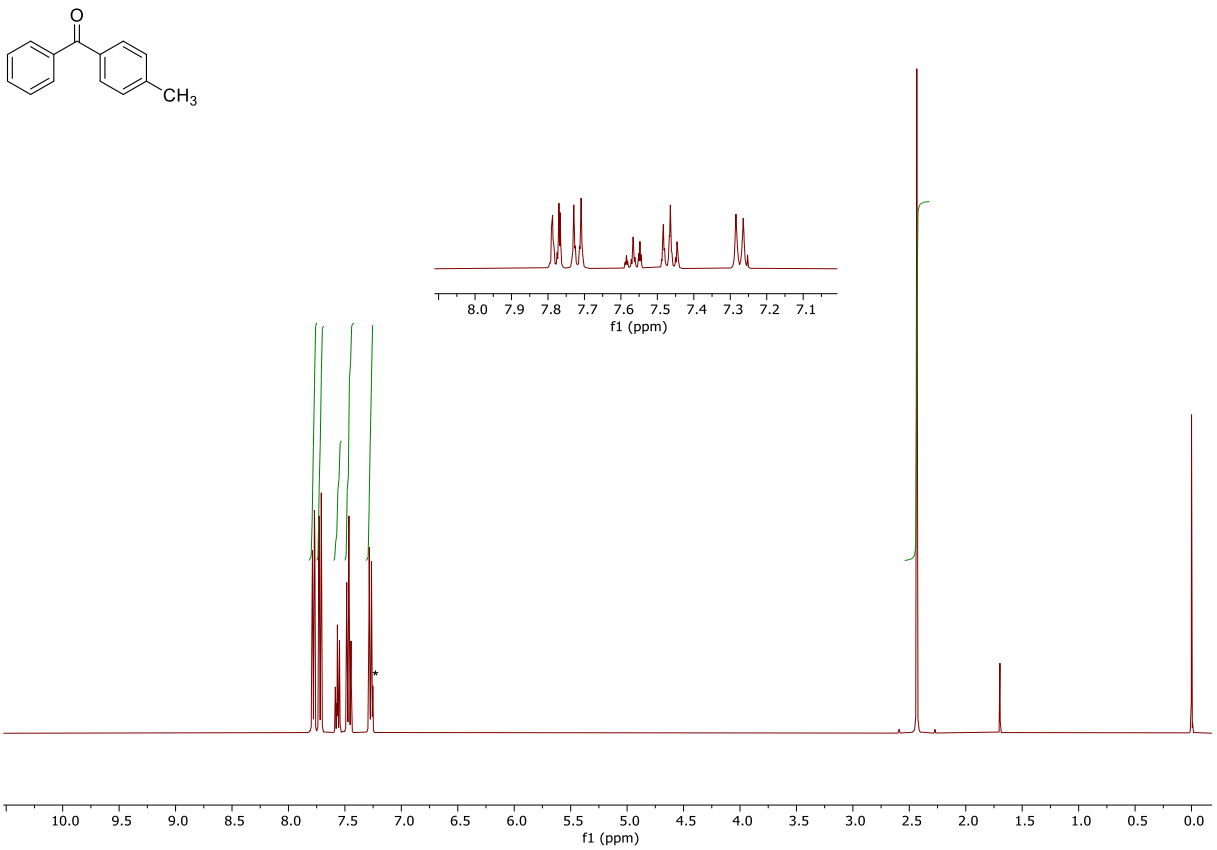

Figure S91. ^{1}H NMR spectrum (400 MHz, $CDCl_3$) of **35-CH$_3$**.

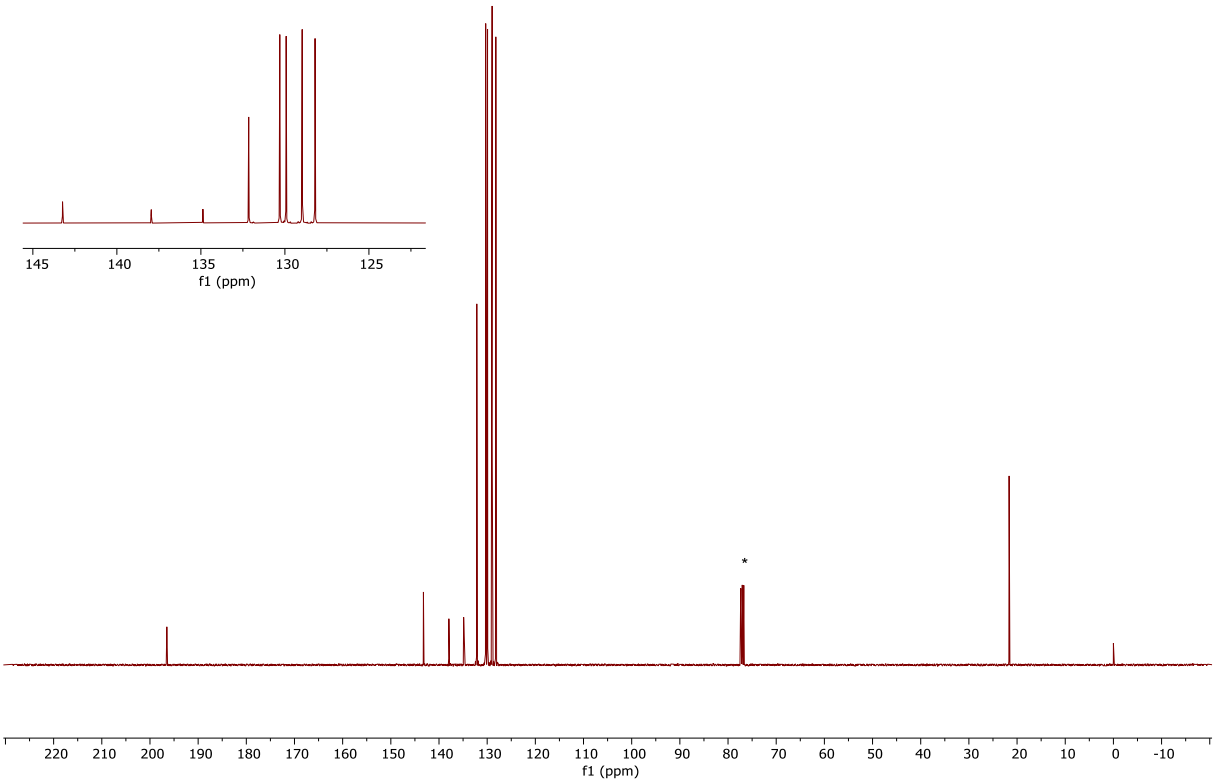

Figure S92. $^{13}C\{^{1}H\}$ NMR spectrum (101 MHz, $CDCl_3$) of **35-CH$_3$**.

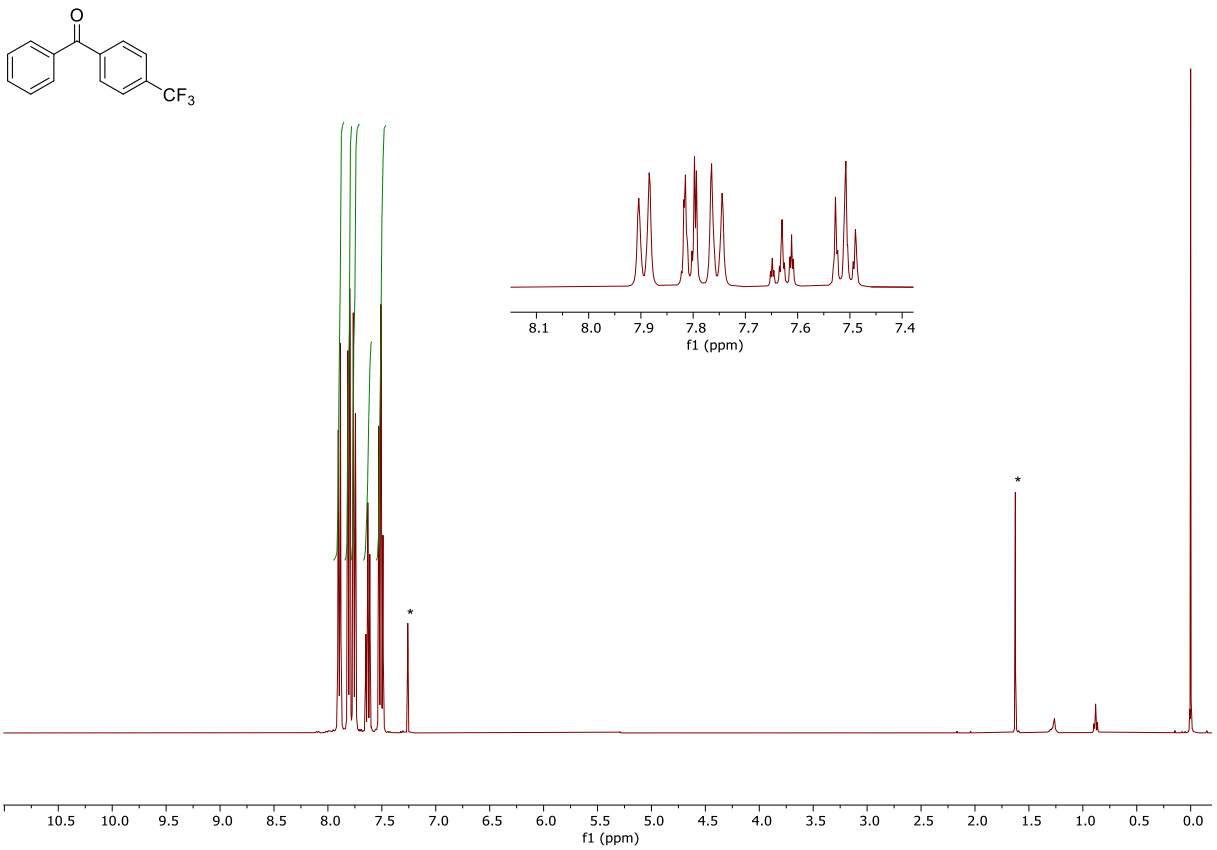

Figure S93. ^{1}H NMR spectrum (400 MHz, $CDCl_3$) of **35-CF$_3$**.

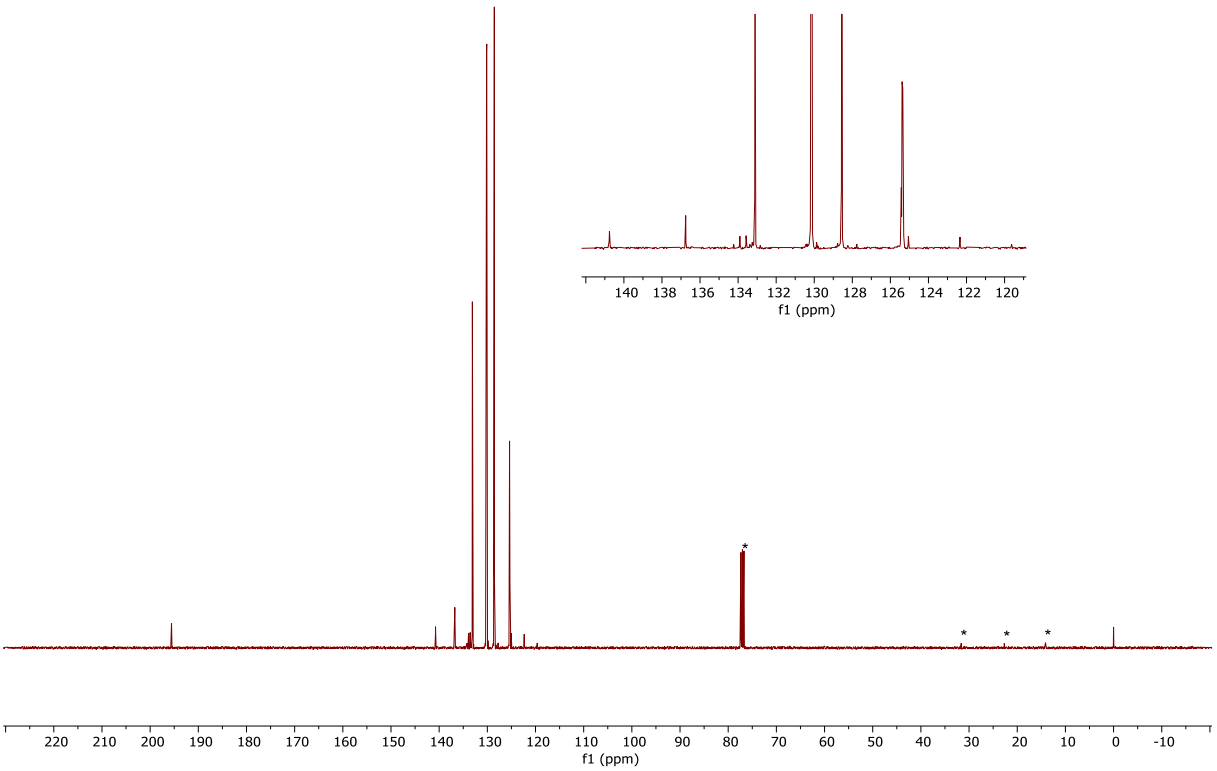

Figure S94. $^{13}C\{^{1}H\}$ NMR spectrum (101 MHz, $CDCl_3$) of **35-CF$_3$**.

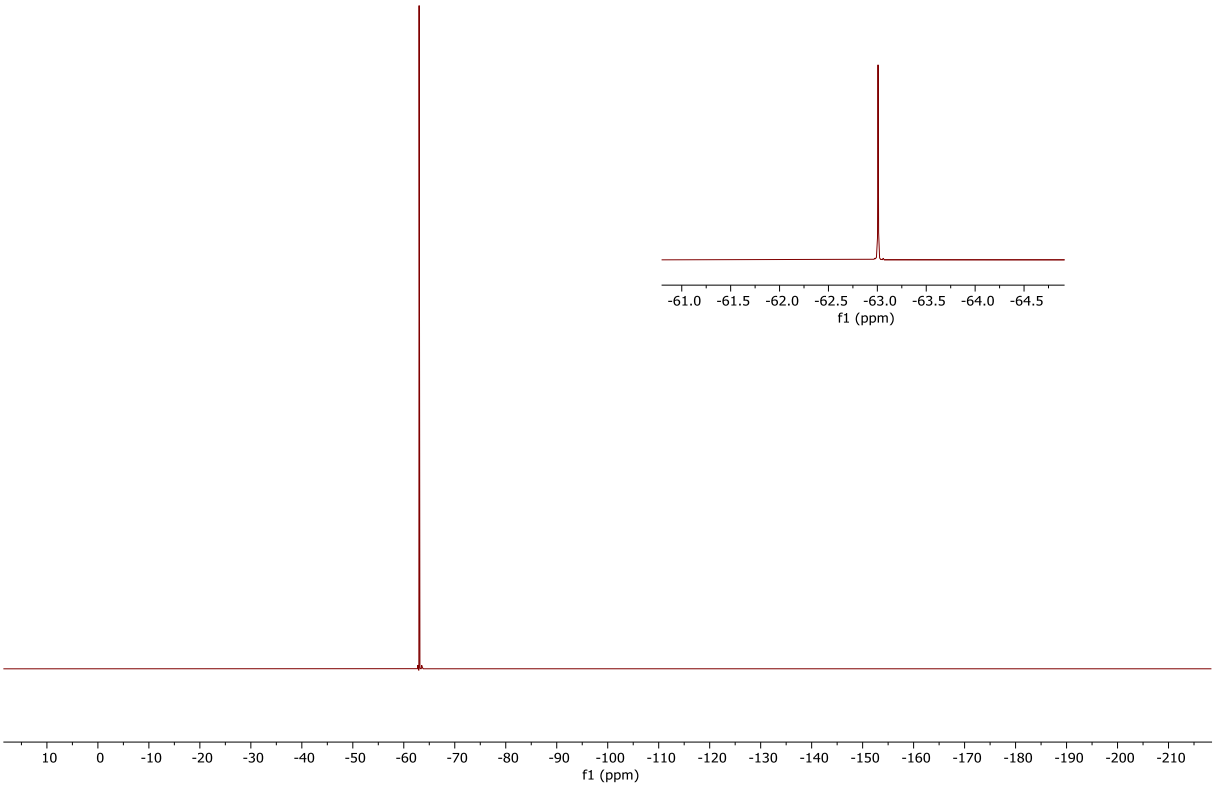

Figure S95. ^{19}F NMR spectrum (376 MHz, $CDCl_3$) of **35-CF_3**.

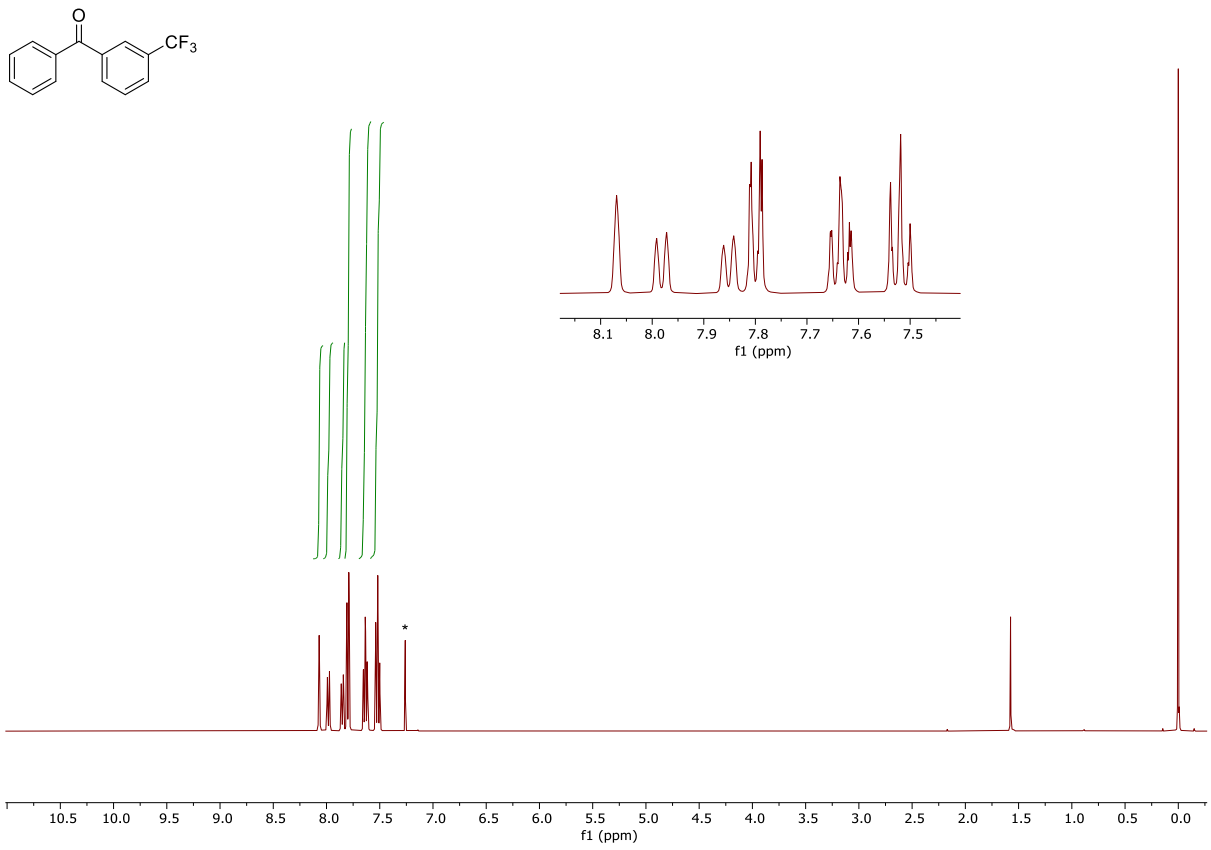

Figure S96. ^{1}H NMR spectrum (400 MHz, $CDCl_3$) of **38**.

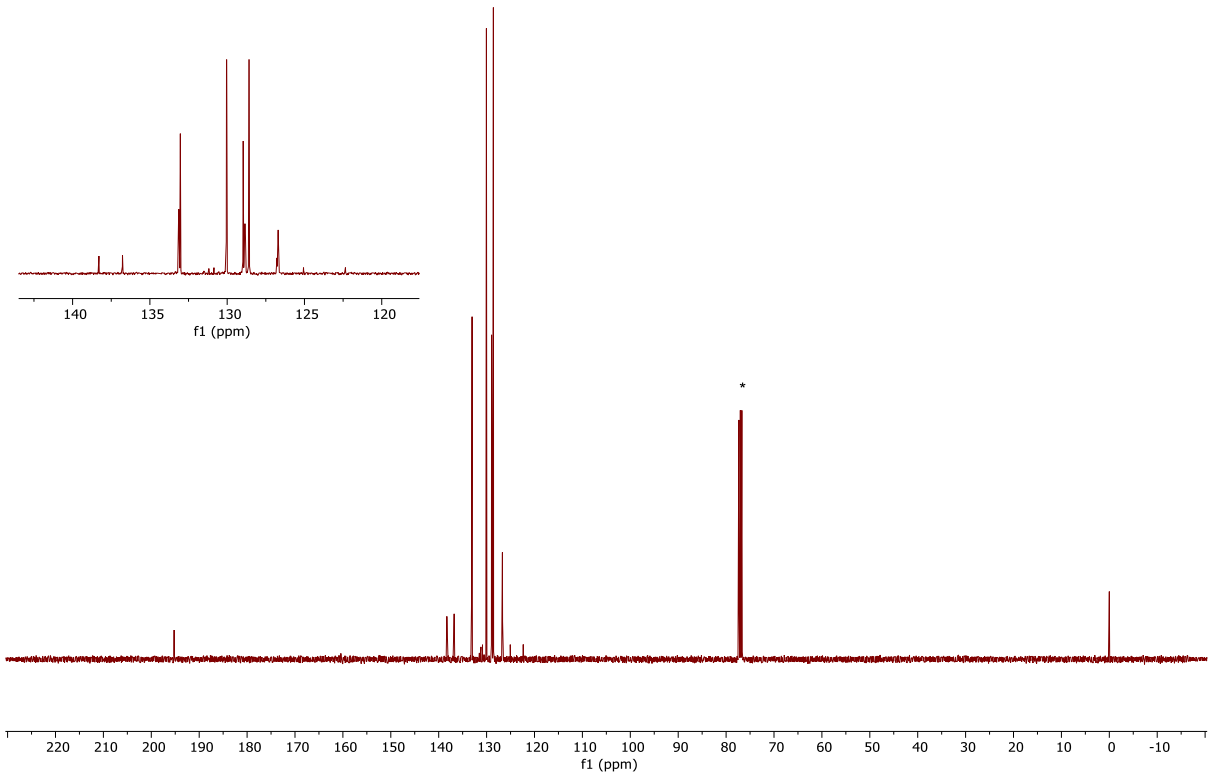

Figure S97. $^{13}C\{^{1}H\}$ NMR spectrum (101 MHz, $CDCl_3$) of **38**.

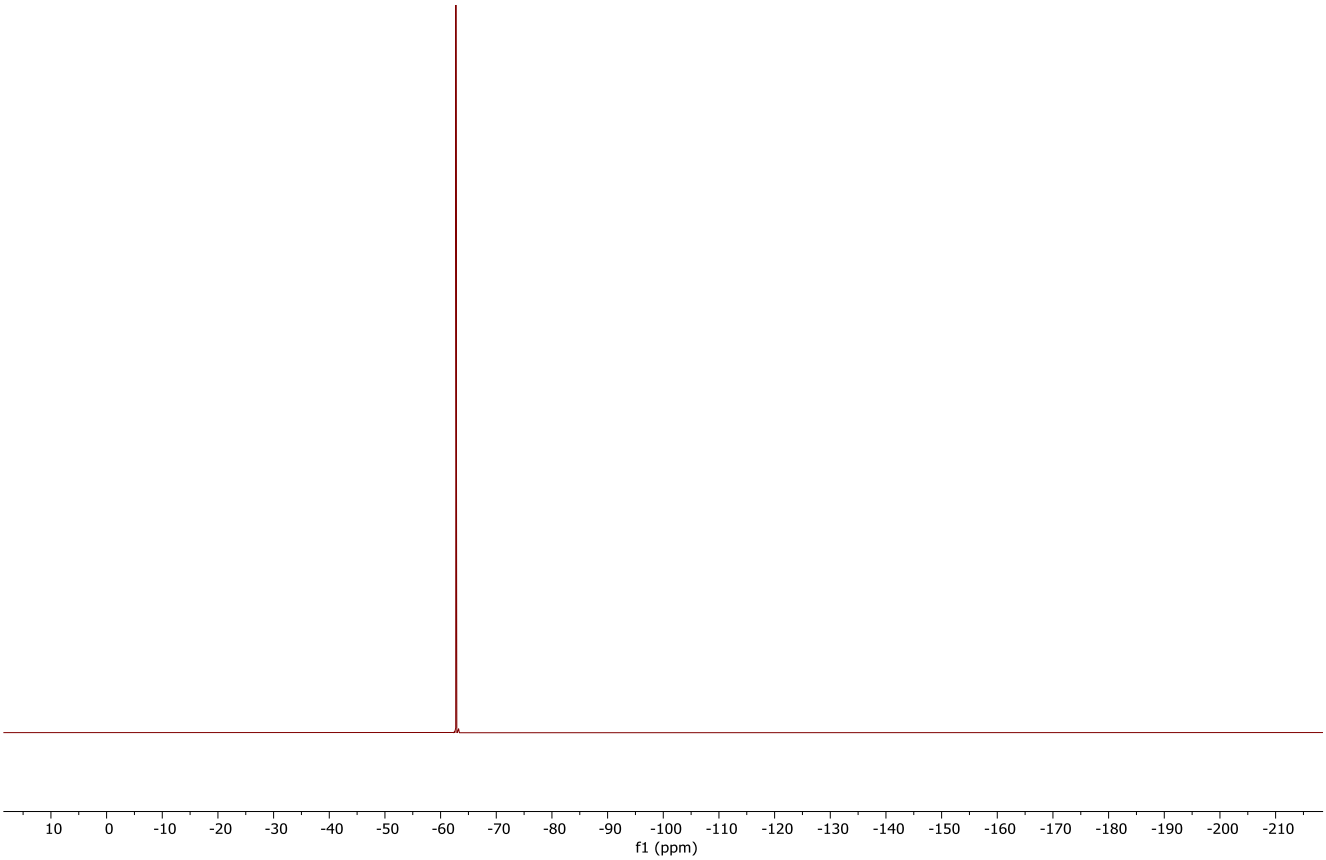

Figure S98. ^{19}F NMR spectrum (376 MHz, $CDCl_3$) of **38**.

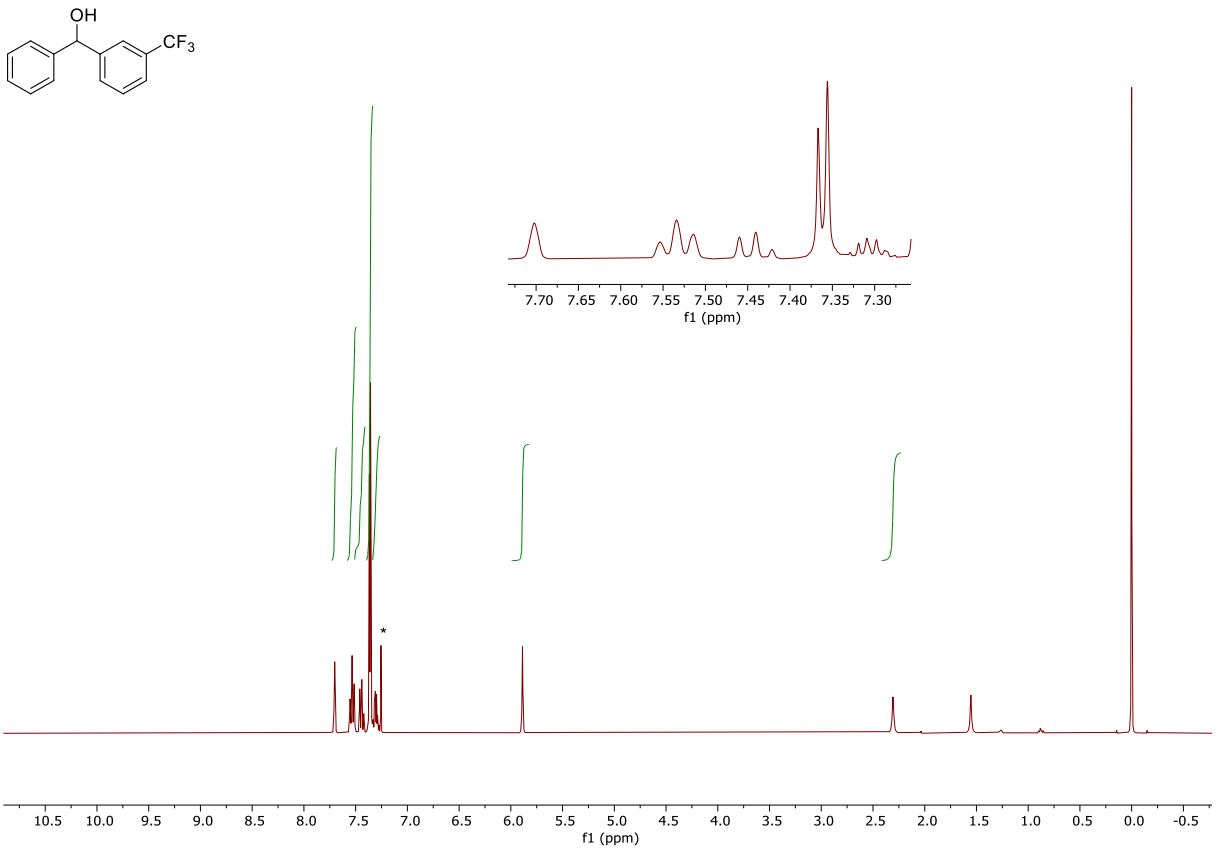

Figure S99. ^{1}H NMR spectrum (400 MHz, $CDCl_3$) of **39**.

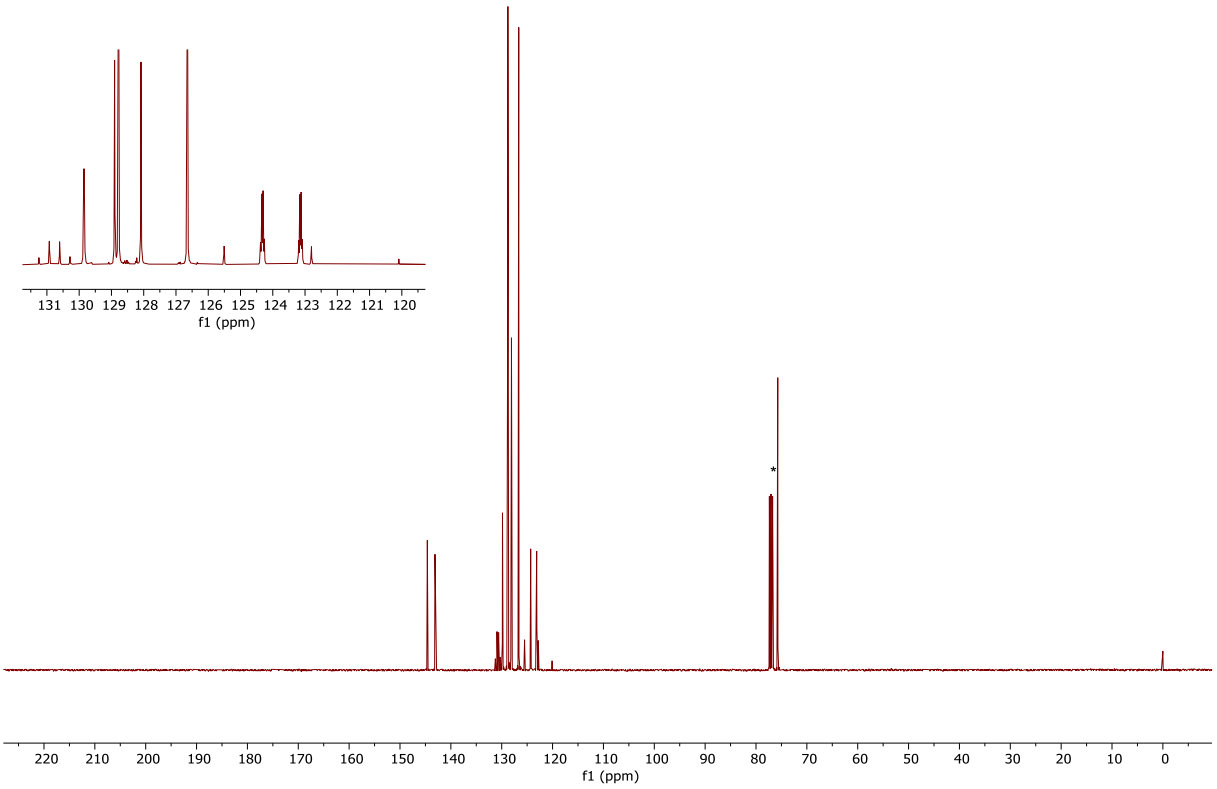

Figure S100. $^{13}C\{^{1}H\}$ NMR spectrum (101 MHz, $CDCl_3$) of **39**.

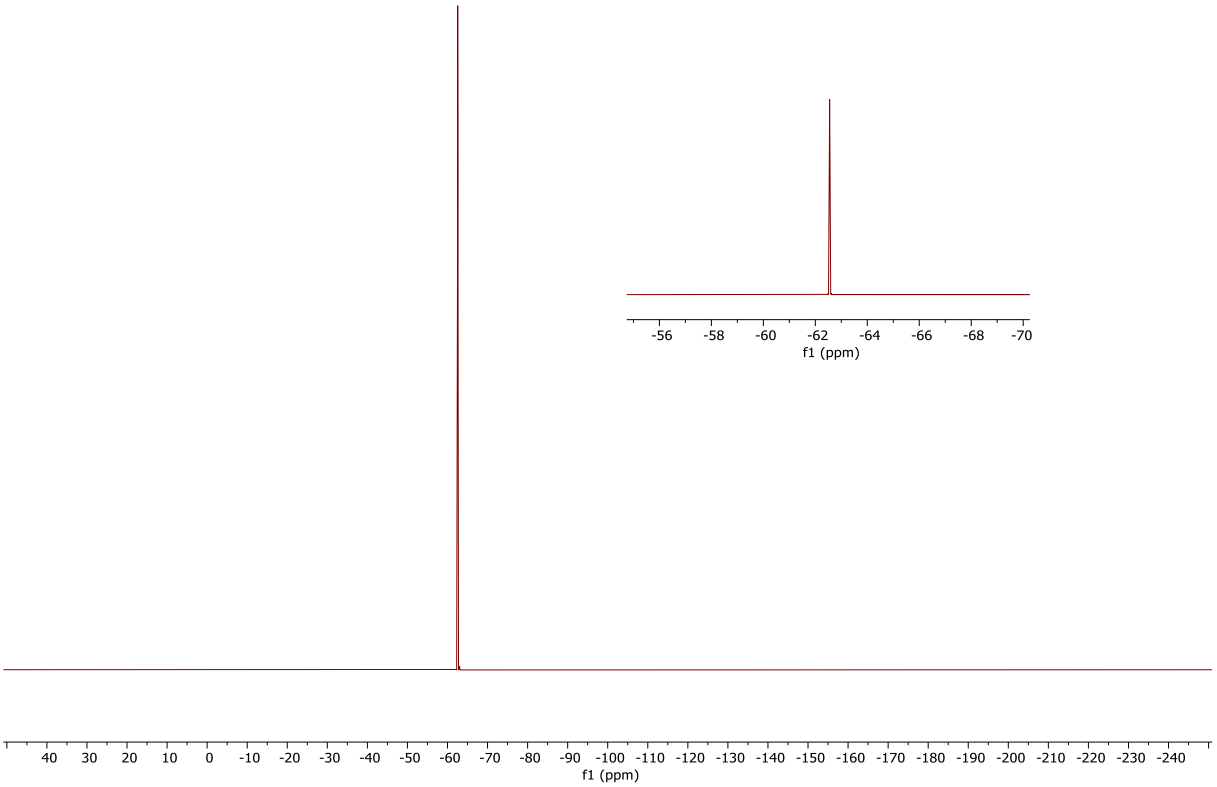

Figure S101. ^{19}F NMR spectrum (376 MHz, $CDCl_3$) of **39**.

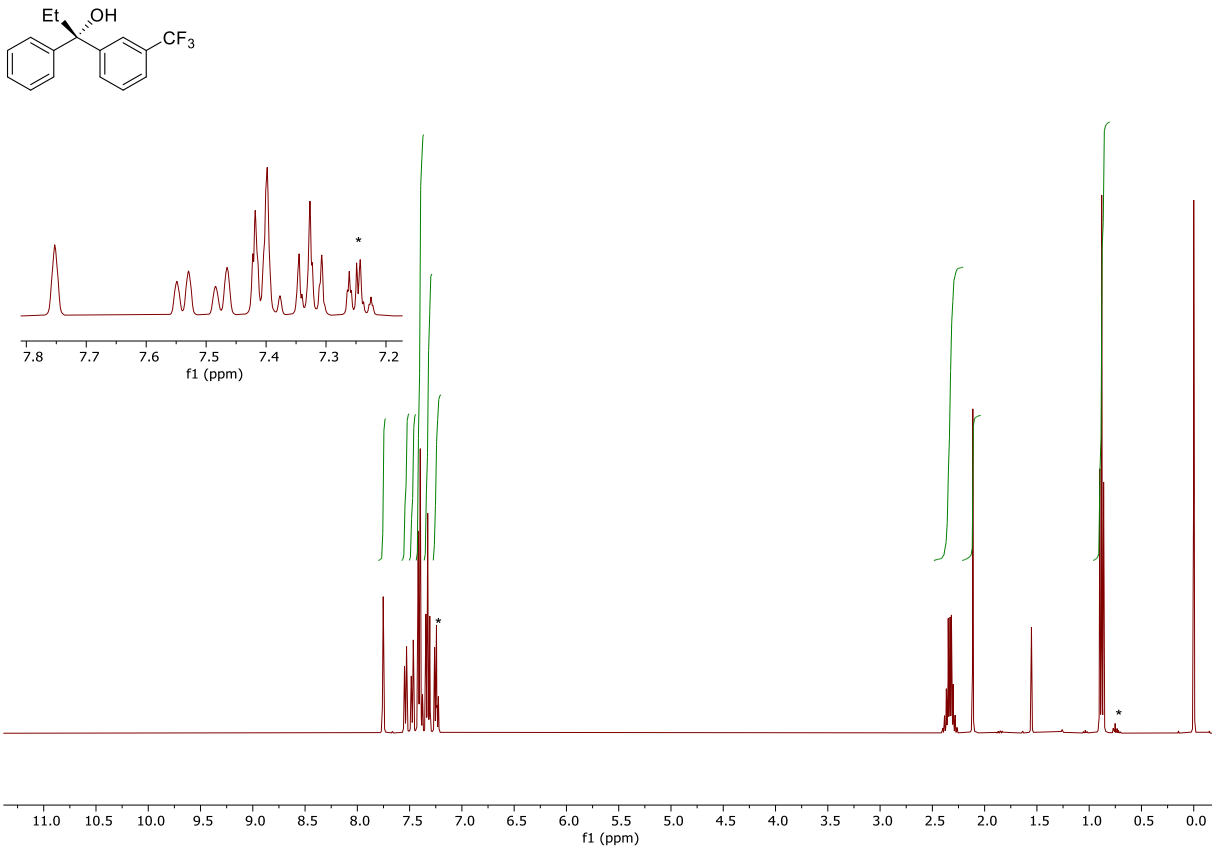

Figure S102. ^{1}H NMR spectrum (400 MHz, $CDCl_3$) of **40**.

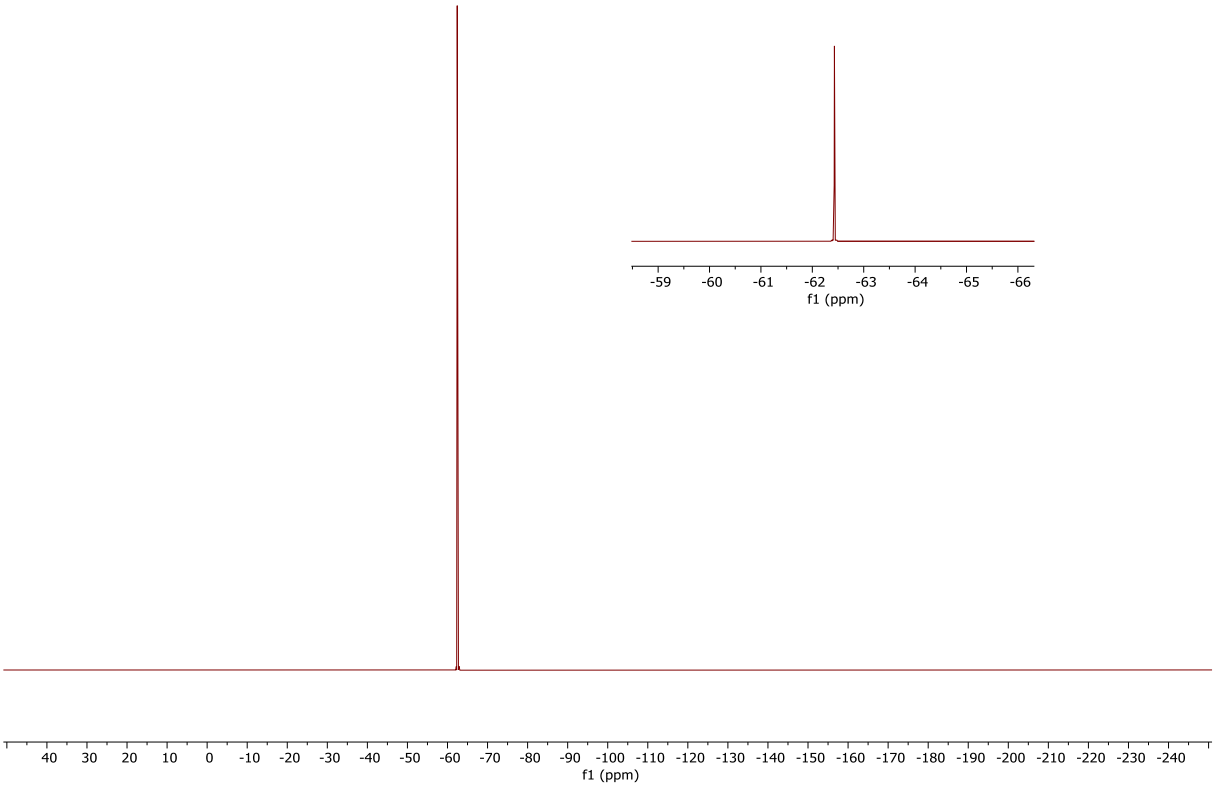

Figure S103. ^{19}F NMR spectrum (376 MHz, $CDCl_3$) of **40**.

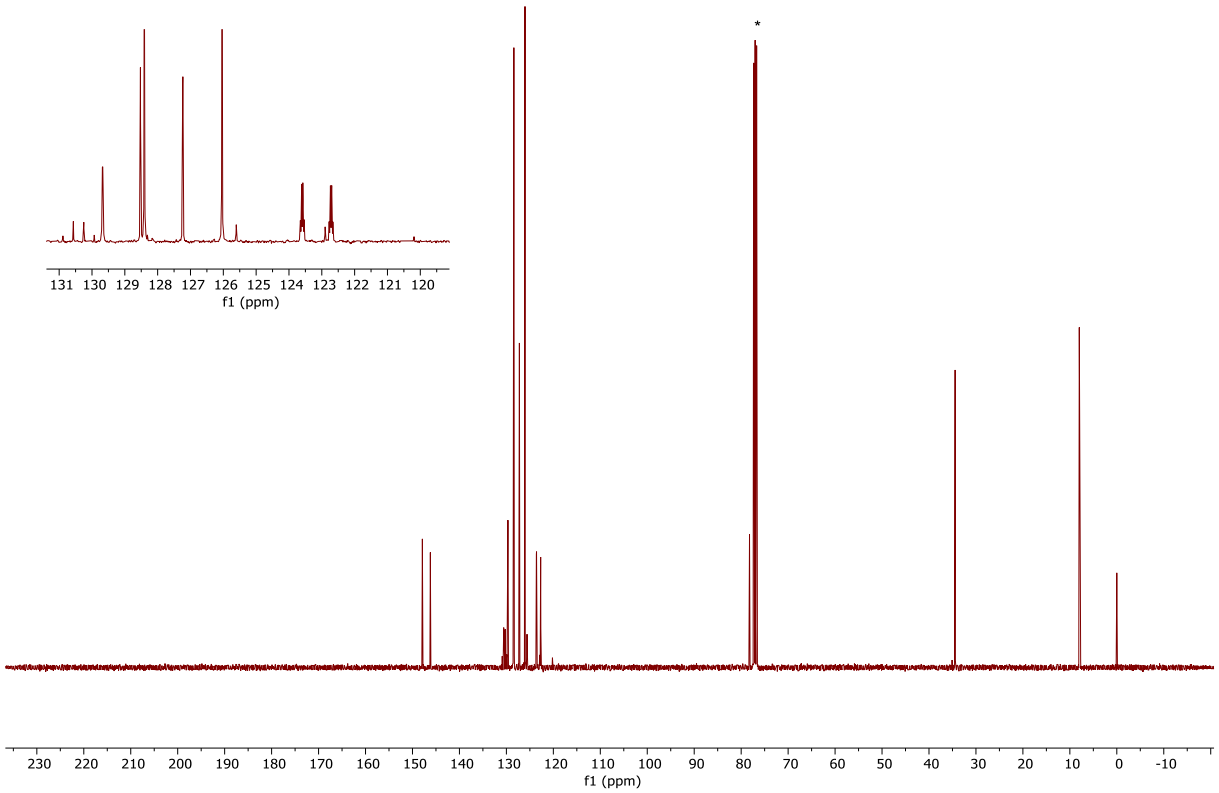

Figure S104. $^{13}C\{^{1}H\}$ NMR spectrum (101 MHz, $CDCl_3$) of **40**.

References

1 G. M. Sheldrick, *Acta Crystallogr., Sect. A: Found. Adv.*, 2015, **71**, 3.

2 G. M. Sheldrick, *Acta Crystallogr., Sect. C: Struct. Chem.*, 2015, **71**, 3.

3 (a) A. L. Spek, *Acta Crystallogr., Sect. D: Biol. Crystallogr.*, 2009, **65**, 148; (b) A. L. Spek, *Inorg. Chim. Acta*, 2018, **470**, 232.